Alternative Refrigerants in Adiabatic Capillary Tubes

J. J. Meyer and W. E. Dunn

ACRC TR-108 December 1996

For additional information:

Air Conditioning and Refrigeration Center
University of Illinois
Mechanical & Industrial Engineering Dept.
1206 West Green Street
Urbana, IL 61801

(217) 333-3115

Prepared as part of ACRC Project 69
Stationary Air Conditioning System Analysis
C. W. Bullard and W. E. Dunn, Principal Investigators

The Air Conditioning and Refrigeration Center was founded in 1988 with a grant from the estate of Richard W. Kritzer, the founder of Peerless of America Inc. A State of Illinois Technology Challenge Grant helped build the laboratory facilities. The ACRC receives continuing support from the Richard W. Kritzer Endowment and the National Science Foundation. The following organizations have also become sponsors of the Center.

Amana Refrigeration, Inc.
Brazeway, Inc.
Carrier Corporation
Caterpillar, Inc.
Copeland Corporation
Dayton Thermal Products
Delphi Harrison Thermal Systems
Eaton Corporation
Ford Motor Company
Frigidaire Company
General Electric Company
Lennox International, Inc.
Modine Manufacturing Co.
Peerless of America, Inc.
Redwood Microsystems, Inc.
The Trane Company
Whirlpool Corporation

For additional information:

Air Conditioning & Refrigeration Center
Mechanical & Industrial Engineering Dept.
University of Illinois
1206 West Green Street
Urbana IL 61801

217 333 3115

Abstract

This study examines the mass flow rate of refrigerants in adiabatic capillary tubes, with an emphasis on the nature of the metastable region for both single component refrigerants and mixtures.

The metastable region of a capillary tube was found to be much more predictable than previously thought. A new and revealing data taking technique, which takes the history of the system into account, allowed for the discovery of a hysteresis effect in the mass flow rate as the level of inlet subcooling is increased and decreased. This finding may have a profound impact on the future of capillary tube data acquisition and modeling.

Table of Contents

page

Abstract iii

List of Tables vi

List of Figures vii

Nomenclature ix

Chapter

1. Introduction 1

2. Capillary Tube Literature Review 2
   - 2.1 Sizing Tools 2
   - 2.2 Friction Factors and Tube Roughness 3
   - 2.3 Flow Regime Analysis 7
   - 2.4 Flash Point Location and Metastability 8
   - 2.5 Two-phase Flow Modeling 17
   - 2.6 Exit Conditions 23
   - 2.7 Experimental Data 28

3. Capillary Tube Study Experimental Facility 31
   - 3.1 Refrigerant Loop 31
     - 3.1.1 Overview 31
     - 3.1.2 Control of Refrigerant Flow Parameters 33
     - 3.1.3 Test Section 34
   - 3.2 Instrumentation 35
     - 3.2.1 Temperature and Pressure Measurement 35
     - 3.2.2 Data Acquisition System 37
   - 3.3 Composition Analysis 37
   - 3.4 Nitrogen Flow Facility 38
   - 3.5 Water Flow Facility 40

4. Capillary Tube Experimental Procedure 42
   - 4.1 System Preparation 42
     - 4.1.1 Charging and Discharging Refrigerant 42
     - 4.1.2 Changing Test Sections 43
   - 4.2 System Operation 43
     - 4.2.1 System Start-Up 43
     - 4.2.2 Data Collection 45
   - 4.3 Refrigerant Sampling Procedure 46
   - 4.4 Data Matrix 46

5. Data Analysis 48
   - 5.1 Capillary Tube Study Data Reduction 48
     - 5.1.1 Determining Capillary Tube Diameters 48
     - 5.1.2 Data Reduction 51

6. Capillary Tube Results 52
6.1 Justification and verification of experimental technique 52
6.1.1 Wall Temperature Measurements 58
6.1.2 Pressure Measurements along the Capillary Tube 59
6.2 Length of the Metastable Regions 60

7. Conclusions and Recommendations 73
7.1 Conclusions and Implications 73
7.2 Suggestions for Future Research 74

References 75

APPENDIX A. MASS FLOW RATE DATA 77

List of Tables

Table ..... Page

2.1 Measured capillary-tube roughnesses, adapted from Sweedyk (1981).....6

2.2 Comparison of calculated and measured exit plane properties for the adiabatic flow of Refrigerant 12 under non-choked flow conditions (Tube: Copper 0.0555-in. ID × 6.0 ft long), adapted from Mikol (1963). 25

2.3 Comparison of calculated and measured exit plane properties for the adiabatic flow of Refrigerant 12 under choked flow conditions. (Tube: Copper 0.0555-in. ID × 6.0 ft long), adapted from Mikol (1963). 26

2.4 Comparison of calculated and measured exit plane properties for the adiabatic flow of Refrigerant 12 under choked flow conditions, but with large pressure drop from tube exit to back pressure region. (Tube: Copper 0.0555-in. ID ×72.0 in. long), adapted from Mikol (1963)..... 27

3.1 Capillary tube dimensions..... 34

4.1 Test matrix for capillary tube studies..... 46

5.1 Comparison of stated and determined tube diameters..... 51

6.1 Capillary tube inlet pressures for the four refrigerants tested 67

6.2 Capillary tube mass flow rates at 10 °F of subcooling for the four refrigerants tested..... 67

6.3 Depressurization rates in the liquid region at 10 °F of subcooling for the four refrigerants tested..... 68

6.4 Calculated critical bubble radius and resulting relative roughness from metastable region data for R-22 in a 0.049-in. ID tube 69

List of Figures

Figure ..... Page

1.1 The ozone depletion potential and the global warming potential of various refrigerants 1
2.1 Mikol's water flow data 5
2.2 Scott's comparison of several two-phase friction factors 5
2.3 Output from thermocouples located along a capillary tube during steady flow conditions (solid lines) and unsteady flow conditions (dashed lines) from Scott 10
2.4 Attempt by Kuijpers and Janssen to correlate the delay of flashing to inlet temperature 13
2.5 Underpressure at the point of vaporization versus expansion rate from Scott 13
2.6 Length of metastable region versus expansion rate from Scott 14
2.7 Length of metastable region versus underpressure at the point of vaporization 14
2.8 Comparison of Equation 3.7 with data from Kuijpers and Janssen 16
2.9 Underpressure at vaporization versus the square of the mass flux form Scott 16
2.10 Typical temperature and pressure profiles in an operating capillary tube with a metastable region 18
2.11 Predicted and experimental temperature and pressure profiles from Li 21
2.12 Variation in void fraction along a capillary tube 22
2.13 Fanno plot calculated for the measured flow rate and the actual flash point from the data of Mikol from Mikol 22
2.14 Refrigerant mass flow rate through a capillary tube as the reservoir pressure is reduced (from Pate) 29
2.15 Critical mass flux for homogeneous frozen and nonhomogeneous models, adapted from Pate 30
3.1 Schematic of capillary tube facility 32
3.2 Capillary tube inlet and outlet connections 35
3.3 Inlet pressure transducer calibration results 36
3.4 Outlet pressure transducer calibration results 36
3.5 Schematic of data acquisition system 37
3.6 Schematic of nitrogen flow facility 38
3.7 Schematic of the water flow facility 41
4.1 Configuration used to add or remove refrigerant charge 44
4.2 Typical data set (R-22 flowing through the 0.039-in. capillary tube) 46
5.1 Resulting fractional deviations from the calculated best diameter for the 0.039 inch ID capillary tube 49
5.2 Resulting fractional deviations from the calculated best diameter for the 0.042 inch ID capillary tube 50

5.3 Resulting fractional deviations from the calculated best diameter for the 0.049 inch ID capillary tube 50
6.1 Mass flow rate data obtained for discrete levels of subcooling for R-22 flowing through a 46-in. long capillary tube with an inlet pressure of 241 psia 53
6.2 Data from Figure 6.1 shown with similar data obtained from one continuous run 53
6.3 Many "identical" trials of R-134a flowing through the 0.049-in. capillary tube 54
6.4 Typical temperature and pressure profile in an operating capillary tube 55
6.5 A double "loop," showing the hysteresis effect resulting from increasing and decreasing the level of inlet subcooling 56
6.6 Mass flow rate and tube wall temperature data for R134a flowing through the 0.049-in. capillary tube 57
6.7 The effect on mass flow rate resulting from an additional wall temperature measurement (Tcap9.5) 59
6.8 R-22 flowing through the 0.039-in. capillary tube 60
6.9 R-22 flowing through the 0.042-in. capillary tube 61
6.10 R-22 flowing through the 0.049-in. capillary tube 61
6.11 R-134a flowing through the 0.039-in. capillary tube 62
6.12 R-134a flowing through the 0.042-in. capillary tube 62
6.13 R-134a flowing through the 0.049-in. capillary tube 63
6.14 R-407C flowing through the 0.039-in. capillary tube 63
6.15 R-407C flowing through the 0.042-in. capillary tube 64
6.16 R-407C flowing through the 0.049-in. capillary tube 64
6.17 R-410A flowing through the 0.039-in. capillary tube 65
6.18 R-410A flowing through the 0.042-in. capillary tube 65
6.19 R-410A flowing through the 0.049-in. capillary tube 66
6.20 Mass flow rates from three different attempts to record data for R-22 flowing through the 0.049-in. capillary tube. Figure "b" shows the same data plotted on an expanded scale 70
6.21 Mass flow rates from three different attempts to record data for R-407C flowing through the 0.042-in. capillary tube. Figure "b" shows the same data plotted on an expanded scale 71

Nomenclature

Roman and script letters

A = cross sectional area [ft^2]

b = microfin height [in]

Bo = Boiling number, $\dot{Q}''/G\,h_{fg}$

c = speed of sound [ft/sec]

C = constant in two-phase flow multiplier equations [-]

C_p = constant pressure specific heat [BTU/lbm-°F]

D = diameter [ft]

D_e = effective diameter [ft]

D_{eq} = equivalent diameter [ft]

f = friction factor [-]

Fr = Froude number, ratio of gravitational forces to inertial effects [-]

g = gravitational acceleration [ft^2/s]

g_c = gravitational constant

G = mass flux [lbm/ft^2-hr]

Ga = Galileo number, ratio of gravitational forces to viscous forces [-]

h = heat transfer coefficient [BTU/ft^2-°F]

h_{fg} = enthalpy of vaporization [Btu/lbm]

k = thermal conductivity [BTU/ft-°F], Boltzman's constant

L = tube length [ft]

$\dot{m}$ = mass flow rate [lbm/hr]

NTU = UA/C_{min}, number of transfer units [-]

Nu = hD/k, Nusselt number, dimensionless heat transfer coefficient [-]

P = pressure [psi]

q = heat transfer rate [BTU]

$\dot{Q}''$ = heat flux [Btu/ft^2-hr]

Re = Reynolds number [-]

T = temperature [°F]

u = velocity [ft/s]

UA = overall heat exchanger thermal conductance [kW/K]

v = specific volume [ft^3/lbm]

X = Lockhart-Martinelli parameter [-]

x = thermodynamic quality [-]

z = distance in refrigerant flow direction [m]

Greek letters

α = two-phase flow void fraction [-]

Δ = denotes change or difference

ε = tube roughness [ft]

ϕ = two-phase flow multiplier [-]

Γ = physical property index used in de Souza pressure drop correlation [-]

μ = absolute viscosity [lbm/ft-hr]

ν = kinematic viscosity [ft^2/s]

ρ = density [lbm/ft^3]

σ = surface tension [lbf/ft]

σ_i = Cavitation index defined by Mikol and Dudley

ω = oil concenntration, mass basis [-]

Ψ = two-phase heat transfer multiplier [-]

Subscripts

c = critical

i = inlet

f = flash, friction

ℓ = quantity pertains to liquid phase

m = mixture, momentum

o = outlet

rd = a "reduced" quantity, as in $P_{rd} = P/P_{crit}$

sat = value evaluated at a saturated conditions

sc = subcooled condition

so = quantity defined by Soliman

tp = quantity pertains to a two-phase condition

v = quantity pertains to vapor phase

wall = quantity pertains to wall

Superscripts

' = denotes a modified quantity

$\dot{}$ = denotes quantity is a rate

$\bar{}$ = denotes quantity is an average

Dimensionless groups

Quantity	Interpretation	Definition
Reynolds number, Re	Ratio of inertial effects to viscous forces	GD/μ
Superficial Reynolds number	Assumes that actual phase flow rate occupies entire tube	$Re_l = \frac{GD(1-x)}{\mu_l}$ $Re_v = \frac{GDx}{\mu_v}$
Liquid or vapor only Reynolds number	Assumes all flow consists of the phase of interest and occupies the entire tube	$Re_{lo} = \frac{GD}{\mu_l}$ $Re_{vo} = \frac{GD}{\mu_v}$
Nusselt number, Nu	Dimensionless heat transfer coefficient	$Nu = \frac{hD}{k_l}$
Prandtl number, Pr	Ratio of momentum diffusivity to heat diffusivity	$Pr = \frac{\mu C_p}{k}$
Galileo number, Ga	Ratio of gravitational to viscous forces	$Ga = \frac{\rho_l(\rho_l-\rho_v)gD^3}{\mu_l^2}$
Froude number, Fr	Ratio of inertial effects to gravitational forces	$Fr_l = \frac{(G/\rho_l)^2}{gD}$
Lockhart-Martinelli parameter, X_{tt}	Dimensionless liquid inventory	$X_{tt} = \left(\frac{\rho_v}{\rho_l}\right)^{0.5}\left(\frac{\mu_l}{\mu_v}\right)^{0.1}\left(\frac{1-x}{x}\right)^{0.9}$

Chapter 1

Introduction

This work focuses on defining the performance characteristics of alternative refrigerants while expanding in an adiabatic capillary tube.

Many uncertainties still surround the specific environmental and safety criteria that future refrigerants may have to meet. The ozone depletion potentials (ODP's) and greenhouse warming potentials (GWP's) of the refrigerants concerned are shown in Figure 1.1.

Due to the wide-spread use of the refrigerants being phased out, every effort is being made to maximize the efficiency of the new refrigerants and the systems designed for them. Performance data are needed to make wise decisions when both choosing the thermodynamically best alternative and designing system components that will use it. In order to take full advantage of the characteristics of future refrigerants, a better understanding of the phenomenology of multiphase flow and heat transfer is needed.

This report begins with an extensive literature review, and then describes experiments conducted on adiabatic capillary tubes using R-22, R-134a, R-407C and R-410A. The data sets span a wide range of subcooled inlet conditions, and the analysis focuses on the existence of metastable behavior near the flash point.

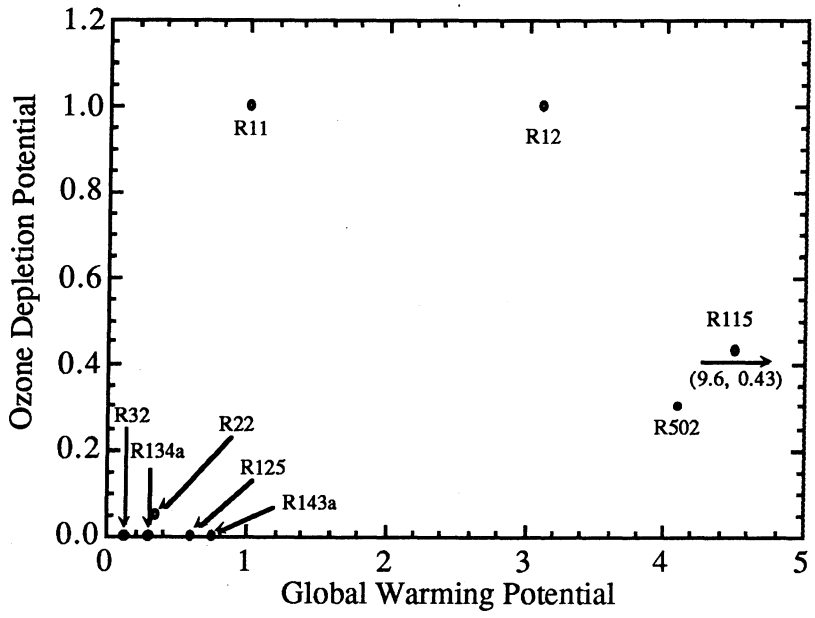

Figure 1.1 The ozone delpetion potential and the global warming potential of various refrigerants.

Chapter 2

Capillary Tube Literature Review

A literature review was conducted to discover the problematic areas of researching and understanding capillary tube flow. Due to similarities in flow conditions, some overlap exists between the ideas presented condensation and the capillary tube literature. For completeness, however, a complete discussion of what was found to be the issues and ideas which need to be considered before capillary-tube results can be interpreted is presented.

2.1 Sizing Tools

Until 1949, capillary-tube literature consisted almost exclusively of capillary-tube flow analyses and general design criteria. Discussions were made concerning the approach to sizing capillary tubes, yet a true technique for selecting a capillary tube, given a specific operating condition, was not available. Marcy (1949) presents a method for calculating the length of capillary tubing required for a desired pressure drop. He also shows how to predict the mass flow rate for a capillary tube of specified dimensions.

In deriving his selection method, Marcy first assumed that the flow was adiabatic. The immediate practicality of the method was questioned since it could not be used for capillary-tube/suction-line heat exchangers. However, it served to lay the ground work for future models. The principle of the model is to integrate the Fanning Equation for fluid friction

$$-\frac{dP}{dz}=\frac{4f\rho u^2}{2g_cD}. \qquad (2.1)$$

If the refrigerant entering the capillary tube is subcooled liquid, the length of tube in which the refrigerant remains liquid can be calculated from the above equation. Because the flow is assumed to be adiabatic the temperature for the subcooled liquid section is approximately constant.

The procedure for calculating the length of the two-phase region is in principle the same as that used for the subcooled length. Marcy arranged the Fanning Equation as follows,

$$dz=-K\frac{\rho}{f}dP, \qquad (2.2)$$

where $K = 72gD/G^2$ and $G = v\rho$. The equation is integrated over the two-phase region with the limits being the saturation pressure at the inception of flashing to the given outlet pressure. Note that there is no allowance for a choked-flow exit condition. Marcy integrated the equation graphically to determine the length of the two-phase region. The total capillary tube length is simply the sum of the liquid length and the two-phase length.

2.2 Friction Factors and Tube Roughness

The determination of tube roughness and its effect on frictional pressure loss has been a focal point of discussion in refrigeration literature since capillary tubes were first introduced as an expansion device. Seemingly, every author of a paper concerning capillary tubes has in one way or another referenced this topic. Despite the fact that frictional pressure drop has received much attention, the exact nature of shear between phases in a two-phase flow is still not adequately understood. Manufacturing variability in the production of capillary tubing has also been discussed with regular frequency in the literature. It is often blamed for the inability of researches to find a universal model for refrigerant flow in capillary tubes. This section outlines the major findings and summaries regarding treatment of this important aspect of capillary-tube flow.

Marcy (1949) assumed that drawn tubes were produced so that tube walls could be considered smooth. Thus, he did not account for tube roughness in his relation between friction factor and Reynolds Number. Tube roughness has since been shown to have a significant effect on flow characteristics.

Hopkins (1950) initially used the friction factor relation from McAdams (1933),

$$f = \frac{0.094}{Re^{0.26}}, \qquad (2.3)$$

for $5000 < Re < 200{,}000$, in his analysis. However, Hopkins found that by using this friction factor, his model predicted capillary-tube lengths an average of 13% greater than the observed lengths. He then arbitrarily set his friction factor to 13% higher than that calculated by McAdams' method. The only other discussion Hopkins makes regarding the friction factor is to acknowledge that this remained a point of question. Hopkins mentions that the manufacturing tolerance of ±0.001 in. for the internal diameter may account for some of the variability in his results. He does not, however, attempt to quantify the variation.

Mikol (1963) notes that previous researchers, including Marcy (1949), Bolstad and Jordan (1948 and 1949), Hopkins (1950), Cooper, *et al.* (1957), and Whitesel (1957a), each used different friction factor correlations. Mikol attempted to resolve the apparent confusion by performing a detailed experimental pressure drop analysis. The object of this analysis was to predict pressure drop within an error of ±1.5%. The limit of ±1.5% was placed after an error analysis was performed on the calculation of the friction factor. Mikol found that the largest contributors to error were tube inside diameter measurement and mass flow rate measurement. A 1% error in either measurement results in a 5% and 2% error in friction factor calculation, respectively. From his error analysis, Mikol determined he could make all measurements so that the maximum predictable error in friction factor would be ±1.5%.

Mikol determined inside tube diameter by weighing the tube dry, then filling it with water and weighing it full. This was done four times. The result for a nominal 0.055 in. diameter tube was 5.5509×10^{-2} in. with an rms error of 6.0×10^{-5} in. Tube roughness was determined independently by a diamond stylus type profilometer and a stereoscopic microscope. The resulting measurements showed tube roughness to be 2.1×10^{-5} in., giving a relative roughness ε/D of 3.8×10^{-4}.

Water was used as the test fluid during the flow experiments. The results are shown in Figure 2.1. The results show good agreement with the standard Moody correlation. Mikol concluded from his results that fluid flow in capillary tubes may be analyzed in the same manner as any other pipe flow, and the same methods for analysis apply. Note though that the Nikuradse correlation for smooth tubes is relatively close to Moody's formula for the measured tube roughness. Also note that the data tend to fall between the two correlations. The curve defined by Bolstad and Jordan (1949) for a nominal 0.055 in. diameter tube is shown on the same plot. The trend for this curve is consistent with the Moody correlation, but is consistently high. Mikol conjectures that the Bolstad data are high because they used the nominal diameter in their calculations and not the actual diameter, and because they had systematic errors in their measurements.

Scott (1976) compares several two-phase friction factor correlations to experimental data from one of Mikol's test runs. He plotted the results as shown in Figure 2.2. There is considerable discrepancy between the correlations. It is interesting that the McAdams' approach, which is a general correlation, appears the most successful. This may not be surprising if one concurs with Mikol's conclusion that refrigerant flow in capillary tubes can be treated as any other pipe flow. Scott also recounts the roughness heights determined by several investigators. Mikol experimentally determined the roughness for his tubing to be 2.1×10^{-5} in. Erth (1970) used the slope of the liquid region pressure profiles of data from Bolstad (1948) and Battelle (1960) to determine roughness heights of 1.43×10^{-5} in. and 2.0×10^{-5} in., respectively. The roughness for drawn tubing is typically considered to be 6.0×10^{-5} in., much higher than the typical values for capillary tubing. For his analysis, Scott used essentially an average value of 1.8×10^{-5} in.

Sweedyk (1981) sought to limit the effect of manufacturing variability by lobbying for a revision in the standard for capillary-tube production. He suggests that a standard for internal surface roughness be added to the existing manufacturing standard. To quantify the variability in roughness between different tubes, Sweedyk measured the roughnesses of a cross section of tube makes and sizes using a profilometer (Sweedyk did not specify what type of profilometer he used). The results are presented in Table 2.1, from Sweedyk. The variability is surprisingly large.

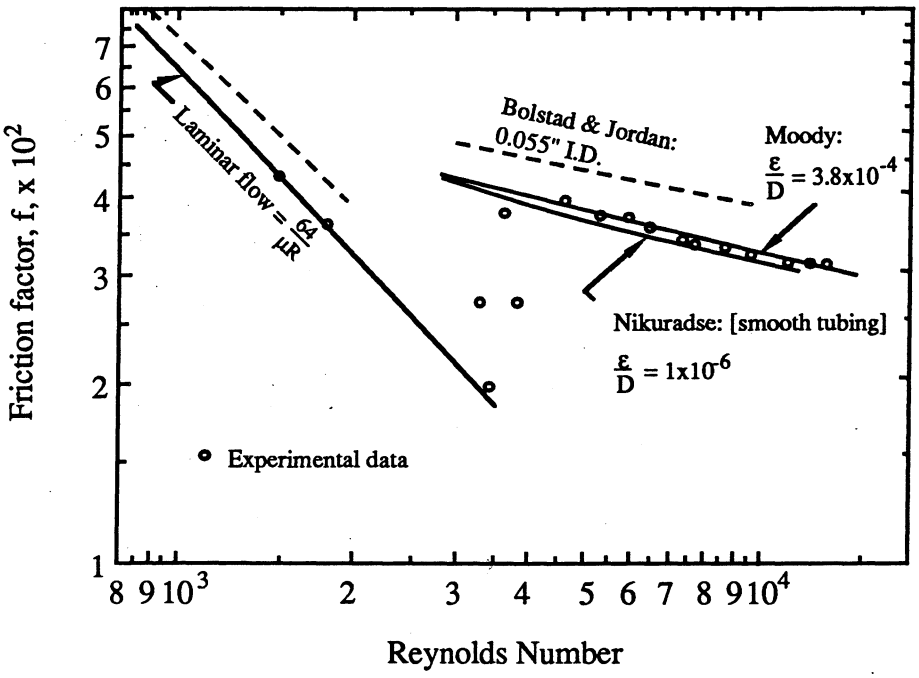

Figure 2.1 Mikol's water flow data

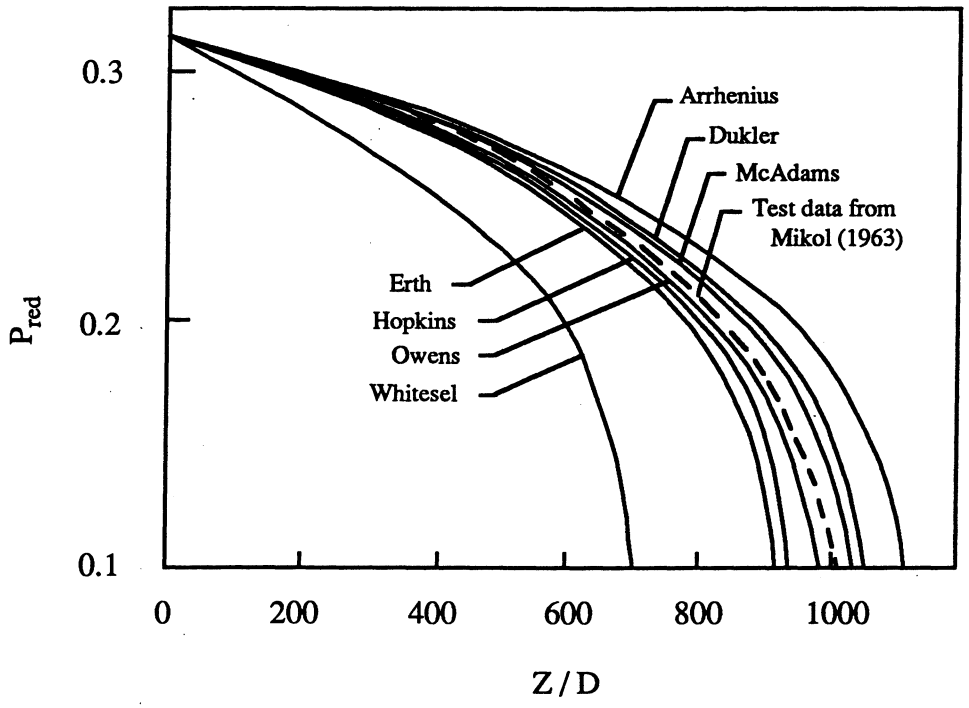

Figure 2.2 Scott's comparison of several two-phase friction factors

However, the tubes tested were obtained from different manufacturers and from different processes. It is known that different manufacturing processes produce different surface finishes. Without more information relating tube roughness to manufacturer and manufacturing process, no conclusive remarks about roughness variability may be made.

Table 2.1 Measured capillary-tube roughnesses, adapted from Sweedyk (1981).

ID (mm)	ID (in.)	ROUGHNESS (μin.)
0.66	0.026	11
0.79	0.031	6 - 8 - 8 - 73 - 6 - 43
0.99	0.039	7.5
1.07	0.042	4.5 - 6 - 4 - 11 - 16
1.17	0.046	9.5 - 10
1.24	0.049	6 - 8 - 7.5
1.37	0.054	13 - 5 - 12 - 5.5 - 7
1.50	0.059	10.5 - 9 - 7
1.63	0.064	3.4 - 5 - 10 - 36 - 32 - 4.5
1.78	0.070	6.5
1.91	0.075	9
2.03	0.080	6 - 9
2.16	0.085	7
2.29	0.090	5
2.79	0.110	7

Pate (1982) acknowledges the fact that several different sources reported a variety of different tube roughnesses. In particular, he mentions that for drawn copper tubing, Moody (1944) found roughness to be 5.0×10^{-6} ft (6.0×10^{-5} in.) and Miller (1978) found the roughness to be 8.2×10^{-6} ft (9.84×10^{-5} in.). With this in mind, Pate determined the friction factor for his tubing experimentally, bypassing the need for determining surface roughness. Upon comparison of his friction factor with the Moody diagram, he found the roughness to be 3.85×10^{-5} ft (4.62×10^{-4} in.), an order of magnitude higher than any other reported roughnesses.

It is clear that there is a variability associated with the treatment of frictional pressure loss, and that there is very little agreement in the literature on this topic. It is also clear that, due to significant differences between manufacturing processes, friction factor correlations are valid only for the tube from which they were determined. Conversely, it may be argued that the Moody friction factor or similar approaches will be successful given an accurate surface roughness of the tube. Nevertheless, one may speculate with some confidence that tubing from the same batch will have surface finishes similar enough so that the Moody chart will provide adequate results.

2.3 Flow Regime Analysis

Researchers have spent considerable effort determining the different flow regimes that occur in two-phase flow. The relative mass fluxes of the liquid and vapor phases are generally regarded as the most important factors in determining the flow regime for a given set of flow conditions. However, tube orientation has also been shown to have a significant effect on flow patterns for most tube diameters; two-phase flows in vertical tubes tend to be annular over a much larger range of operating conditions than flows in horizontal tubes. Tube diameter has been shown to have relatively small impact on flow regime, although very little work has been done with tube diameters on the order of capillary-tube sizes.

Different flow regimes can be characterized by different physical phenomena. For example, heat transfer to an annular flow, in which a thin liquid film contacts the entire tube wall, behaves much differently than stratified flow, in which the liquid lies in the bottom half of the tube and vapor is in the upper half of the tube. As another example, the drag forces on vapor bubbles suspended in a liquid continuum are significantly different from those on slug-flow bubbles sandwiched between liquid slugs. A major key necessary to correctly model a two-phase flow is knowing the flow regime. To better understand the flow regimes present in capillary-tube flow, visualization studies have been performed.

Cooper, et al. (1957) sought more insight into the question of metastability in the development of their selection criteria. Their observations and conclusions concerning the metastable region will be discussed in a later section. Secondary to their main objective was the observation and analysis of the two-phase flow regimes, and their discussion is correspondingly brief. To the naked eye, the flow was reported to appear fog-like; the presence of bubbles or slugs of liquid and vapor were not observed. A photograph of the flow is presented, but no details of how it was obtained are given.

Mikol (1963) conducted flow tests with R-12 in a 0.049-in. ID glass tube. During his tests, Mikol observed that under different operating conditions the flow may be either steady or pulsating. No attempt at explaining the existence of the two modes is made. Photographs of each mode are presented. The pulsating mode is characterized by larger bubbles, visible to the naked eye. Downstream of the vaporization point, additional vapor bubbles appeared to be forming in the bulk fluid. Liquid was present on the tube wall along the entire length of the tube. The stable mode appeared fog-like, in agreement with Cooper, et al. (1957). However, high speed photographs were taken to "stop" the flow. These revealed the flow was comprised of very small bubbles. The bubbles appeared to form on the tube wall and move to the center of the tube. Again, liquid was present on the tube wall along the entire tube length. As the flow progressed down the tube, the size of the center vapor region became larger. Toward the end of the tube, virtually the entire diameter was comprised of the vapor region. A fine spray was observed exiting the tube.

Koizumi and Yokoyama (1980) performed a visualization study using a 1-mm (0.03937-in.) ID glass tube. Their observations agree with those of Mikol. They observed one initial vaporization point on the wall. Downstream of this point the bubbles moved toward the center of the tube. Once initiated, vaporization continued "in all parts of the liquid." Bubbles coalesced as the fluid moved farther downstream. Toward the exit, bubbles began to break up, giving the flow an almost homogeneous appearance.

2.4 Flash Point Location and Metastability

As mentioned earlier, visualization studies were performed to determine the location of the flash point as well as to determine the flow regimes present. These studies sought to ascertain whether the so-called metastable region actually exists. Unfortunately, however, the capillary tube visualization studies used glass tubing, leaving the conclusions open to the argument that flow through a glass tubes does not accurately represent what happens in a copper capillary tube. Nonetheless, these visualization studies have added much to our understanding of the behavior of refrigerant flow in capillary tubes.

By using a glass capillary tube, Cooper, et al. (1957) were able to observe that the length of the liquid region was longer than that predicted by equilibrium saturation calculations, confirming the existence of the metastable phenomena. Curiously, the vaporization point in the test sections oscillated within a section of tube a few inches long. Cooper, et al. sought to explain this by noting the lack of nucleation sights on the smooth internal surface of the glass tube. A thin wire was inserted into the tube in an effort to stabilize the flow. With the wire installed, the flash point moved "regularly" along the tube as the amount of inlet subcooling was varied.

Mikol and Dudley (1964), in a paper related to Mikol (1963), examined the phenomena of metastability utilizing cavitation theory. In their data analysis, Mikol and Dudley included results from other investigators who used both glass tubes and copper tubes. The unstable, pulsating flow mentioned in Mikol (1963) was also discussed in more detail. These pulsations in the flow were attributed to instabilities in the inception of vaporization. Evidence from photographs taken of the pulsating flow indicated that vaporization occurs in the bulk liquid. Further observation showed that the pulsating flow was not a transient phenomena that would eventually decay; rather, once initiated, the pulsating flow persist if operating conditions were left unchanged. Mikol and Dudley were unable to characterize the nature of the instabilities further, however.

In an attempt to reach stable flow operation more consistently, Mikol and Dudley (1964) inserted a thin wire in their tubes in a fashion similar to Cooper, *et al.* (1957). Unlike Cooper, *et al.*, however, Mikol and Dudley did not find that the flash point moved smoothly as the inlet subcooling was changed. Instead, they found that once a stable flash point was initiated, it was quite stable until large changes in operating conditions were imposed. Once the vaporization point

was unseated by increased changes in operating conditions, an unstable flow pattern appeared. Further changes in conditions eventually led to the emergence of a new vaporization site.

Mikol and Dudley sought to correlate the length of flashing delay with a cavitation index σ_i defined as

$$\sigma_i = \frac{P_{static} - P_{vapor}}{\frac{\rho u^2}{2g_c}} . \qquad (2.4)$$

They report much scatter in the data, with only data for the copper tube showing an obvious trend. Visual observations indicated that the cavitation index increased as velocity increased. Plots of cavitation index versus velocity for the copper tube confirm this trend, despite the velocity term in the denominator. Mikol and Dudley attribute the large scatter in their data to the fact that inception of vaporization is not a continuous function of the parameters used in their plots, namely velocity, Reynolds Number, and Weber Number. They also report the findings of other investigators who reached a similar conclusion: vaporization inception is not a continuous function of any known parameter. This manifests itself in the observation that the inception point changed from test run to test run and that it moves in discrete jumps rather than smoothly along the tube.

Erth (1970) studied the data of Bolstad and Jordan (1948) and Mikol (1963) as well as Whirlpool proprietary data taken by Battelle Memorial Institute in 1960. No detailed information concerning the Whirlpool data was given. The data of Mikol showed a metastable region for every run, however neither the data of Bolstad nor Battelle indicated the existence of a metastable region. Erth quotes a private communication from Mikol in which he stated that the pressure taps served as the initiation site for vaporization in his glass tube and that he believed the same was true for his copper tube. Considering this information, Erth deduced that the metastable region was an "anomaly" and did not consider it in his model.

Scott (1976) measured the wall temperature profile for adiabatic capillary tube flow. He did not take pressure measurements along the tube to avoid the situation described by Mikol wherein the pressure taps served as nucleation sites. Scott's data exhibit a metastable region. Scott also observed preferential initiation sites. Consistent with the observations of Mikol, Scott found that the flash point did not move in the tube despite minor changes in operating conditions. Scott presented an example from his data in which the flash point was initially located 20 in. from the inlet. Inlet pressure was increased until the flash point jumped to 60 in. from the inlet. Inlet pressure was then dropped to below the initial value before flash point returned to the original position 20 in. from the inlet. Flow between the two stable operating points was observed to be erratic. Figure 2.3 from Scott is an example of the thermocouple readings from this test. Scott

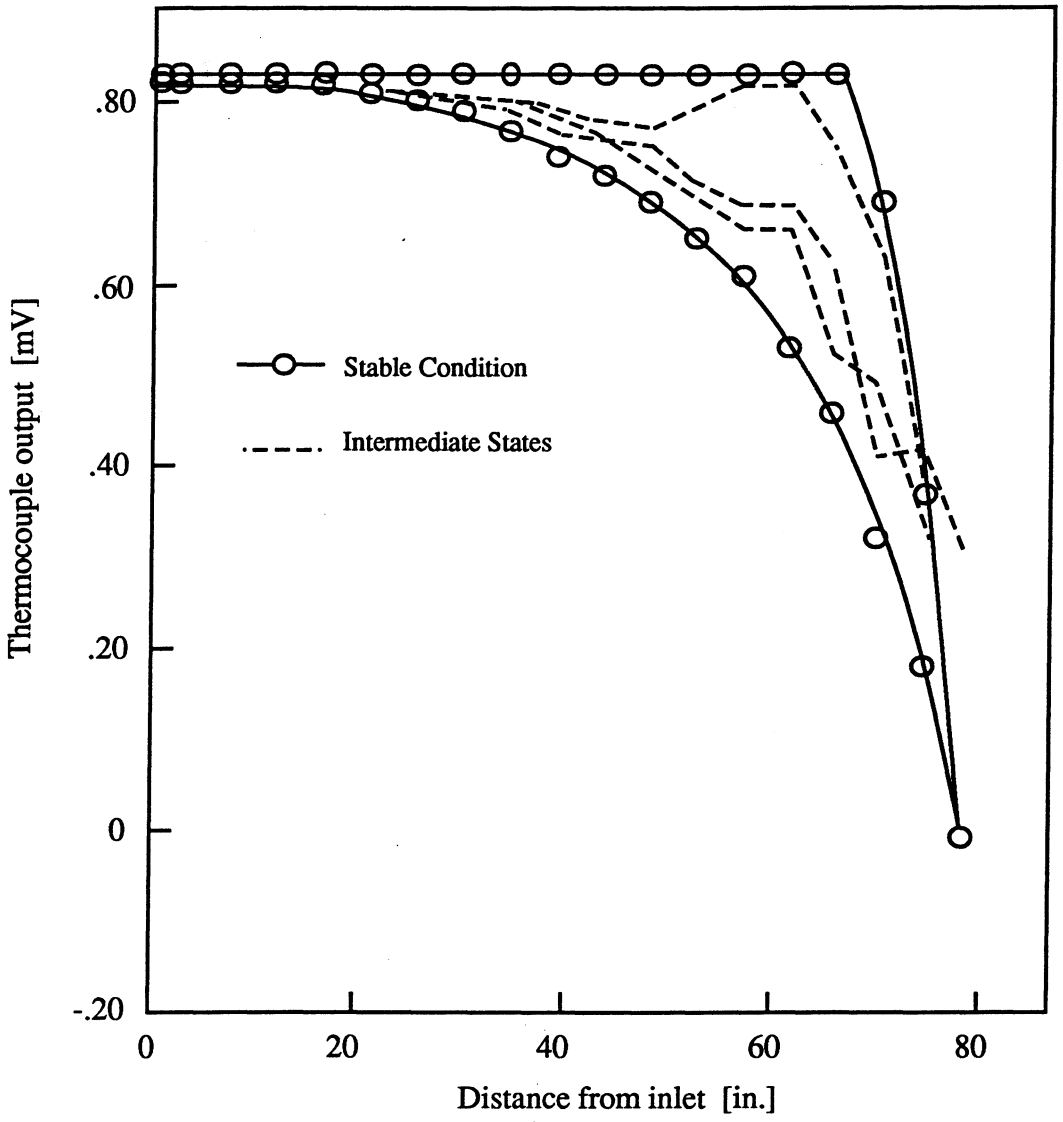

Figure 2.3 Output from thermocouples located along a capillary during steady flow conditions (solid lines) and unsteady flow conditions (dashed lines) from Scott.

concluded that the pressure taps made by Bolstad, Battelle (under contract with Whirlpool), and Mikol altered the flow pattern from the actual patterns found in normal operation, and thus considered the data unreliable.

Having determined that the metastable region must be considered in a model of capillary tubes, Scott sought to formulate a model of this section of the flow. Scott argued that nonequilibrium effects need to be considered, and that in order to model this, a semi-empirical approach is required. Scott assumed that within the delay length, bubbles were formed and destroyed. The flash point corresponded to the point where the formed bubbles were of some critical radius, at which time they would no longer be destroyed but would continue to grow.

Scott then attempted to develop a semi-empirical model derived from the momentum equation for the initial stage of bubble growth. The delay length was equated with the time elapsed before rapid bubble growth begins. Scott nondimensionalized this equation, creating a dimensionless delay length as a function of the initial disturbance to the equilibrium bubble.

Koizumi and Yokoyama (1980), in addition to their visualization study, instrumented an adiabatic copper capillary tube for pressure and temperature measurements along the tube. Their data show a metastable region in agreement with the literature published in the last 10 years. They summarize their results in terms of two parameters; the superheated liquid length and the delay of vaporization, which is the difference between the measured fluid temperature at vaporization and the saturation temperature at the measured pressure at vaporization, symbolically written as

$$\text{Delay} = T_{observed} - T_{sat}(P_{observed}). \qquad (2.5)$$

During the tests, they observed that both an increase in flow rate and a decrease in internal diameter decreased the superheated liquid length and increased the delay of vaporization.

Koizumi and Yokoyama state that the reliability of their capillary-tube sizing model depends on the accuracy of the estimated superheated liquid length. Over the range of their experiments, the mean superheated liquid length was 39 cm with a relatively large mean error of ± 14 cm. No analytical means of determining superheated liquid length is provided, however. Using their experimental data to determine the superheated liquid length inherently introduces significant error to their model.

Kuijpers and Janssen (1990) developed a theoretical model for refrigerant flow in capillary tubes that included thermal nonequilibrium effects; they then took experimental data to validate their model. Their model predicted flow rates for a given capillary tube that averaged 5% less than the measured values, with a maximum deviation of 10% less than observed values. They attribute the discrepancy to the existence of the metastable region. To account for this discrepancy, Kuijpers and Janssen sought to correlate the delay of vaporization with inlet temperature at various amounts of subcooling. The results are less than encouraging, as shown in Figure 2.4 from Kuijpers and

Janssen. Unsatisfied, they then attempted to correlate the underpressure at vaporization with a constant static underpressure and turbulent pressure fluctuation, following the work of Jones (1980).

Jones (1980) attempted to characterize decompressive flashing inception based on initial temperature, decompression rate, and amount of liquid turbulence. Based on the limited amount of data available, Jones states that boiling inception models for static liquids had two shortcomings in modeling flowing liquids. First, static liquid models for the inception of vaporization tend to predict lower vapor content in two-phase flows than do equilibrium models. Second, static liquid models predict increasing superheat, or underpressure, at vaporization with increasing expansion rate. This trend correctly predicts homogeneous nucleation behavior, but it conflicts with the data presented by Jones for flowing liquids.

The data of Scott show further evidence that static liquid boiling models do not adequately predict flashing delay in flowing fluids. Figure 2.5 shows a plot of underpressure versus expansion rate from Scott's (1976) data. The temperature and pressure profiles from the Scott (1976) data were used to determine the underpressure and expansion rate. There is considerable scatter in the data, and no trend is discernible. Flashing delay is plotted against expansion rate in Figure 2.6. As expansion rate increases, the flashing delay approaches zero. Typical values for the expansion rate in capillary tubes are approximately 0.5 to 2 psia/in. At this expansion rate there is considerable scatter in the delay of flashing data. Flashing delay is plotted against underpressure in Figure 2.7. Again, there is considerable scatter in the data. From the Scott data, it is clear that static liquid boiling models are inadequate for predicting the delay in vaporization in flowing liquids. Jones (1980) attributes the discrepancy to the turbulent pressure fluctuations in flowing liquids.

On this basis, Jones combined the effects from static flashing over expansion and turbulent pressure fluctuation. Turbulent pressure fluctuations increase with mass flux, and the amplitude of these fluctuations add to or subtract from the static pressure in the fluid to give the net pressure. The minimum underpressure in the liquid at vaporization can be written as

$$\Delta P = \Delta P_o - \mathrm{Max}|P'|, \qquad (2.6)$$

where P' is the turbulent pressure fluctuation. Assuming pressure fluctuation coincides with kinetic energy fluctuation, Jones rewrote Equation 2.6 as

$$\Delta P = \Delta P_o - 27\frac{u'^2}{u^2}\frac{G^2}{2\rho_\ell} . \qquad (2.7)$$

In this manner, it is assumed that the minimum pressure in the liquid exists long enough for a vapor bubble to be generated and grow. This model correlated well with the data presented by Jones.

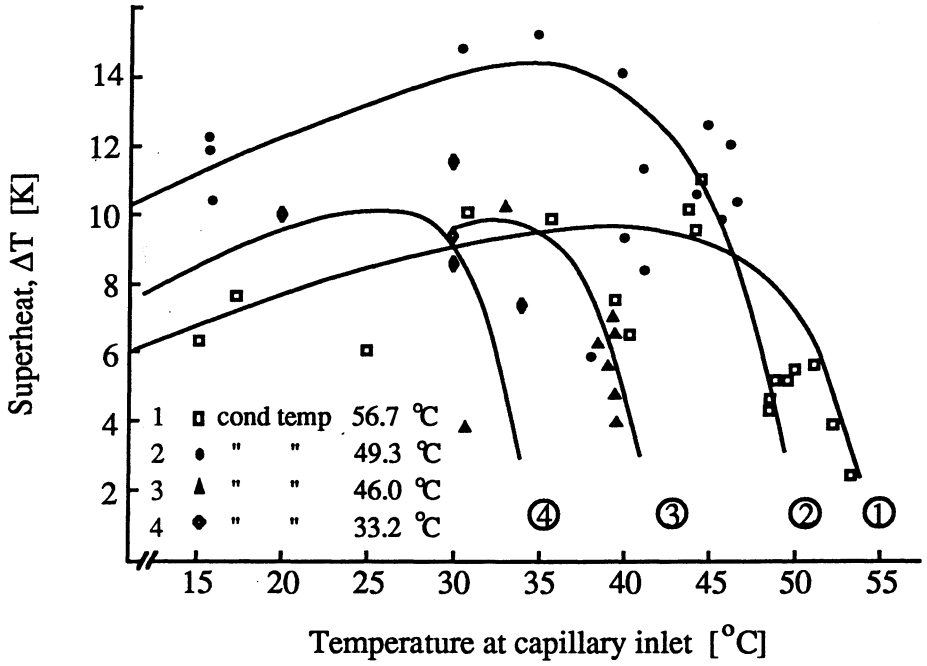

Figure 2.4 Attempt by Kuijpers and Janssen to correlate the delay of flashing to inlet temperature.

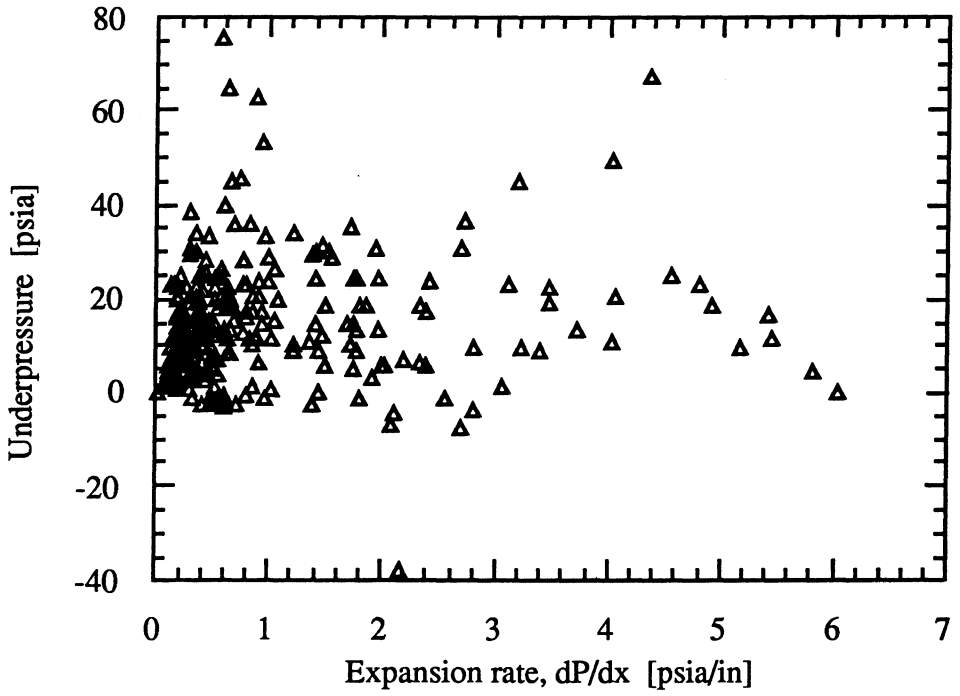

Figure 2.5 Underpressure at the point of vaporization versus expansion rate from Scott.

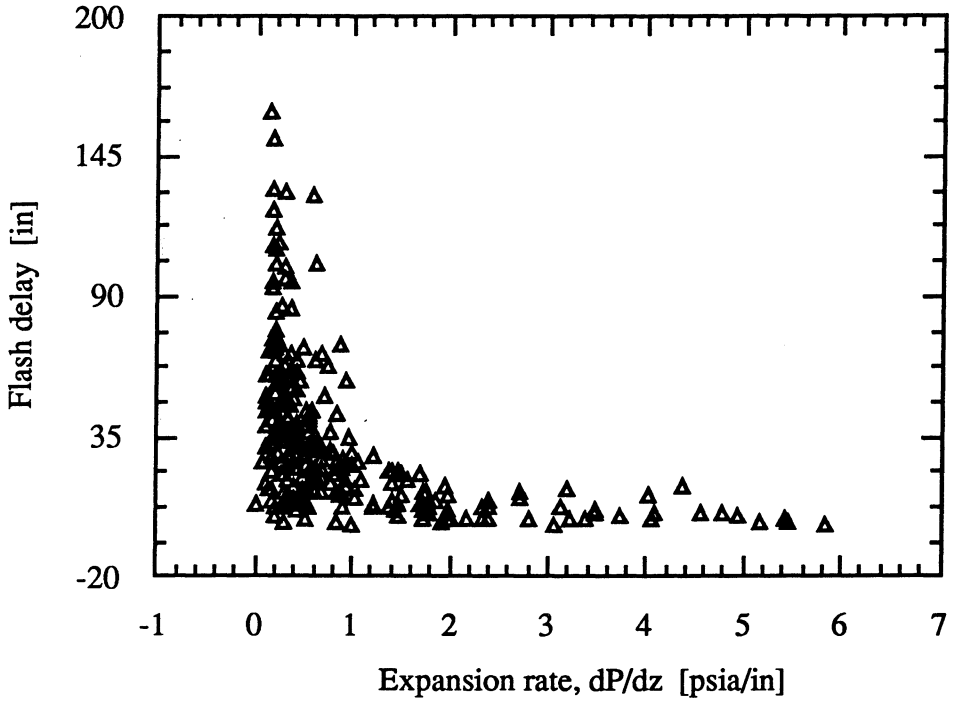

Figure 2.6 Length of metastable region versus expansion rate from Scott

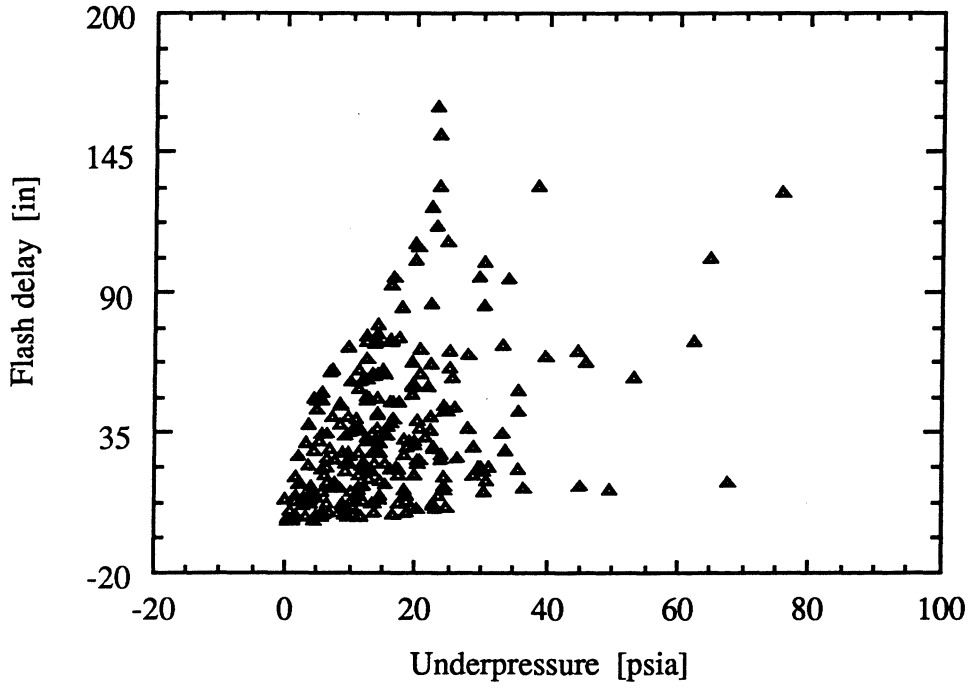

Figure 2.7 Length of metastable region versus underpressure at the point of vaporization from Scott.

Figure 2.8 shows a comparison of Equation 2.7 with the data of Kuijpers and Janssen. The error band is for 20% uncertainty in static underpressure. The correlation captures the trend in their data that underpressure does tend to decrease at the higher mass fluxes. Figure 2.9 is a plot of data from Scott (1976) showing underpressure as a function of mass flux squared. A trend in Scott's data is difficult to find. If a trend does exist, it appears that undershoot increases at lower mass fluxes, reaches a maximum, then decreases at higher mass fluxes. A closer look at the data of Kuijpers and Janssen reveals that the same trend may be surmised from their data. However, no clear pattern exists in either data set. In addition, recall that Koizumi and Yokoyama observed that underpressure increased with increasing mass flux. It is clear that this type of correlation does not completely capture the flow phenomena.

Chen, *et al.* (1990) developed one of the first theoretically based models for predicting the level of underpressure present at the incepting of flashing. Starting with Equation 2.8, from classic nucleation theory, and an experimental parameter that accounts for tube roughness, flow turbulence, non-uniformity of nuclei formation, the distribution of the nuclei, and the impurity contained in the refrigerant, they used 238 data sets to determine the best values for the constants C, n_1, n_2, and n_3. The final correlation is Equation 2.9

$$r_c = \frac{2\sigma}{P_s - P_f}. \tag{2.8}$$

$$P_s - P_f = 0.679\left(\frac{\sigma^{3/2}}{\sqrt{kT_s}}\right)\left(\frac{v_g}{v_g - v_\ell}\right)Re^{0.914}\left(\frac{\Delta T_{sc}}{T_c}\right)^{-0.208}\left(\frac{D}{D'}\right)^{-3.18}, \tag{2.9}$$

where

$$D' = 10^4\sqrt{kT_s/\sigma}, \tag{2.10}$$

and k is the Boltzman constant. This effort resulted in predicting the underpressure of vaporization with a standard error of 26%. They claim the error is caused "mainly by the fluctuation and the contingency of the position of the inception of vaporization."

Recent literature for adiabatic capillary tube flow has given substantial support for the existence of the metastable region. Until details of the Battelle experiments are known, no explanation can be given as to why their data did not exhibit a delay in vaporization. The metastable phenomenon seems real and has been shown to have a significant impact on the prediction of mass flow rates.

The mechanics of this phenomenon are still not understood. Although one may draw analogies between boiling of static liquids and flashing of flowing fluids, the method of predicting boiling inception in static liquids has proven unsuccessful when modeling refrigerant flashing in a capillary tube. One may also logically argue that the effects of the flow field should affect flashing inception. Although models based on this premise have shown agreement with some data,

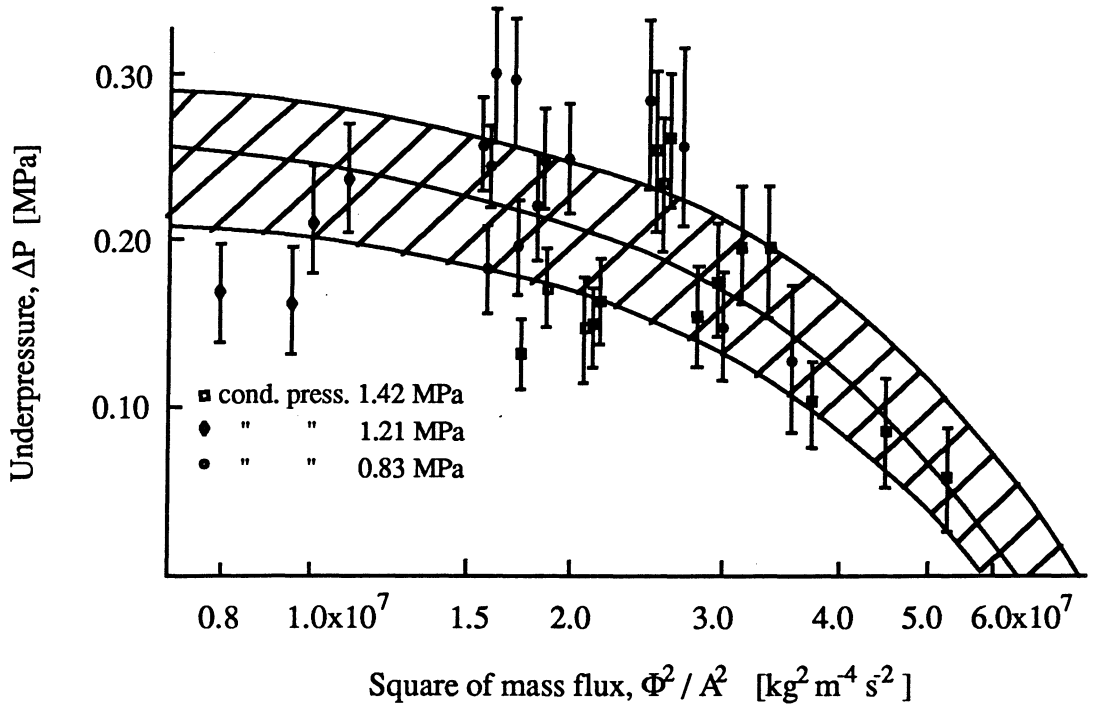

Figure 2.8 Comparison of Equation 3.7 with the data from Kuijpers and Janssen.

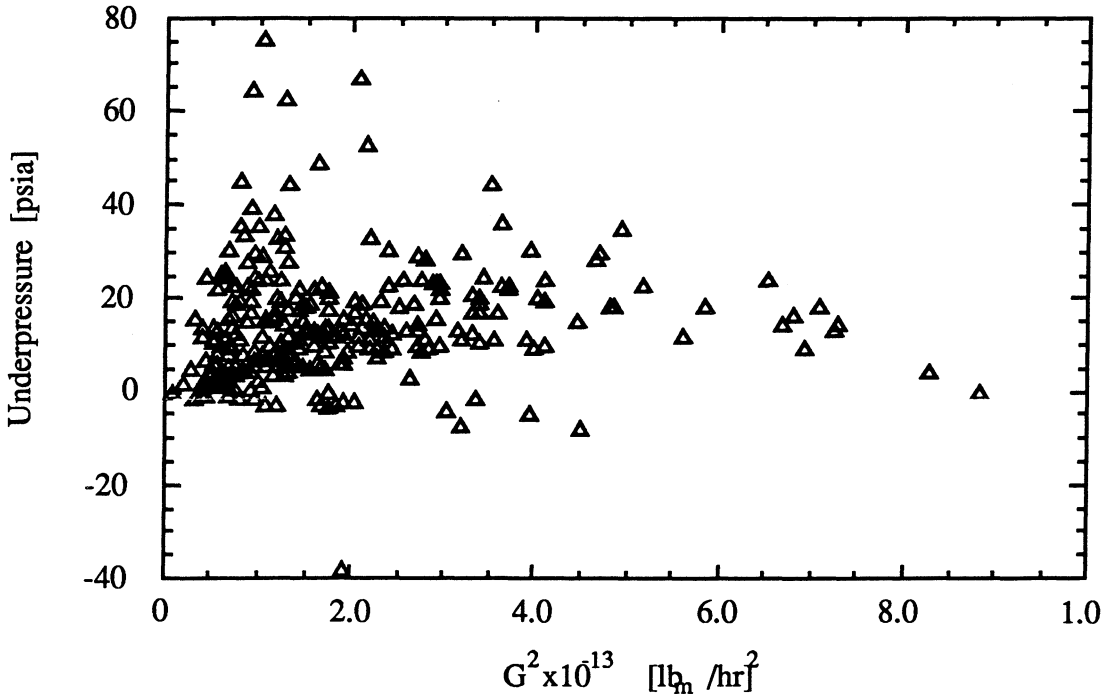

Figure 2.9 Underpressure at vaporization versus the square of the mass flux from Scott.

they also predict results which are completely contrary to other data. Clearly, more work focused on the physics of phase change in flowing fluids is needed to better understand the phenomena.

2.5 Two-phase Flow Modeling

Several two-phase flow models found in the literature were discussed by Wallis (1980, 1982). The models fall into two general categories: equilibrium and nonequilibrium. Equilibrium models assume the phases of the flow are in equilibrium, thus simplifying the modeling process. Nonequilibrium models attempt to account for interphase heat, mass, and momentum transfer, as well as multidimensional effects and flow-regime transitions.

Of the equilibrium models, the most straightforward is the homogeneous equilibrium model (HEM). This model assumes the equations describing a two-phase mixture can be reduced to a single set of equations describing a "pseudo-fluid" with appropriate properties. Included in this assumption is that the phases are in equilibrium with each other, have the same velocity, and are at the same temperature. This model does a good job of predicting the critical mass flux if the tube is long enough so that equilibrium is reached by the exit and if the flow pattern is such that relative motion between phases is minimized (Wallis 1980). The observations of temperature and pressure profiles which indicate equilibrium being reached in the later section of the capillary tube along with the typical "fog-like" flow observed exiting from capillary tubes (Mikol 1963) indicate both of these conditions are met.

Wallis groups the non-equilibrium models into three categories: i) completely empirical, ii) physically based models for thermal non-equilibrium, and iii) two-fluid models. Although some of the empirical models show strikingly good agreement with the data, their range of applicability is limited.

The thermal non-equilibrium models account for mass transfer between phases due to a temperature difference between the phases. These models typically rely on boiling theory to determine the rate of mass transfer. Some models consider bubble nucleation and vapor generation as the modes of mass transfer, yet still rely greatly on empirical correlations. These correlations are typically needed to determine the nucleation site densities and initial bubble number densities.

For two-fluid models separate conservation equations are written for each phase. The equations require auxiliary relations for interphase heat, mass, and momentum transfer. The key to this type of model is determining the interphase transfer relations. Two-fluid models show the most promise at the present time, but they are still in the developmental stages, and much work is needed before they can be widely applied with success.

A few investigators have attempted to model the two-phase portion of the flow in multiple sections, at least one of which is non-homogeneous. The motivation for this approach stems from an examination of the temperature profile along an adiabatic capillary tube. If a metastable region exists, the temperature drop associated with the inception of flashing is initially steeper than the

corresponding pressure drop. Shortly after flashing begins, the temperature and pressure profiles match, indicating that the refrigerant is once again in a saturated state. These regions are shown explicitly in Figure 2.10 and in the data of Figure 2.9. One obvious division of the two-phase flow is to model two sections, one thermal nonequilibrium section and one equilibrium section, which may or may not be considered homogeneous.

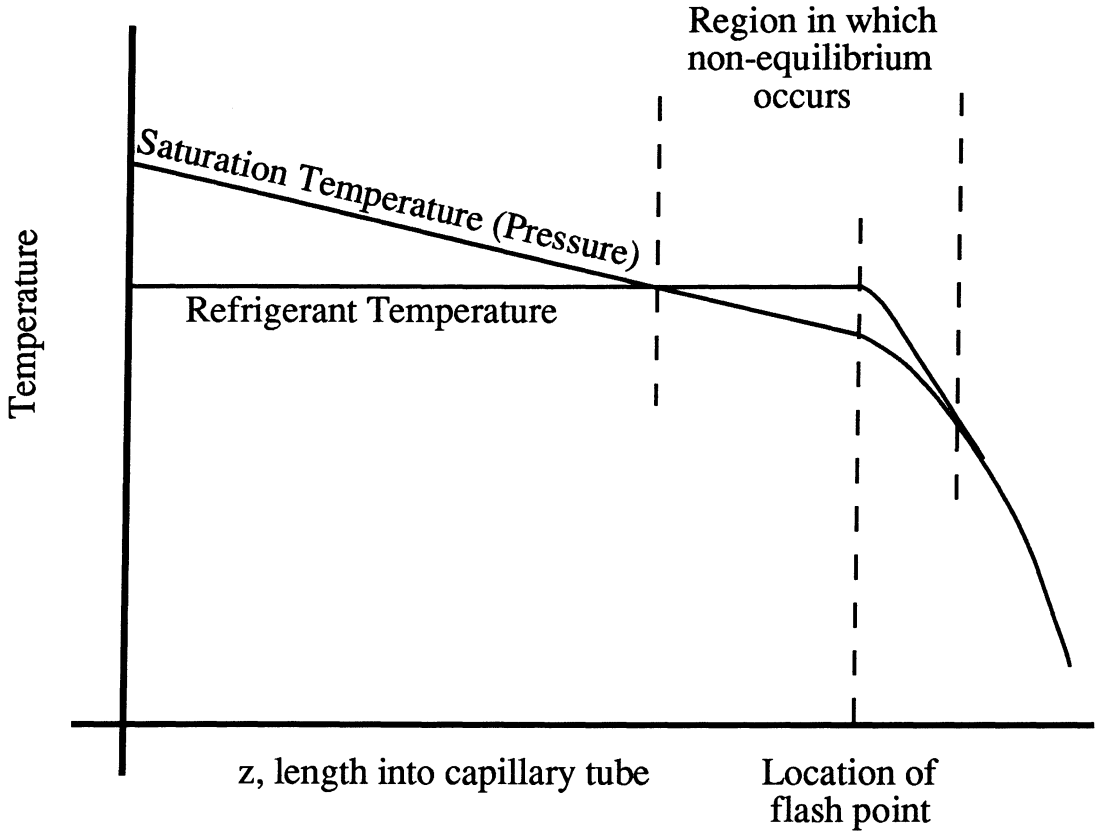

Figure 2.10 Typical temperature and pressure profile in an operating capillary tube with a metastable region

The thermal nonequilibrium model of Kuijpers and Janssen (1990) is a good example of a model that allows for a temperature difference between the phases. Initial conditions set the magnitude of this difference, which is then correlated with another flow variable, such as void fraction, as the flow proceeds. Kuijpers and Janssen selected a function of the form

$$\Delta T_{fi}'(\alpha) = (1-\alpha)^n \Delta T_{fi}, \qquad (2.11)$$

where ΔT_{fi} represents the delay of vaporization as defined by Koizumi and Yokoyama, α represents void fraction, and n is determined experimentally. Although the meaning of $\Delta T_{fi}'$ is not explicitly stated, it appears to be the derivative of ΔT_{fi} with respect to tube position. At some point

along the tube the calculated temperature difference is small enough that the two phases may be considered in equilibrium and a homogeneous flow model may be employed.

Scott (1976) presents a model based on the same premise: the two-phase flow is initially in a non-equilibrium state, determined by the temperature difference between the liquid and vapor phases. The calculated difference vanishes at some point along the tube; then a different model is used to describe the flow. Scott assumed that the two-phase flow was governed by the growth of vapor bubbles. In order to simplify the governing equations, Scott introduced the following additional assumptions: 1) once initialized, the bubble growth is controlled by thermal effects, 2) pressure in both phases is the same, 3) the quality remains small, 4) fluid properties remain constant. Scott only presented the model, as implementation of the model into computer code was beyond the scope of his thesis. The accuracy of this model is therefore unknown.

Li, et al. (1990) provided for the mass transfer between liquid and vapor due to thermal non-equilibrium. The mass transfer was assumed to be proportional to the latent heat of vaporization and took the form

$$\dot{m} = \frac{k_\ell (T_\ell - T_s) S}{h_{fg} Le}, \qquad (2.12)$$

where k_ℓ is the thermal conductivity of the liquid, T_ℓ and T_s are the liquid temperature and saturation temperature, respectively, S is the surface area per unit volume between the liquid and vapor phases, h_{fg} is the latent heat of vaporization, and Le is an apparent length of heat transfer characterizing the thermal boundary layer over which the liquid temperature changes from T_ℓ to T_s. The values of S and Le are dependent on the flow regime.

Based on the observations of Mikol and Dudley (1964), Li, et al (1990). assumed two flow regimes to exist. First, a bubble flow pattern was assumed for void fractions up to 0.3. Mist annular flow was then assumed to exist for the remaining section of tube. The initial total surface area between the phases is defined as the surface area of a single bubble of some critical radius times the number of bubbles per unit volume generated at the vaporization point. This approach is commonly found in the two-phase flow literature for nuclear power applications.

The initial size of the bubble is taken to be a critical radius defined by surface tension as

$$r_c = \frac{2\sigma}{P_s - P_f}, \qquad (2.13)$$

where the initial pressure difference $P_s - P_f$ is given from the correlation of Chen, et al. (1990). The number of bubbles per unit volume is also given by a correlation of Chen, et al. The apparent

length, Le, is determined by a relation from Hirt (1979). For the mist annular flow regime, Li, et al. (1990) expresses the interfacial surface area as

$$S = \frac{4\alpha}{D}, \tag{2.14}$$

where D is the capillary-tube internal diameter, and α is the void fraction. The apparent length is expressed as

$$Le = \frac{c}{\alpha}, \tag{2.15}$$

where c is determined from experimental data.

Comparisons of the predicted temperature and pressure profiles against their experimental data are shown in Figures 2.11a-d from Li, et al (1990). The agreement appears encouraging. The prediction of the vaporization point and non-equilibrium section of the two-phase flow show the trends of the data. Figure 2.12 shows void fraction development along the tube length for the cases shown in Figure 2.11a-d. By comparing Figures 2.11a-d and 2.12, one can see the how the temperature difference between the phases and the rate of vaporization of liquid are related. At the flash point, the rate of vaporization is quite high, due to the relatively high temperature difference between the phases and large interfacial surface area. As the temperatures of the two phases become nearly equal, the rate of void fraction development decreases to an almost constant value. This result makes sense intuitively, since one expects the rate of vaporization, and thus void fraction, to decrease as the driving potential, which is the temperature difference between phases, decreases.

The methods for modeling two-phase flow are widely varied. The success of a given method depends upon, among other things, the agreement between the actual and predicted flow regimes. Homogeneous flow models offer an attractive simplicity, yet they are also restrictive in the types of flows that can be accurately represented. Two-fluid models are more complicated in nature and are correspondingly more difficult to implement. The treatment of the phase interaction is of paramount importance. However, they do reduce to the homogeneous model in limiting cases.

Separate phase models also show better agreement with the experimental data, and considering the experimental observations from visualization studies, they seem best suited for modeling capillary tube flow.

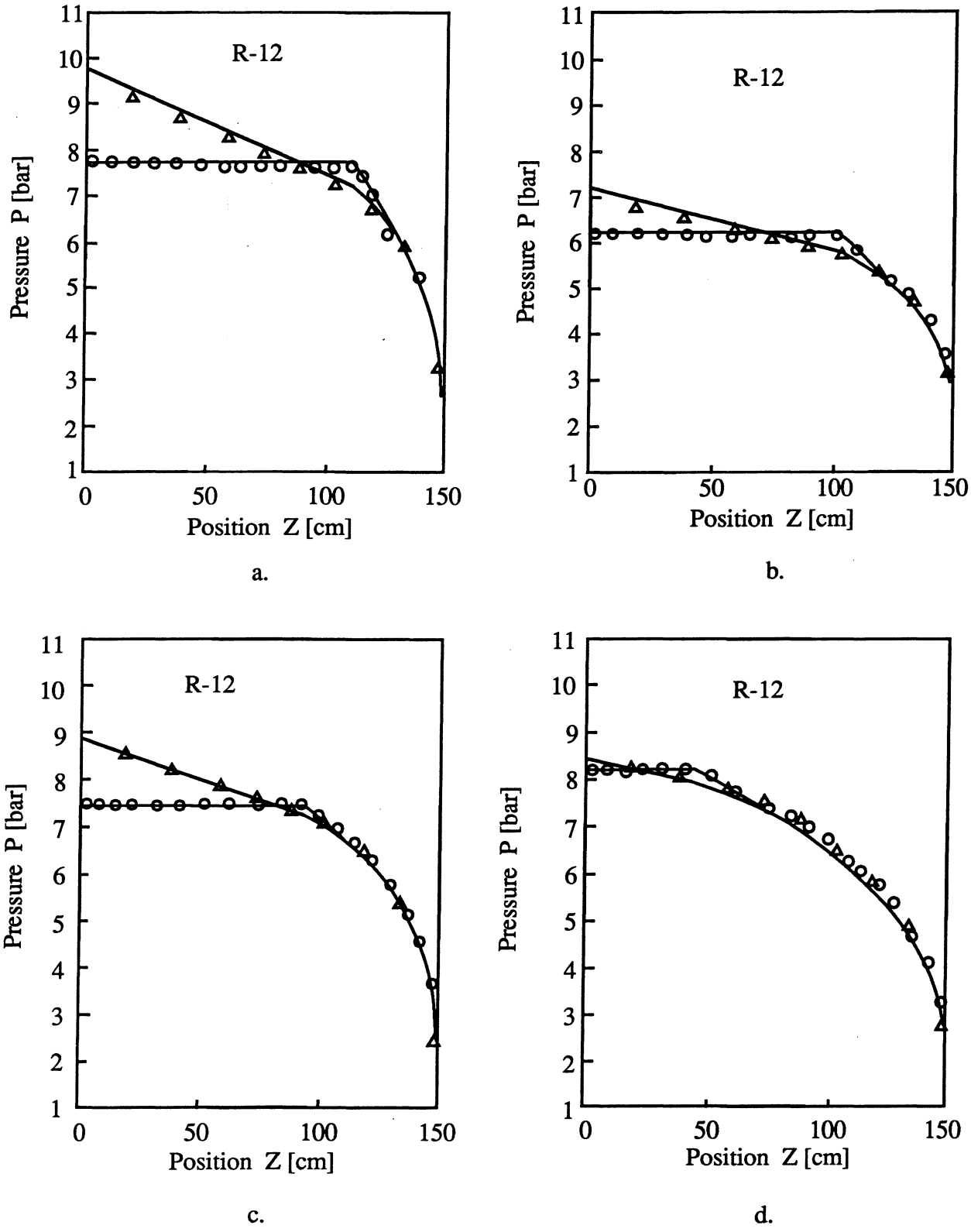

Figure 2.11 Predicted and experimental temperature and pressure profiles from Li.

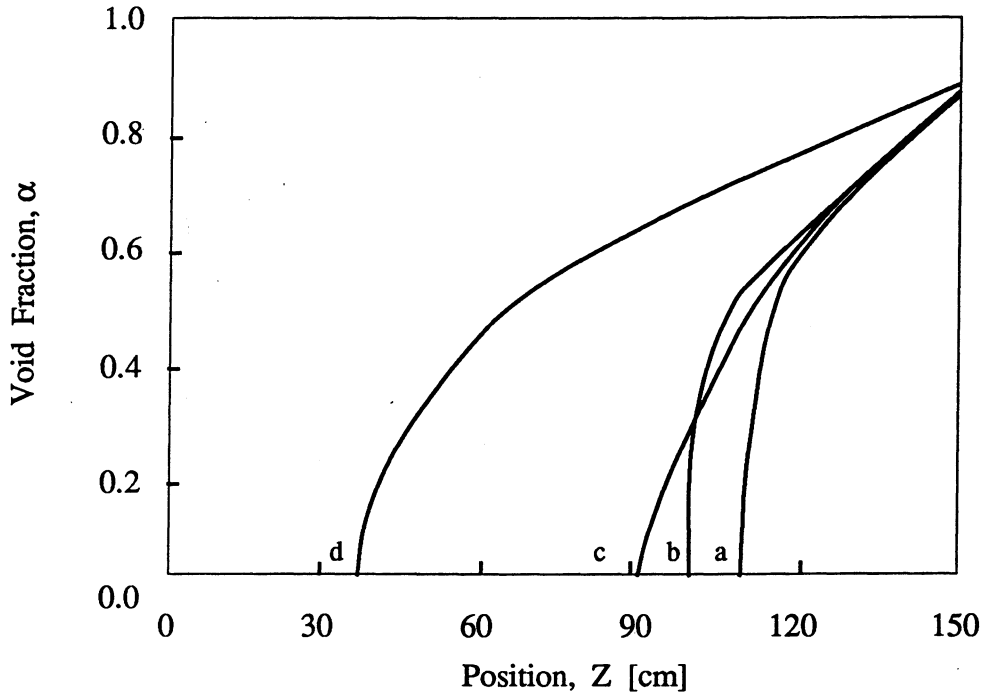

Figure 2.12 Variation in void fraction along a capillary tube. The curves a-d correspond to the conditions represented in Figure 3.11 a-d.

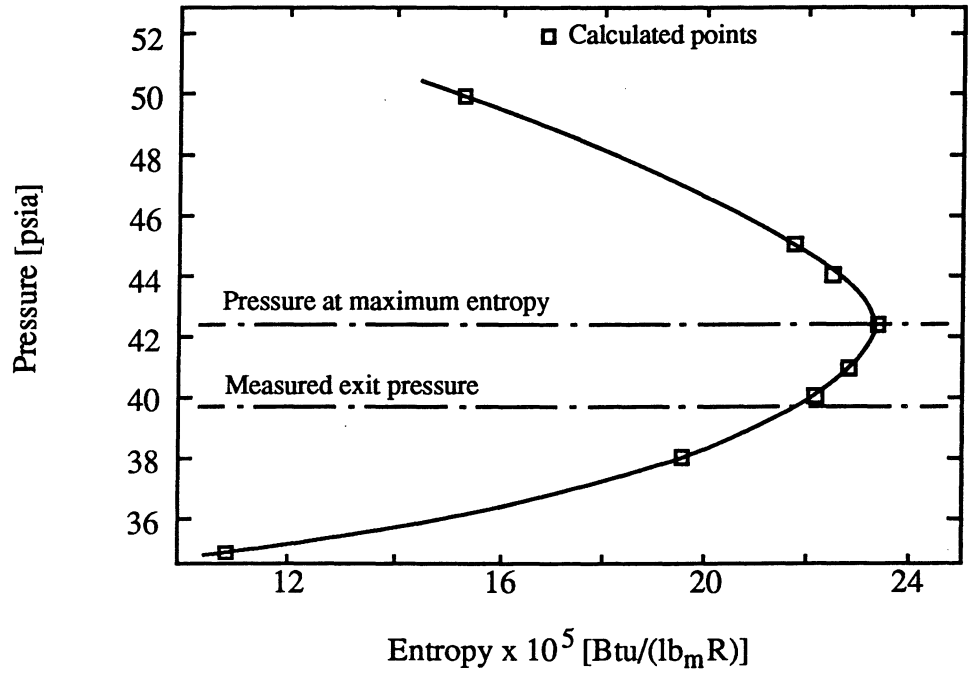

Figure 2.13 Fanno plot calculated for the measured flow rate abd the actual flash point from a data run of Mikol from Mikol.

2.6 Exit Conditions

Gases that flow in piping systems from an upstream reservoir at relatively high pressure to a downstream receiver at a lower pressure can reach critical conditions, whereby further reduction of the downstream receiver pressure does not further increase the mass flow rate. The gas velocity at the exit of the piping system is the sonic velocity; thus the "information" of the pressure drop cannot be "communicated" upstream. In analyzing this type of flow, the gas at the exit is considered to be at thermodynamic equilibrium. The presence of two phases in the flow stream complicates the physics; the phases may not reach thermodynamic equilibrium by the time they enter the exit plane. Thus, one may expect treatment of two-phase flows under critical conditions to be different from that of a single-phase flow analysis.

To date, the thrust of investigation into the phenomena of critical two-phase flow has come from the nuclear industry, where reactor safety under extraordinary conditions is of paramount importance. Since the nuclear industry has been the major driving force in two-phase flow research, there has been little emphasis on the use of fluids other than water as the working fluid. Relatively little work in critical two-phase flows has been done with refrigerants. A review of the common critical flow models found in the nuclear literature will give background information and insight into the phenomena peculiar to two-phase critical flows.

The homogeneous models are derived from an expression for pressure drop via a one-dimensional steady-state analysis which typically takes the form shown by Wallis (1969) as

$$-\frac{dP}{dz}=\frac{C_f+C_x\frac{dx}{dz}+C_a\frac{1}{A}\frac{dA}{dz}+C_g g\cos\theta}{1-M^2}, \qquad (2.16)$$

where the coefficients C_f, C_x, C_a, and C_g determine the relative importance of friction, phase change, area change, and gravity, respectively, on pressure drop. The M^2 term in the denominator serves the same function as does the square of the Mach Number in a single-phase flow analysis. Thus, the resulting relation for M^2 from any one-dimensional derivation can be solved for an equivalent sonic velocity. A "choked" flow condition can be defined when the average velocity across the tube exit is equal to the sonic velocity. The exact form of the M^2 term depends on the state variables used in the derivation.

Equilibrium models can be grouped further by the types of limiting assumptions made to avoid accounting for nonequilibrium effects. The Homogeneous Equilibrium Model (HEM) is an extension of the homogeneous two-phase flow model, and assumes the two phases are in complete equilibrium, i. e., equal pressures, temperatures, and velocities. In this way, the fluid acts as a single-phase fluid with properties equal to some average of the properties of the two phases. The HEM analysis is the simplest of the models and is the one most often cited in the literature.

Other equilibrium models include the Frozen Model, in which the time scale is so short that there is essentially no time for phase change to take place. Quality, then, is considered constant throughout the expansion process.

Slip flow models assume quality is known *a priori*, such as from the Frozen Model. The velocity ratio can then be treated as an unknown, and the conservation equations solved for the value of the velocity ratio for which mass flow is a maximum. Slip flow models tend to predict higher critical mass flow rates than the HEM.

If the fluid is in a flow regime that may be approximated by a homogeneous fluid, this model should give adequate results. However, if the piping system is such that the phases cannot reach equilibrium, as with short pipes, or such that the primary flow regime allows for significantly different phase velocities, as with annular flow, use of a model other than the HEM should be considered.

A few investigators have studied the exit conditions of capillary-tube flow. Mikol (1963) studied the phenomena occurring at the exit of a capillary tube in two ways. First, he developed a model for the exit conditions of two-phase refrigerant by calculating a Fanno flow line using quality weighted properties of the refrigerant. Measured values of pressure at the capillary-tube exit can be plotted on the calculated Fanno line and compared with the minimum pressure given by maximum entropy for the calculated Fanno line. Figure 2.13 shows one such comparison. The measured pressure is shown to be less than the calculated minimum pressure, which is physically impossible. Mikol notes that other investigators had observed similar results. The discrepancy was stated to be a result of two-dimensional effects occurring in the real flow that were not accounted for in the one-dimensional analysis.

Mikol's second approach was based on a homogeneous two-phase flow. The speed of sound can then be calculated from the equivalent single-phase flow relationship

$$c = \sqrt{\left(\frac{\partial P}{\partial \rho}\right)_s}. \qquad (2.17)$$

The average velocity at the exit is calculated and compared with the calculated speed of sound. The observed exit pressure is also compared to the calculated exit pressure using the Fanno line. Mikol grouped the data into three categories for discussion. The first group, summarized in Table 2.2, from Mikol, shows the observed exit pressure to be higher than the calculated critical exit pressure. For each of these cases, the calculated exit velocity is less than the calculated speed of sound. This result agrees with the classic compressible flow theory. Further supporting this conclusion is the magnitude of the pressure drop at the exit of the tube ΔP_{exit}. For each of the cases presented in Table 2.2, both observed and calculated ΔP_{exit} are less than 3 psi, which is of the order one would expect for subsonic flow.

Table 2.3 shows the experimental data for which ΔP_{exit} is greater than 3 psi but less than 11 psi. These pressure drops are considered large enough to indicate significant pressure drop over and above any experimental error. Mikol concluded that this magnitude of pressure drop was representative of what one could expect for sonic flow. For these cases, the observed and calculated exit pressures are approximately equal, as are the observed exit velocity and calculated speed of sound. Again the results agree with the trends for classical compressible fluid flow theory for choked flow.

Table 2.2 Comparison of calculated and measured exit plane properties for the adiabatic flow of Refrigerant 12 under non-choked flow conditions (Tube: Copper 0.0555-in. ID × 6.0 ft long), adapted from Mikol (1963).

			Pressure Comparisons		Velocity Comparisons			
Run No.	Flash point Temp	Mass Flow Rate	Exit Plane Press. (Pexit) observed	Exit Plane Press. (1) (Pexit) Fanno	Exit Velocity (observed) (2)	Speed of Sound (3)	ΔPexit observed	ΔPexit Fanno (4)
	F	lb_m/hr	psia	psia	ft/s	ft/s	psi	psi
14	81.5	56.16	50.4	48	121	129	3.1	(5)
15	81.5	55.44	51.3	46	115	127	2.5	(5)
18	85.3	51.84	54.1	45	105	130	1.4	(5)
19	85.8	51.84	52.4	45	111	133	1.9	(5)
29	119.0	67.68	73.8	64	147	158	1.3	(5)
30	117.6	67.68	76.3	64	136	162	1.1	(5)
36	124.6	63.00	68.3	62	170	188	2.4	(5)
37	125.2	61.56	70.0	60	161	186	1.6	(5)
38	126.5	59.04	76.7	58	136	180	0.1	(5)
39	126.5	59.40	80.1	58	127	175	0.3	(5)

(1) Corresponds to point of maximum entropy on Fanno line for the measure mass flow rate and flash point temperature.

(2) "Observed" only in the sense that the calculation of exit velocity uses the measured mass flow rate and measured exit plane pressure, but it uses the assumption of equilibrium, one-dimensional adiabatic flow to calculate exit quality and exit velocity.

(3) Speed of sound determined from a finite difference approximation to $c^2=(\partial P/\partial \rho)_S$ for the temperature and quality at the exit plane.

(4) $\Delta P_{exit\ Fanno} = (P_{exit\ Fanno}-P_{back})$.

(5) These values would be negative and lack significance in this case.

Table 2.3 Comparison of calculated and measured exit plane properties for the adiabatic flow of Refrigerant 12 under choked flow conditions. (Tube: Copper 0.0555-in. ID × 6.0 ft long), adapted from Mikol (1963).

			Pressure Comparisons		Velocity Comparisons			
Run No.	Flash point Temp	Mass Flow Rate	Exit Plane Press. (Pexit) observed	Exit Plane Press. (1) (Pexit) Fanno	Exit Velocity (observed) (2)	Speed of Sound (3)	ΔPexit observed	ΔPexit Fanno (4)
	F	lb_m/hr	psia	psia	ft/s	ft/s	psi	psi
10	90.5	47.16	41	42	173	168	5.0	6.2
11	90.1	47.88	40	42	182	170	7.4	9.7
12	82.2	55.44	46	46	141	139	4.4	4.0
16	85.9	51.84	43	45	159	154	8.2	9.8
17	86.0	51.84	44	45	153	151	10.1	10.7
27	117.0	73.44	65	69	175	173	4.0	-0.1

(1) Corresponds to point of maximum entropy on Fanno line for the measure mass flow rate and flash point temperature.

(2) "Observed" only in the sense that the calculation of exit velocity uses the measured mass flow rate and measured exit plane pressure, but it uses the assumption of equilibrium, one-dimensional adiabatic flow to calculate exit quality and exit velocity.

(3) Speed of sound determined from a finite difference approximation to $c^2=(\partial P/\partial \rho)_s$ for the temperature and quality at the exit plane.

(4) $\Delta P_{exit\ Fanno} = (P_{exit\ Fanno}-P_{back})$.

Table 2.4 shows observed and calculated pressure drops at the tube exit greater than 13 psi. One would expect, from compressible ideal gas theory, that the greater reduction of back pressure would have no effect on flow conditions. However, note that the observed values of ΔP_{exit} are much less than the calculated values of ΔP_{exit}. The observed values of the exit pressure are also much less than the values of calculated exit pressure. The exit velocity is correspondingly higher than the calculated speed of sound. The one-dimensional ideal gas approach appears to have broken down. Mikol pointed to earlier investigators who have attributed similar results, at least in part, to the actual two-dimensional nature of the flow at the exit. If the experimental results of Mikol are valid, then a more sophisticated model than a homogeneous one-dimensional flow model is required to capture the physics governing the flow.

Table 2.4 Comparison of calculated and measured exit plane properties for the adiabatic flow of Refrigerant 12 under choked flow conditions, but with large pressure drop from tube exit to back pressure region. (Tube: Copper 0.0555-in. ID × 72.0 in. long), adapted from Mikol (1963).

			Pressure Comparisons		Velocity Comparisons			
Run No.	Flash point Temp	Mass Flow Rate	Exit Plane Press. (Pexit) observed	Exit Plane Press. (1) (Pexit) Fanno	Exit Velocity (observed) (2)	Speed of Sound (3)	ΔPexit observed	ΔPexit Fanno (4)
	F	lb_m/hr	psia	psia	ft/s	ft/s	psi	psi
24	110.2	76.68	61	69	200	170	17.0	25.0
25	114.5	74.16	61	69	209	179	13.5	21.9
26	116.2	72.72	57	69	231	188	21.7	33.7
33	118.5	67.68	57	64	220	192	14.6	21.2
34	122.8	63.00	55	62	230	204	14.9	21.8
35	125.7	66.24	55	64	254	210	15.2	24.6

(1) Corresponds to point of maximum entropy on Fanno line for the measure mass flow rate and flash point temperature.

(2) "Observed" only in the sense that the calculation of exit velocity uses the measured mass flow rate and measured exit plane pressure, but it uses the assumption of equilibrium, one-dimensional adiabatic flow to calculate exit quality and exit velocity.

(3) Speed of sound determined from a finite difference approximation to $c^2=(\partial P/\partial \rho)_s$ for the temperature and quality at the exit plane.

(4) $\Delta P_{exit\ Fanno} = (P_{exit\ Fanno}-P_{back})$.

Pate and Tree (1987) considered several critical flow models for inclusion in his capillary-tube model. He compared a total of nine models which he divided into three categories: homogeneous equilibrium models (HEM), homogeneous frozen models (HFM), and nonhomogeneous models. From the HEM group, Pate considered an isentropic and isenthalpic model from Lahey and Moody (1977), and a model from Smith (1963). He compared HFM from Smith (1963), Semenov and Kosterin (1964), and Wallis (1969). He also examined nonhomogeneous models from Fauske (1962), Levy (1964), and Moody (1968).

Before comparing models, Pate plotted mass flow rate versus downstream reservoir pressure for three upstream pressures. This is shown in Figure 2.14 from Pate. Note that although mass flow rates tend to level off at low reservoir pressures, it never reaches a constant value. Instead it continues to rise slightly. This is consistent with the data of Mikol, and further indicates that refrigerant flow does not completely choke in the classical sense. Pate states that the isenthalpic model of Smith varied only 4% from the isentropic model, and therefore only showed results from the isentropic model. Figures 2.15a and 2.15b show how the various models predict critical mass

flow rate for various exit qualities. Although Pate's data lie closest to the isentropic HEM prediction, the data are too few to show any trends, and conclusions drawn must be evaluated accordingly.

The concept of a "choked" condition existing in a two-phase flow is predicated on the assumption that the flow is homogeneous. The further the characteristics of the flow are from homogeneous, the less well defined the concept of speed of sound and critical mass flow become. Indications from experimental data show that there is a pseudo "critical" back pressure, at which point further reduction in back pressure has little effect on flow rate. However, there is little conclusive evidence that shows a true "critical flow condition" exists for capillary-tube flow. In this light, homogeneous flow models should be taken only as first approximations. Still, nonhomogeneous models have not shown significantly better results.

2.7 Experimental Data

The vast majority of researchers publishing articles on the various aspects of capillary-tube flow modeling used their own experimental data to develop correlations and validate their work. The actual amount of published data available to the public is, however, relatively small. Major contributors to this data base include Scott (1976), Bolstad and Jordan (1948), DuPont, (Technical Bulletin RT-31F, published to aid in capillary-tube applications), Whitesel (1957), Mikol (1963), Mikol and Dudley (1964), Battelle, (under contract with Whirlpool and reprinted by Scott (1976)), and Pate (1982). The data of Bolstad have been considered suspect by Erth (1970) and Scott (1976) since it does not exhibit a metastable region. Over half of Scott's data are for tubes of internal diameter larger than that used in household refrigerators. Since surface tension effects are not significant for internal tube diameters greater than those found in household refrigerators, that data may not be considered suitable for validation for the model presented in this report.

Clearly, there are many aspects of capillary tube flow which remain a mystery. Even though this is the case, methods for predicting capillary tube performance for the more complicated case of refrigerant mixtures, including possibly zeotropes, is going to be in strong demand in the very near future. It is hoped that the discoveries and insights offered by this work will help develop a better fundamental understanding of capillary tube flow.

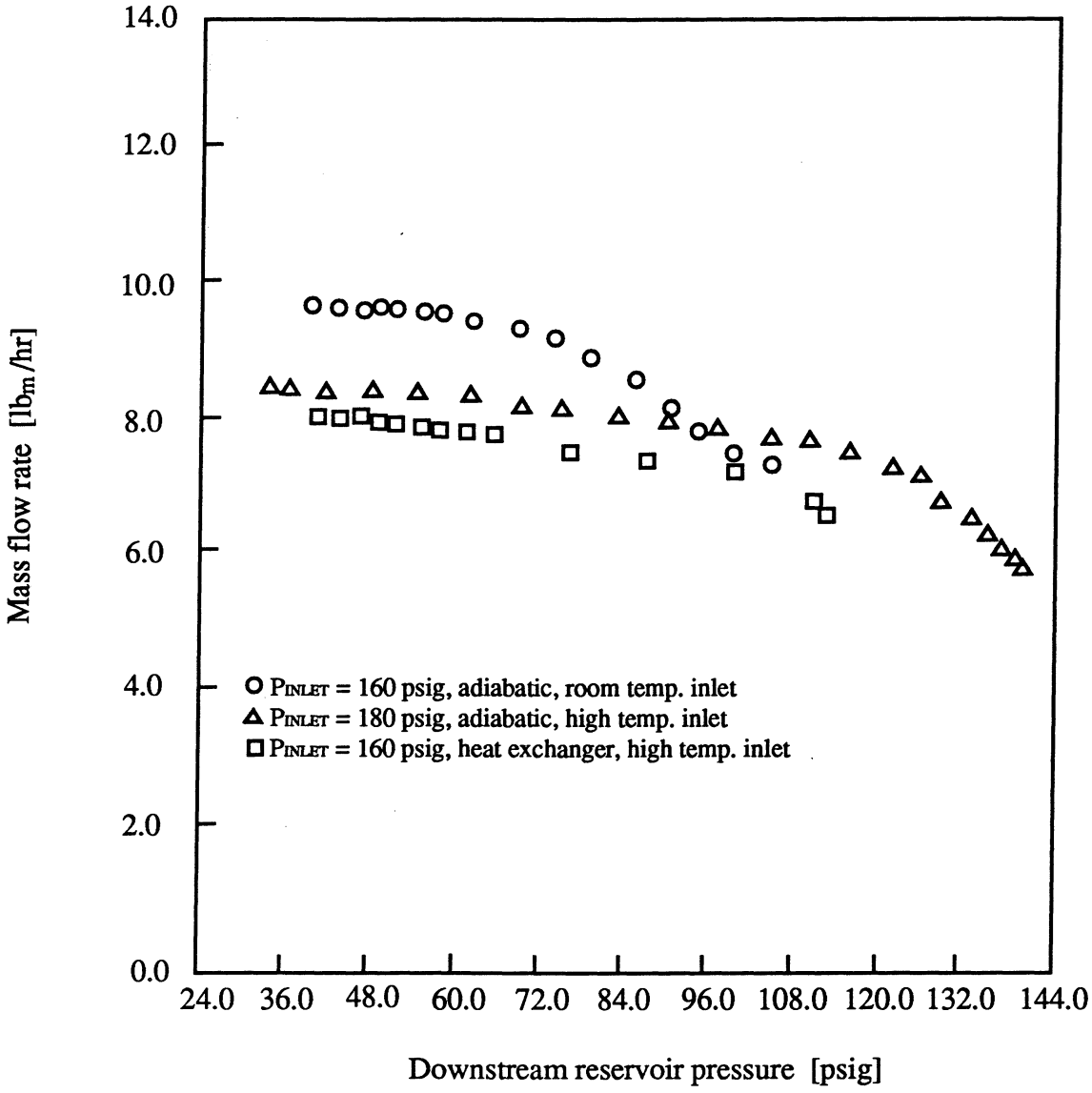

Figure 2.14 Refrigerant mass flow rate through a capillary tube as the reservoir pressure is reduced from Pate.

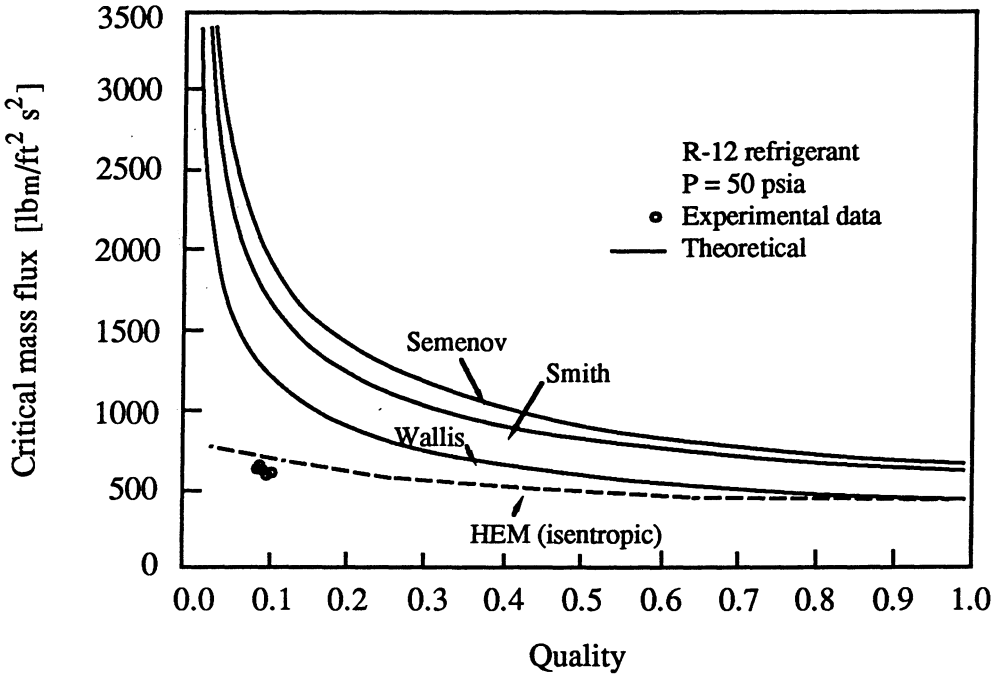

Figure 2.15a Critical mass flux for homogeneous frozen models adapted from Pate.

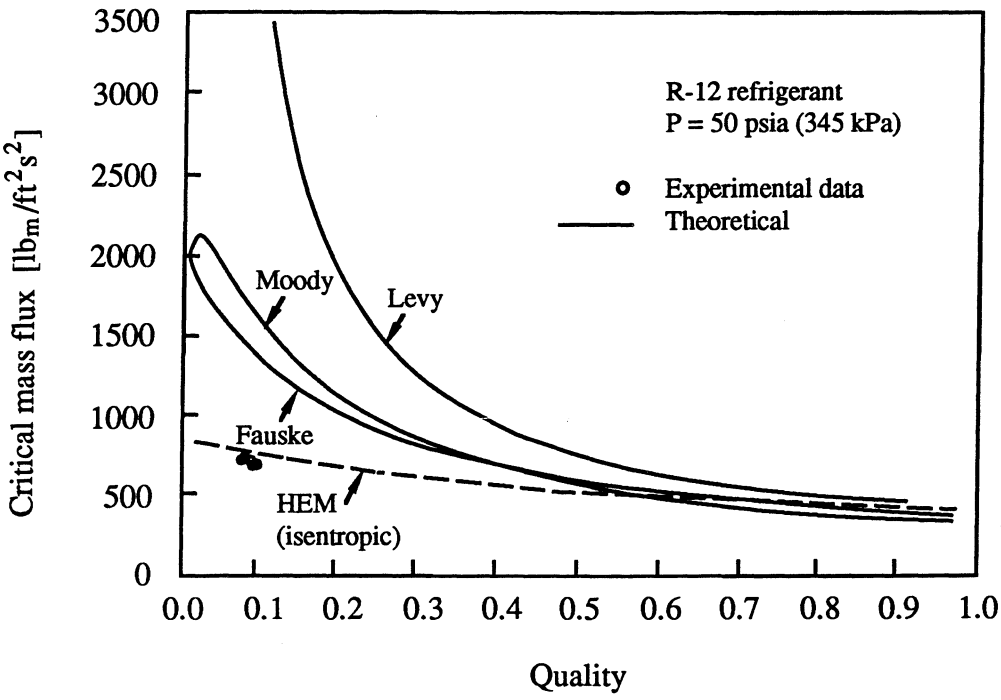

Figure 2.15b Critical mass flux for nonhomogeneous models, adapted from Pate.

Chapter 3

Capillary Tube Study Experimental Facility

This chapter describes the apparatus used to obtain capillary tube data for this study. The facility, shown in Figure 3.1, allows data to be obtained in a unique and informative way. Because of the high pressure drop associated with flow through a capillary tube, using a positive displacement pump to achieve the desired mass flow rates is impossible. Other facilities designed to obtain refrigerant flow data through capillary tubes have utilized either a "blow-down" system or a compressor to achieve the desired flow conditions. Each of these systems has drawbacks which have been avoided with the current design.

With a "blow-down" system is used, the pressure difference across the capillary tube is maintained by placing the refrigerant source cylinder in a hot bath and the receiving cylinder in a very cold bath. After all of the refrigerant has passed through the capillary tube, data acquisition must stop while steps are taken to pump the refrigerant back into the source cylinder. If a compressor is used to supply the desired flow rate, an oil separator must be installed if "pure" refrigerant data is of interest. However, oil separators cannot remove all of the oil from the circulating refrigerant. Both of these potential problems have been avoided with the current facility.

The facility consists of two separate loops: i) the refrigerant test loop and ii) that of a 5-hp R-502 condensing unit that provides the necessary cooling. Four heat exchangers, each with its own R-502 expansion valve to control capacity, are used to remove heat from the system.

3.1 Refrigerant Loop

Because long runs of oil-free refrigerant are desired, using the blow-down technique or a compressor to achieve the desired refrigerant flow rates was deemed unacceptable. A diaphragm pump, capable of producing a 1000 psi pressure increase, was selected as a viable option. Although the pump created a few complications, the loop was modified to accommodate it.

3.1.1 Overview

The diaphragm pump, which requires subcooled liquid at its inlet, is very oversized for this application. Therefore, most of the flow exiting the pump is routed through a bypass line. To ensure that subcooling is maintained in the bypass line, a heat exchanger cools the flow before it is delivered back to the pump's inlet line. The flow that is directed towards the test section is circulated first through the pressure setting tank (PRT), setting the high-side, or "condensing," pressure. Saturated liquid is removed from the bottom of the PRT and flows through a sub-

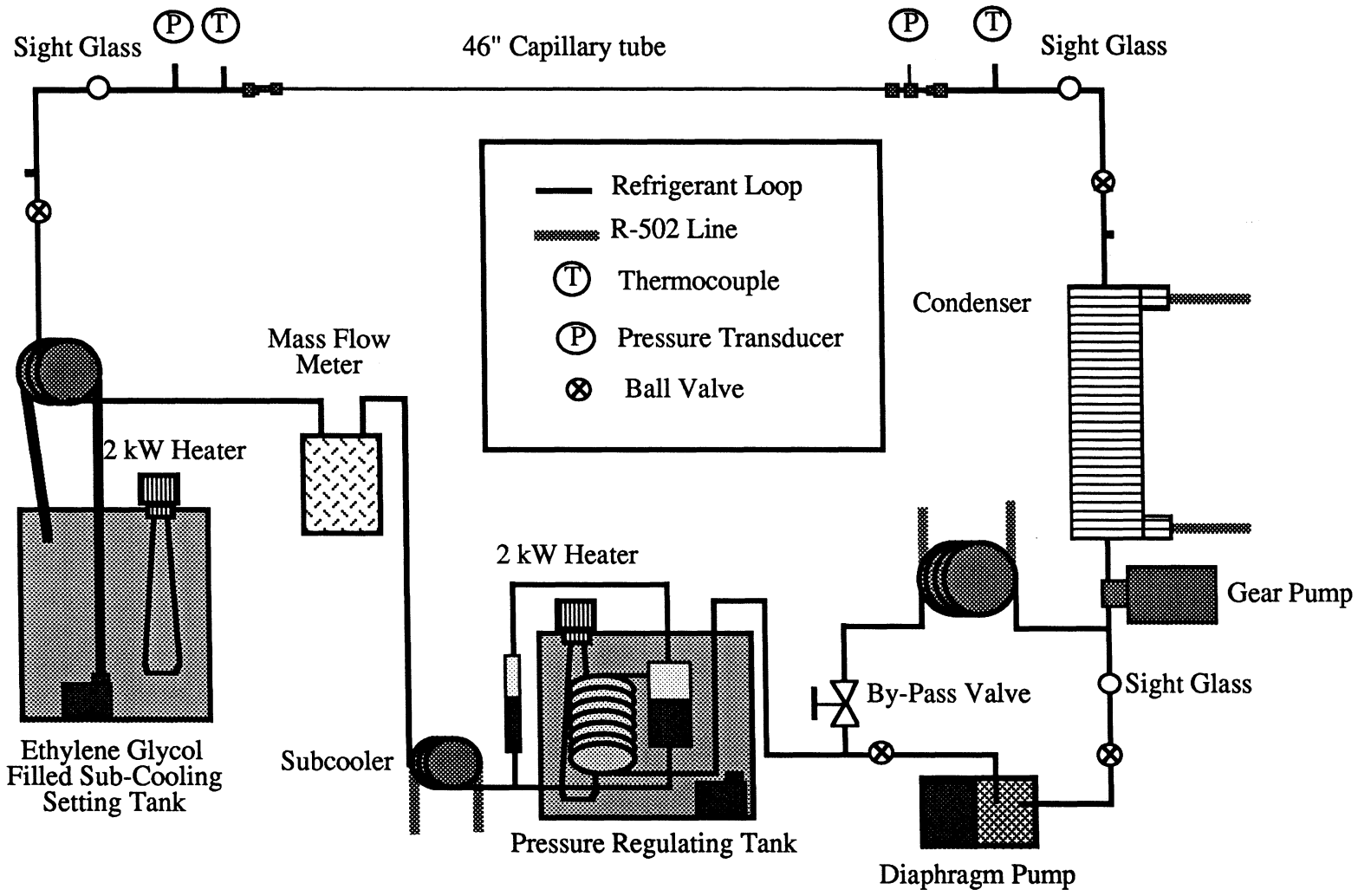

Figure 3.1 Schematic of capillary tube facility.

cooling heat exchanger. The mass flow rate is then measured with a Coriolis effect mass flow meter before the refrigerant is heated to the temperature that will define, along with the pressure, the amount of subcooling at the capillary tube inlet. Upon exiting the capillary tube, the flow is condensed in a large, R-502 cooled heat exchanger. The resulting subcooled liquid then joins with the refrigerant from the bypass line and flows back into the diaphragm pump. For flow observations, sight glasses are located at the inlet and outlet of the test section, and at the inlet of the diaphragm pump.

3.1.2 Control of Refrigerant Flow Parameters

When the diaphragm pump was first installed in the loop, use of the bypass valve alone (without the PRT) was used to set the inlet pressure. Simply adjusting the bypass valve changed the inlet pressure. It was quickly discovered, however, that due to the pulsations created by the pump, having single phase liquid between the pump outlet and the test section resulted in very large (40-50 psi), high frequency pressure oscillations. To overcome this problem, a two-phase mix is created as the refrigerant passes through a warm, well mixed, thermally controlled, ethylene-glycol tank which is located just down stream of the pump. As the refrigerant flows through a coil in the bath, it is heated to a two-phase mix before ending up in a submerged reservoir. The reservoir, by holding a two phase mix, totally dampens the pressure oscillations and sets the high-side system pressure. A vertical sight glass mounted outside the tank enables the liquid level within the reservoir to be monitored. The tank temperature is maintained with a 2-kW heater connected to a Capp Model 535 controller.

After the saturated liquid from the PRT is subcooled in an R-502 cooled heat exchanger, it passes through a Micro Motion Model DS012S100 mass flow meter. The refrigerant is often 50 °F to 130 °F subcooled as it passes through the meter.

To set the appropriate amount of subcooling at the capillary tube inlet, another well mixed, temperature controlled, ethylene-glycol filled tank is used. A pump submersed in the tank is used to circulate warm ethylene glycol through the subcool setting heat exchanger, which is so oversized that the refrigerant exits at very nearly the tank temperature. Thus, by setting the temperature of the PRT and the subcool setting tank (SST), the inlet pressure and temperature, and thus the amount of subcooling, is controlled. The SST temperature is also maintained with a 2-kW heater connected to a Capp Model 535 controller.

After exiting the capillary tube, a large, R-502 cooled heat exchanger condenses the two-phase flow so that it once again may be pumped. Because this condenser is extremely cold (down to -40 °F), some trouble was experienced maintaining a high enough pressure at the inlet to the pump. Also, if the condenser starts to fill with liquid, the exit pressure climbs to unacceptable levels. A small gear pump was therefore installed after the condenser to help keep it as empty as possible and to provide a higher pressure at the inlet of the pump. To verify that subcooled liquid

was reaching the pump, a sight glass is located just downstream of the point where the bypass line and the condensed flow merge.

3.1.3 Test Section

Owing to the fact that different capillary tubes were to be tested, ball valves and charging ports are located just up and down stream of the test section. These valves allow a new capillary tube to be installed without discharging the system. Before entering, and after exiting the capillary tube, the pressure and temperature of the refrigerant is measured.

The inner diameters and lengths of the three test sections used in this study are shown in Table 3.1 They are all copper tubes manufactured by Wolverine Tube, Inc. Great care was taken when cutting the tubes to ensure that the openings were not affected by the cutting process. The tubes were first etched, with the corner of a file, around the entire circumference. They were then gently bent back and forth until they separated into two pieces. This technique was used for all tubes, including the ones used in the nitrogen and water flow tests.

Table 3.1 Capillary tube dimensions

Tube number	Inner Diameter (in.)	Length (in.)
1	.03920	46.0
2	.04202	46.0
3	.04915	46.0

Connecting a capillary tube to the 1/4-in. tubing of the test facility was accomplished with 1/2-in. long brass cylinders machined so that the capillary tubes fit in one side and 1/4-in. tubing fit in the other. The tubes were then brazed in place. The inlet and outlet connections are shown in Figure 3.2. Because the pressure drop of liquid flow is much lower than that of a two-phase flow, the inlet pressure is measured upstream of the test section connections and the exit pressure is measured in the connector, very close to the actual exit. The test section terminates with 1/4-in. male flare fittings. Female flare fittings are located at the points where the facility connects with the test section. With ball valves to isolate the test section and the simplicity of the test section connections, a new capillary tube can be completely installed in less than 1 hr.

No thermocouples are mounted on the test section due to the effect they have on the refrigerant mass flow rate. For similar reasons, no pressure taps are introduced through the capillary tube wall. Melo, *et al.* (1995) found that introducing pressure taps along the capillary tube wall reduced the mass flow rate by about 6%. Making pressure and temperature measurements along the capillary tube and and their possible effects on the mass flow rate are discussed further in the results section.

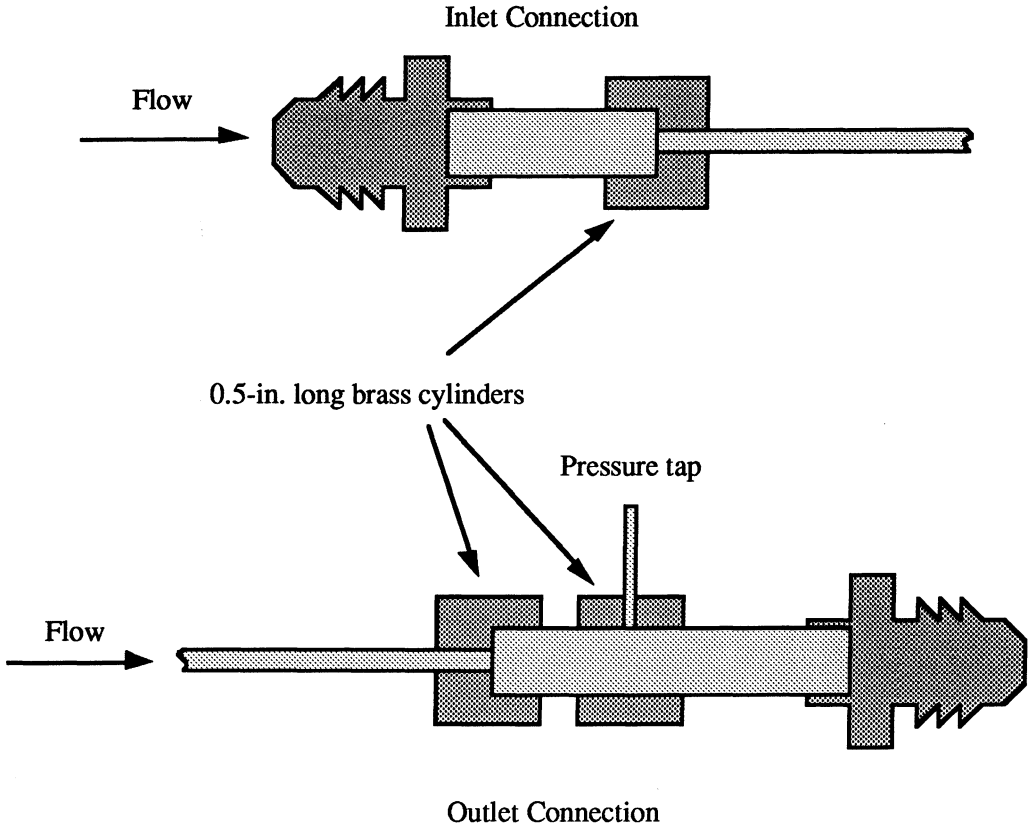

Figure 3.2 Capillary tube inlet and outlet connections.

3.2 Instrumentation

Compared to the condensation facility, the capillary tube data acquisition system records very few measurements. When analyzing the data, for example, the refrigerant mass flow rate and the inlet pressure and temperature are the only flow measurements of interest.

3.2.1 Temperature and Pressure Measurement

Because of the need for high quality data, all temperature measurements are made with Type-T thermocouples constructed from special limits of error wire. The thermocouples are connected to an isothermal board that is part of a Campbell Scientific data acquisition system. All thermocouples were calibrated while attached to the data acquisition system so as to include any uncertainties resulting from converting the voltage signal to a temperature. For the calibration procedure, the thermocouples were placed in an isothermal calibration bath along with an ASTM-grade, NIST-traceable, mercury-glass thermometer. The deviations between the thermocouple reading and that of the glass thermometer were used to calculate the uncertainty. The thermocouples were found to be accurate to within ±0.4 °F with 95% confidence.

The inlet and outlet pressures are measured with a Setra Model C280E 0-500 Psia (0.11% full scale accuracy) and a Setra Model 206 0-250 Psig (0.13% full scale accuracy) pressure transducer, respectively. Calibration curves for these transducers can be seen in Figure 3.3 and 3.4. Analysis of this data gives the experimentally determined uncertainties to be ±0.42 psi and ±0.40 psi, based on a 95% confidence interval, for the inlet and outlet transducers, respectively.

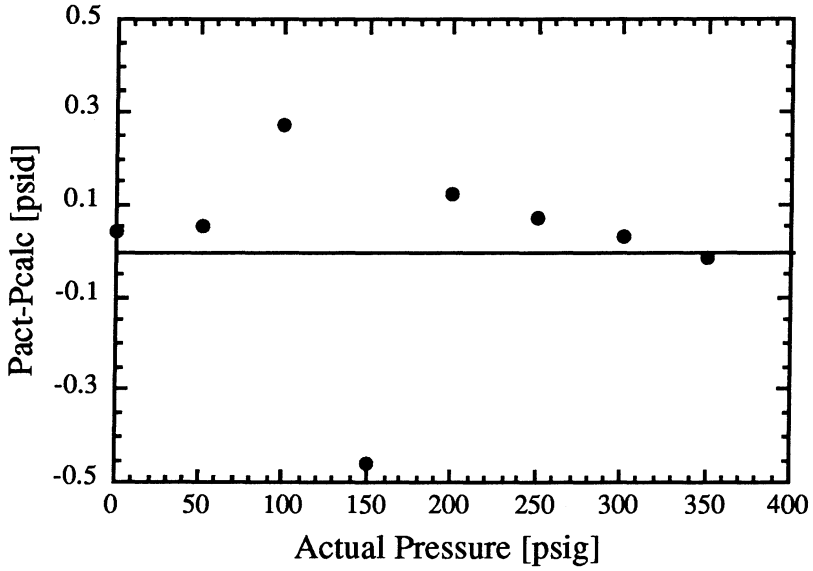

Figure 3.3 Inlet pressure transducer calibration results.

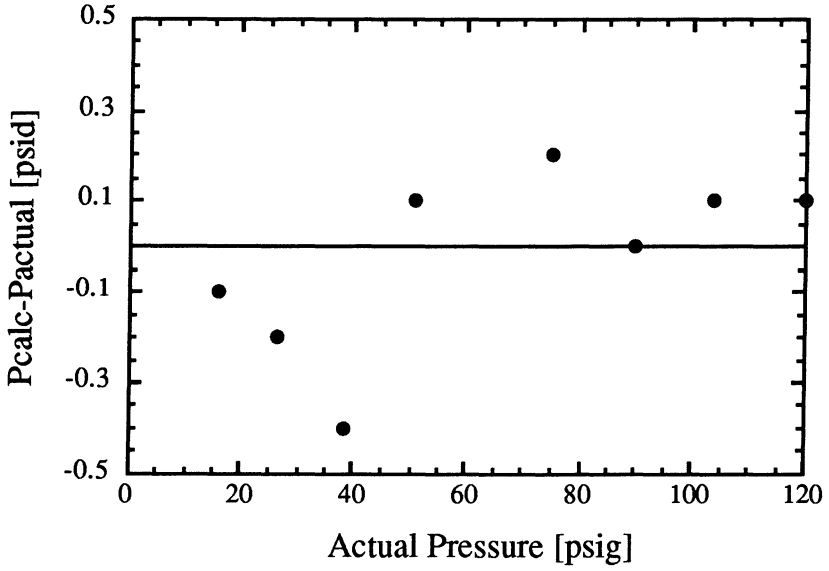

Figure 3.4 Outlet pressure transducer calibration results.

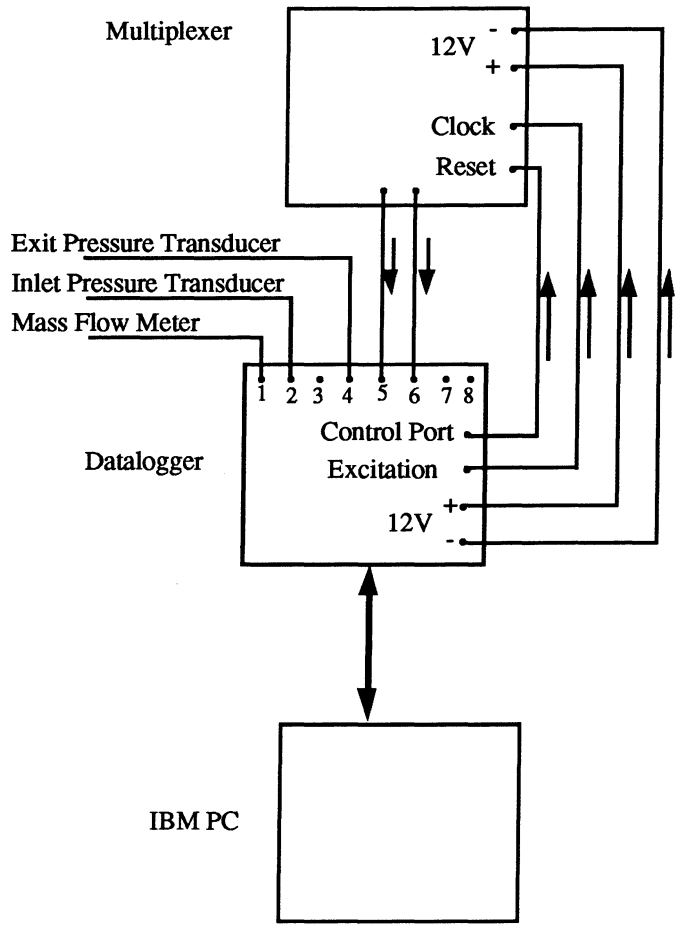

Figure 3.5 Schematic of data acquisition system.

3.2.2 Data Acquisition System

A Campbell Scientific Model 21X Micrologger interfaced to an IBM PC is used to collect data. A schematic of the data acquisition system is shown in Figure 3.5. The datalogger, shown in the middle of the figure, has only eight terminals for receiving information. Because many temperature measurements are made, a Campbell Scientific Model AM 416 Multiplexer is used to scan the thermocouple signals. As shown in the figure, only the mass flow meter, the pressure transducers, and two channels from the multiplexer are connected to the datalogger. Each scan of the datalogger consists of receiving and manipulating signals from the mass flow meter, the pressure transducers, and all of the thermocouples connected to the multiplexer. These scans are averaged over a minute and saved in the datalogger memory. On a given command, the data is transferred to the hard drive.

3.3 Composition Analysis

To determine the composition of a blended refrigerant, the same techniques and gas chromatograph that are used in the condensation study is used.

3.4 Nitrogen Flow Facility

Before analyzing the data, it was necessary to determine the wall roughnesses of the tubes. A separate experimental test facility, which uses nitrogen as the flow fluid, is used to obtain the high Reynolds number flow data required to determine tube roughness. Friction factor, and thus tube roughness, along with entrance loss values were calculated from the data gathered.

There are several reasons for using nitrogen as the working fluid. Because it is chemically inert, nitrogen is noncorrosive with regard to the copper capillary tubes and test facility components. It is also inexpensive, readily available, and easily handled. Nitrogen may be safely discharged into the laboratory atmosphere, provided that adequate ventilation exists. Finally, the thermodynamic and transport properties of nitrogen are well defined, which is an important feature for data analysis.

Figure 3.6 is a schematic representation of the test facility, hereafter referred to as the Nitrogen Test Facility (NTF). Nitrogen is delivered at a very high pressure from a tank containing the gas in compressed form. Attached to the tank is a pressure regulator which is used to set and maintain a steady supply pressure. After exiting the pressure regulator, the mass flow rate is measured with a Micro Motion model DS006S100SU mass flow meter. Next, the nitrogen flows through a tempering coil, which is designed to bring the nitrogen temperature into equilibrium with the atmospheric temperature. The flow proceeds through the transition section, where the gauge pressure and the temperature are measured. Finally, the nitrogen enters the capillary tube, which is thermally insulated to ensure an adiabatic flow. At the exit of the test section, the nitrogen is discharged into the atmosphere.

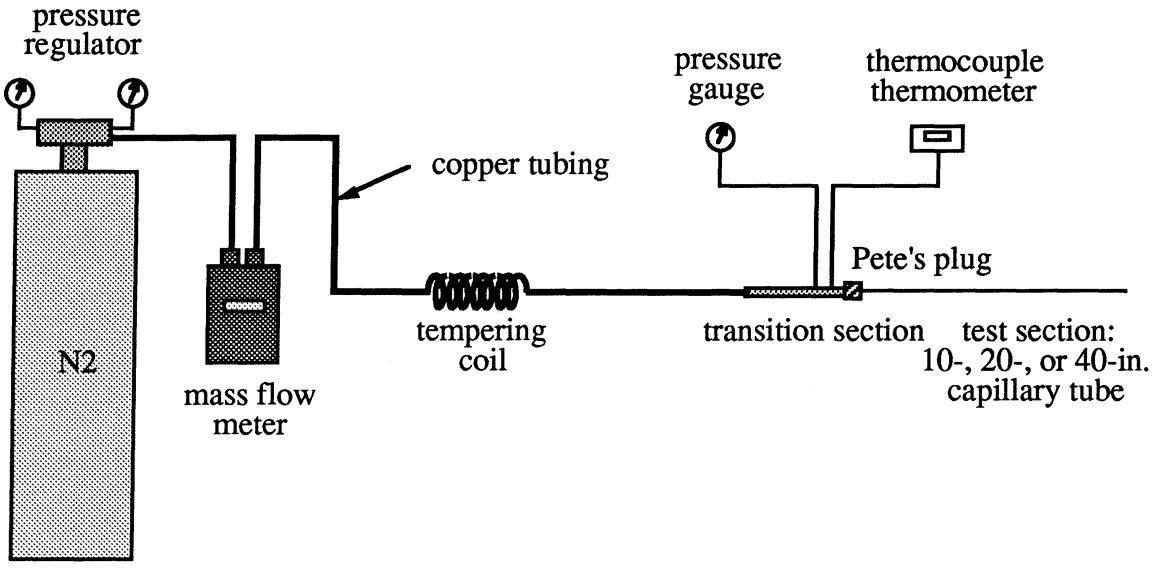

Figure 3.6 Schematic of the nitrogen flow facility.

The components of the NTF are connected by 1/4-in. copper tubing. Permanent joints are soldered, whereas others are connected by compression fittings to allow easy removal. The components of the NTF measure and maintain the desired flow conditions for a given capillary tube. In the paragraphs that follow, the components are described in more detail.

The Micro Motion flow meter is advantageous because it measures and displays the mass flow rate directly, without the need for a conversion factor or a data acquisition system. In addition, the measurement is unaffected by changes in fluid temperature, viscosity, conductivity, or flow profile. The flow meter, which has a range of 0-0.05 kg/min, is accurate to within 0.5% when operating above 20% of the maximum flow rate. The mass flow rates measured while obtaining data ranged from 0.0078 to 0.0370 kg/min, corresponding to 16% and 74% of the maximum flow rate, respectively.

The tempering coil is necessary because of the cooling associated with the throttling process at the exit of the supply tank. For all cases, the coil brings the nitrogen temperature into equilibrium with the temperature of the laboratory. As a result, the potential for heat transfer between the test section and its surroundings is minimized. The coil is comprised of 37 windings, each having a diameter of 4 in. With a copper tube diameter of 1/4 in., the coil offers approximately 365 sq. in. of heat exchange area.

By manually adjusting the pressure regulator, the pressure at the inlet of the test section is set to a desired value in the range of 0–60 psig. Although the depletion of nitrogen in the tank is a transient process, the flow in the nitrogen line is steady because the regulator maintains a constant pressure at its outlet.

So that the pressure and temperature of the nitrogen flow can be measured, the transition section is instrumented with a pressure tap and a Type-T thermocouple probe. A "Pete's Plug", which is nothing more than a tube cap containing a septum with a very small cross cut into it, is used to connect capillary tubes to the transition section. For a given test, the appropriate capillary tube is simply inserted through the septum, which creates an air tight seal around the tube. When the test is finished, the tube is withdrawn and another is inserted.

The nitrogen pressure at the inlet of the test section is measured using an Ashcroft analog gage, with a range of 0–60 psig and a reported accuracy of 0.25% of the span. The gauges were calibrated with a deadweight tester to validate the stated accuracies. The nitrogen temperature at the inlet of the test section is measured using an Omega thermocouple probe, which is inserted into the temperature tap in the transition section. A Thermo Electric thermometer measures the output of the thermocouple and provides a digital display of the temperature. The thermometer has a range of 77–672 K and an accuracy of 0.07% of the span.

At the exit of the test section, the nitrogen discharges freely into the atmosphere. Accordingly, the exit pressure is assumed to be equal to atmospheric pressure. A Nova barometer, fastened to a wall in the laboratory, is used to measure atmospheric pressure.

Nitrogen flow data were obtained for three lengths of each of the tube diameters used in the capillary tube studies. After a tube was inserted into the Pete's Plug, the inlet pressure was increased to about 60 psig. The nitrogen mass flow rate, inlet pressure, outlet pressure, and inlet temperature were then recorded. The inlet pressure was then reduced and new data recorded. This was repeated 10-15 times for each tube. By analyzing the data for the various tube lengths, an estimate of the entrance loss as a function of Reynolds number was obtained for each tube.

3.5 Water Flow Facility (a.k.a. The Monkey Rig)

Because the mass flow rate of laminar nitrogen flow through a capillary tube is below the useful range of the Micro Motion mass flow meter, a separate experimental facility was designed and constructed to investigate the laminar flow characteristics of the capillary tubes. Using water as the flow fluid, accurate values of laminar flow parameters allowed us to determine the capillary tube diameters. The same transition section and capillary tubes were used in the water flow studies as in the nitrogen flow studies.

The facility, which is shown in Figure 3.7, relies on gravitational head pressure to supply the various laminar flow conditions. The pressure that drives the water flow corresponds to the height at which the source tank is suspended. Water is drained from the bottom of the source tank, flows through a 3/8-in. ID tygon tube, and into the transition section. To keep the water level in the source tank constant, a pump, which is submersed in a water reservoir, continuously adds water to the tank. A drainage hole is cut in the side of the bucket so that excess water can return to the reservoir, thus maintaining a constant pressure at the inlet of the capillary tube. In total then, there are three tubes that have water flowing through them: i) from the source tank to the capillary tube, ii) from the reservoir to the source tank, and iii) overflow from the source tank returning to the reservoir.

To measure the inlet pressure, a 1/8-in. ID tygon tube is connected to the pressure tap and attached to the side of the source tank. The inlet pressure is determined by measuring the height of the column of water supported by the inlet flow. The water temperature is measured with a mercury-glass thermometer immersed in the source tank. To determine the mass of water that has passed through the capillary tube, the water exiting the capillary tube is captured in a small bucket on a scale. By measuring the mass of water that has passed through the capillary tube and the time elapsed, the mass flow rate is calculated.

Data were taken at five different inlet pressures, all of which resulted in laminar flows with Reynolds numbers ranging from 200 to 2100.

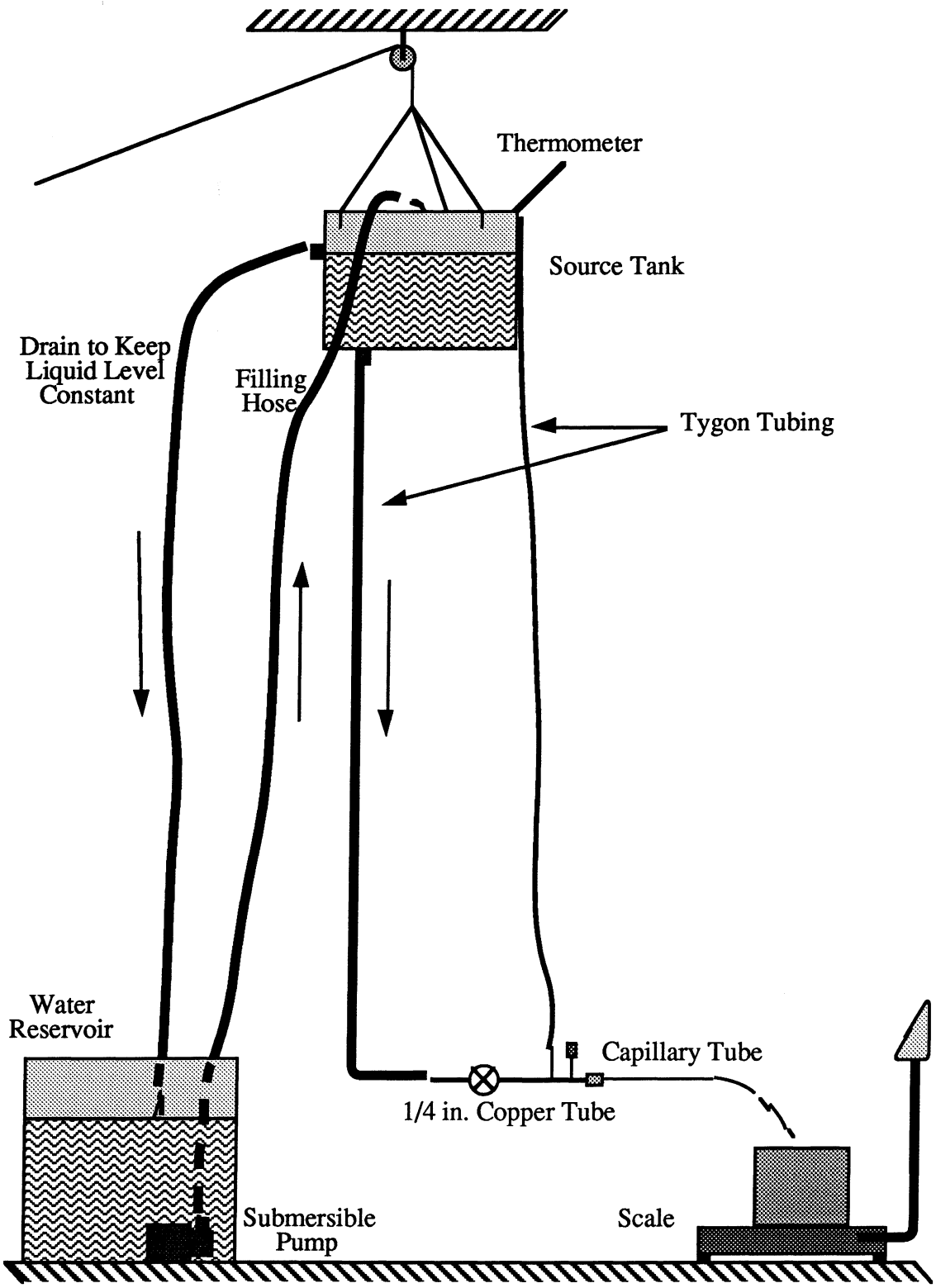

Figure 3.7 Schematic of the water flow facility.

Chapter 4

Capillary Tube Experimental Procedure

This chapter describes the techniques used to acquire data from the capillary tube facility. Also, the complete data matrix is outlined and explained.

4.1 System Preparation

Due to environmental concerns and possible fractional distillation of refrigerant mixtures, every effort is made to ensure that the test facility is leak free before it is charged with refrigerant. This is accomplished after the loop was constructed and again after any modifications are made. Once the loop is verified as being leak free, it is charged with the desired refrigerant. Great care is taken to avoid allowing air into the test stand.

4.1.1 Charging and Discharging Refrigerant

Because of the way the neoprene diaphragms are seated in the diaphragm pump, the manufacturer cautions against subjecting the seals to a vacuum. To isolate the pump when the loop is evacuated, ball valves were added near the inlet and outlet of the pump.

The discharging procedure starts with creating an environment at a lower pressure than the experimental facility. This is accomplished by immersing a recovery cylinder in ice water. After the liquid refrigerant has been captured by the recovery cylinder, a reclamation unit is used to recover the remaining vapor. As the pressure in the loop approaches atmospheric, the valves around the diaphragm pump are closed, trapping a small amount of refrigerant vapor. The reclamation unit is able to reduce the pressure in the loop to about 4 psia. When this level is reached, a vacuum pump is used to complete the evacuation process. Although the refrigerant has been removed from most of the loop, a small amount of vapor remains around the diaphragm pump. To flush the previous refrigerant from the region around the pump, appropriate valves are closed and a small amount of the next refrigerant to be tested is charged into one side of the loop. It is then bled slowly through the pump section, into the evacuated side of the facility, flushing out the old refrigerant. The valves around the pump are then shut, this time trapping vapor of the next refrigerant to be tested. The portion of the loop now contaminated with a mixture of the two refrigerants is re-evacuated before the next refrigerant is added.

When removing the mixture of two refrigerants from the system, a charging manifold is used to connect the loop, vacuum pump, and cylinder of new refrigerant. After the loop is evacuated, the valve on the vacuum-pump side of the manifold is closed, thus isolating the vacuum pump. The valve on the refrigerant cylinder is then opened, allowing refrigerant to flow into the loop. To facilitate the charging procedure, the R-502 unit is used to cool the heat exchangers, thus

maintaining a low pressure in the loop as it fills with refrigerant. After about 12 lbm of refrigerant enter the loop, the cylinder valve is shut and the pump turned on.

If the capillary loop is overcharged, the sight glass that shows how full the PRT reservoir is fills completely with liquid. The pressure then rises sharply, and large pressure fluctuations are sent through the loop. To remedy this problem, liquid refrigerant is removed from the high pressure side of the facility. If the loop is undercharged, no liquid is visible in the sight glass and the inlet pressure is lower than what corresponds to the PRT temperature. In this case, liquid refrigerant is added through the charging port on the low pressure side of the capillary tube. The configuration used to achieve a proper charge can be seen in Figure 4.1. In most cases, once the loop is running with a satisfactory charge, no charge adjustments are necessary for the remainder of the tests for that capillary tube.

4.1.2 Changing Test Sections

Before a test section is removed, the charge in the region between the valves that isolate the test section is minimized. The liquid is removed from this region by turning on the R-502 unit, hus lower the temperature and pressure if the heat exchangers. A heat gun is then used to heat the test section and surrounding tubing. In this way it is assured that there is only low pressure vapor in the test section, thus minimizing the disturbance, both in terms of amount and composition, to the charge in the system. After the test section is removed, a new one is installed and evacuated before the isolating valves are opened, flooding refrigerant vapor into the test section.

4.2 System Operation

As mentioned, once the loop is charged properly and running, very few adjustments are necessary as data are being recorded. Getting the facility operating from a cold start, however, can present a challenge.

4.2.1 System Start-Up

The first task when starting up the loop is to get the PRT and SST to the correct temperature. This is accomplished by turning the heaters up to 100% and turning on the submersible pumps. Depending on the amount of temperature rise necessary, heating the tanks usually takes between 20 and 90 minutes. As the temperatures get close to the desired values, the R-502 loop and the gear pump are turned on. The R-502 loop cools the refrigerant in the heat exchangers and therefore allows the gear pump to start circulating cold refrigerant. The circulating refrigerant cools the inlet line of the diaphragm pump. If this is not done before the diaphragm pump is turned on, the refrigerant will boil violently when it hits the warm copper, resulting in cavitation at the entrance to the diaphragm pump and negligible flow.

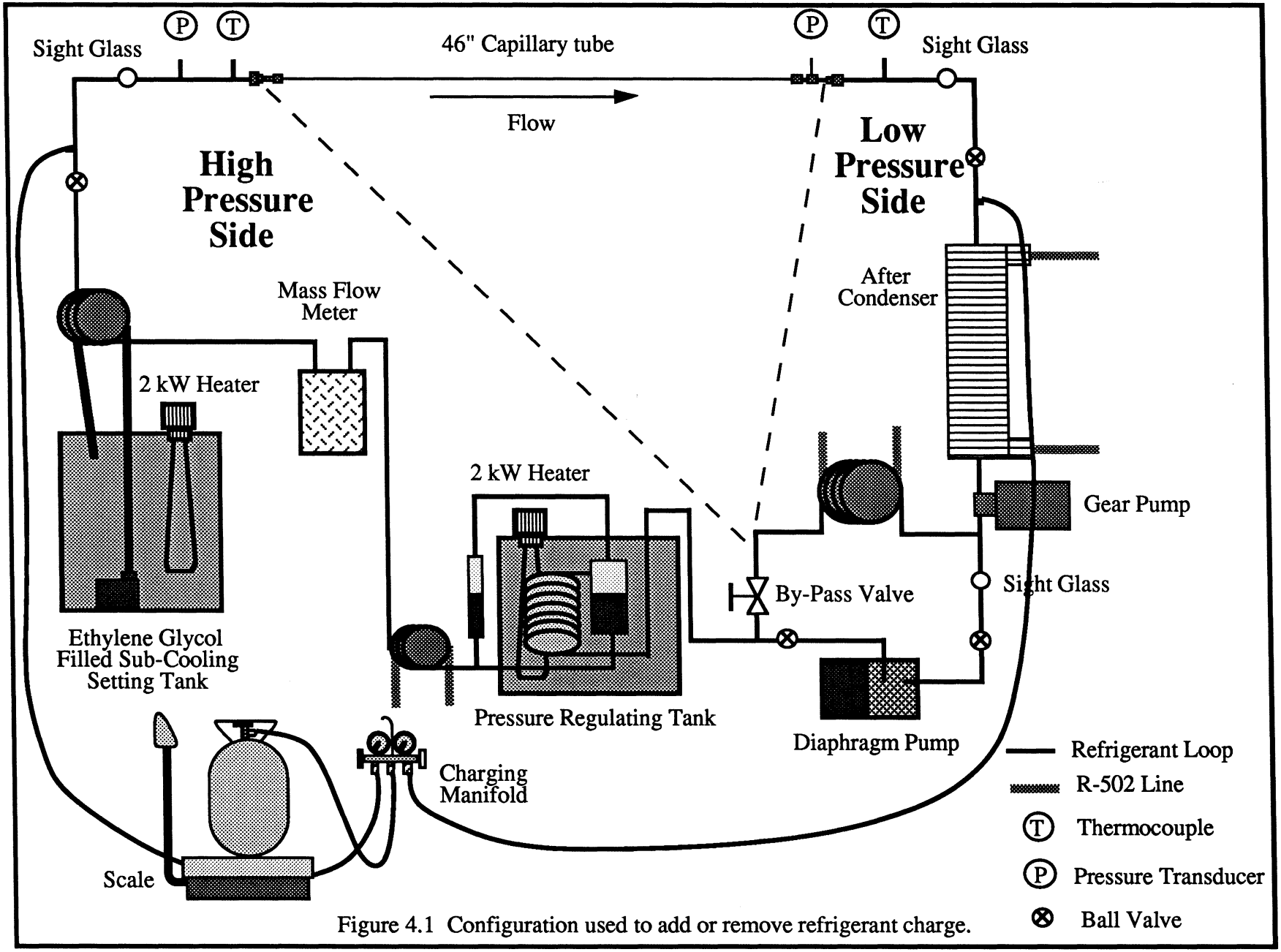

Figure 4.1 Configuration used to add or remove refrigerant charge.

On occasion, the diaphragm pump does not prime, resulting in no refrigerant flow. The pump is then shut off, the gear pump turned up a little to increase the inlet pressure, and the diaphragm pump turned back on. The process might have to be repeated a couple of times before satisfactory flow is attained. When the pump does start moving refrigerant, it sounds very different, the outlet pressure increases, and the inlet pressure decreases. The most important consequence of the pump operating correctly, visible on the computer screen, is that the mass flow rate increases to a stable value. The liquid level in the vertical sight glass is then noted and charge is removed or added accordingly.

Once the loop is running smoothly, with an acceptable liquid level in the vertical sight glass and a stable mass flow rate, the temperatures of the PRT and SST are adjusted to appropriate values for the data collection to begin.

4.2.2 Data Collection

Each data set begins with the PRT at the desired temperature and two-phase flow entering the capillary tube. The SST is then slowly cooled at a rate of about 0.2 °F to 0.3 °F per minute, thus increasing the amount of subcooling at the capillary tube inlet. As data are obtained, the system operator regularly records the time, temperature of the refrigerant entering the test section, percentage power given to the SST, PRT temperature, and the percentage power given to the PRT. By recording all of these values, the operator can "see" the history of the data run and better predict what changes may become necessary as the run proceeds. Of the values recorded, the PRT temperature and the SST temperature are the most important. These values determine the high side pressure and the amount of subcooling at the test section inlet, and are altered by changing the percentage power to each of the tanks. Therefore, knowing past power input values to the PRT and SST prove helpful when an adjustment becomes necessary.

The data are taken in a very systematic and reproducible way. The 130 °F condensing temperature data is taken first, followed by a loop at the 110 °F condensing temperature condition, followed by the 90 °F condensing temperature data. After the 130 °F data is completed, the SST is at about 105 °F and the PRT is at about 131 °F. The PRT is then cooled to 111 °F by circulating the ethylene glycol from the tank through an R-502 cooled heat exchanger. While the PRT is being cooled, the SST is heated to about 112 °F. Once both tanks are at a steady, acceptable level, the SST is again cooled slowly as the 110 °F data are recorded, until 25 °F of subcooling is reached. At this point, the power to the heater in the SST is turned up, so that the subcooling slowly decreases to zero. In this fashion, a complete "loop" is taken for every 110 °F run. The SST and PRT are then cooled to appropriate values and the 90 °F condensing temperature data are taken. About ten hours are required to test a tube at all three temperatures. A typical data set is shown in Figure 4.2.

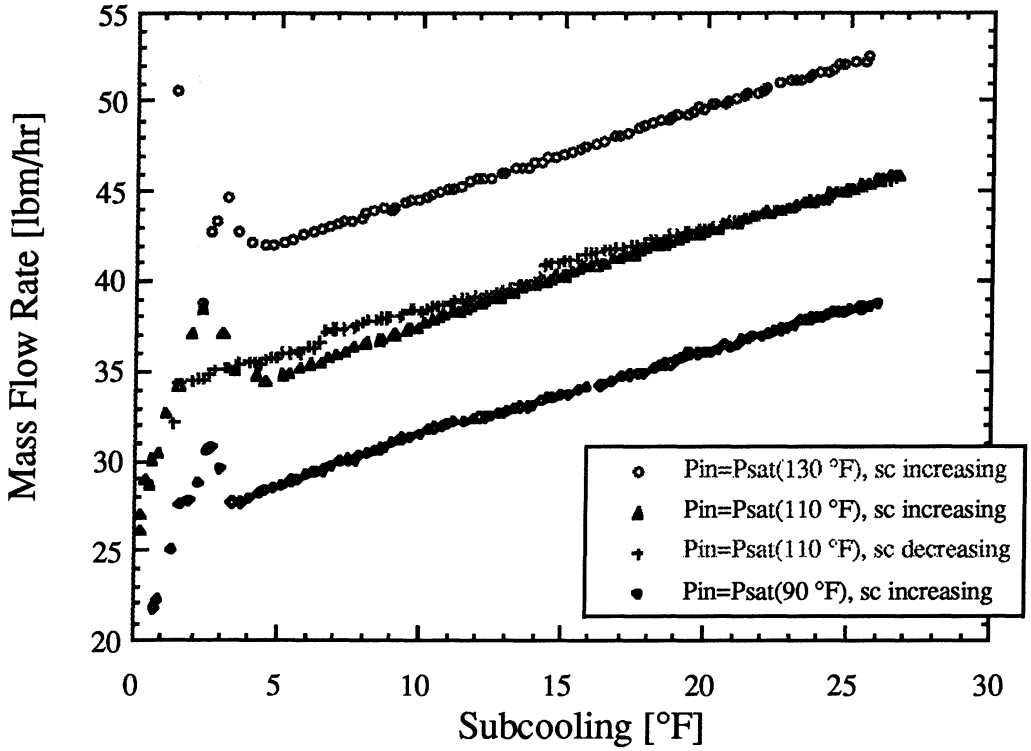

Figure 4.2 Typical data set (R-22 flowing through the 0.039-in. capillary tube).

The 110 °F loops are taken to investigate the magnitude of path dependent effects on mass flow rate. To investigate the effect of temperature on the hysteresis, loops were run at all temperatures for R-22 flowing through the 0.049-in. ID tube.

4.3 Refrigerant Sampling Procedure

For sampling purposes, refrigerant is removed as a liquid from the high pressure side of the test facility. About three grams of liquid refrigerant is trapped and the composition is analyzed by a gas chromatograph.

4.4 Data Matrix

The complete data matrix for the capillary tube studies is outlined in Table 4.1. Data were taken at all three condensing temperatures for every tube/refrigerant pair. An "**I**" in the table indicates that the data were obtained by starting with two-phase at the capillary tube inlet and increasing the subcooling to 25 °F. An "**L**" in the table indicates a loop, starting with two-phase at

the inlet, was taken at that condition. Because of its extremely high operating pressures, the mass flow rate, and thus pressure drop, was much higher for R-410A flow for the highest inlet pressure. An "**X**" in the table indicates that the test was not taken.

Table 4.1 Test Matrix for Capillary Tube Studies

	90 °F			**110 °F**			**130 °F**		
	0.039	0.042	0.049	0.039	0.042	0.049	0.039	0.042	0.049
R-22	**I**	**I**	**L**	**L**	**L**	**L**	**I**	**I**	**L**
R-134a	**I**	**I**	**I**	**L**	**L**	**L**	**I**	**I**	**I**
R-407C	**I**	**I**	**I**	**L**	**L**	**L**	**I**	**I**	**I**
R-410A	**I**	**I**	**I**	**L**	**L**	**L**	**I**	**I**	**X**

Chapter 5

Data Analysis

In this chapter, the data reduction processes involved in the capillary tube study is presented.

5.1 Capillary Tube Study Data Reduction

Because the mass flow rate, temperature, and pressure are recorded directly by the data acquisition system, very little data analysis is necessary for the capillary tube study. Also, we are interested in how the data change from minute to minute, so we do not average values over longer time spans. The data acquisition system scans the measured parameters 39 times per minute, and records the average. These averaged values are then taken to be the data points for that minute.

5.1.1 Determining Capillary Tube Diameters

Due to manufacturer variability, the actual inner diameter of a capillary tube can vary by as much as 0.001 in., or about 2 - 3%. Because uncertainties of this magnitude result in unacceptably high uncertainties in mass flow rate, the actual diameter of each capillary tube was determined experimentally. A water flow facility was constructed to meet this need. Reducing the water flow data to obtain tube diameters proved to be a very complicated matter. Measured quantities include total mass flow of water, elapsed time for the water flow, inlet pressure (gage), and inlet temperature. The inlet pressure was kept low enough to ensure laminar flow in the capillary tube. The mass flow rate is obtained by dividing the total mass flow by the elapsed time. The pressure drop across the tube is simply the gage pressure at the inlet. So the pressure drop, tube length, mass flow rate, and fluid properties are all known. The difficulty resides in separating the frictional pressure drop from other losses. The following equation is used to model the pressure drop:

$$\Delta P = \frac{1}{2}\rho u^2\left(K + \frac{64}{Re}\frac{L}{D}\right), \qquad (5.1)$$

where K represents the non-frictional losses and may be a function of Reynolds number. The magnitude of K results from two different phenomenon; i) contracting the flow from a large diameter tube to a small diameter tube and ii) the additional pressure drop resulting from developing flow in the first few inches of the capillary tube. The loss resulting from the sudden contraction and resulting vena contracta is a function of diameter ratios, and the loss resulting from the developing region is a function of Reynolds number. For these reasons the value of K in Equation 5.1 may be a function of both Reynolds number and tube diameter. For a given mass flow rate, however, the Reynolds number is a function of diameter, confounding the problem further.

In an attempt to separate K from frictional losses, the manufacturer's diameter was assumed to be correct and Equation 5.1 was used with the experimental data to find a K for each water flow data point. When the "nominal" K values are plotted versus Reynolds number it becomes clear that the 10-in., 20-in., and 40-in. tubes have different K values and change in different ways with respect to Reynolds number. It is believed that these differences are not necessarily due to the different diameters, lengths, and Reynolds numbers alone, but may also result from unique geometries at the inlet of each of the nine capillary tubes tested with water. If the diameter used in the water flow calculation is changed by 0.0001 in. (0.26%, 0.24%, or 0.20% for the 0.039, 0.042, and 0.049-in. ID tubes, respectively), the values of K change significantly. For this reason it is apparent that almost any diameter has the possibility of being determined as the best one, depending on the K values chosen.

An Engineering Equations Solver (EES) program was written to simultaneously solve for the best K values for each length of tube and the best diameter for all three tubes. This procedure was then repeated for each diameter. Although this program is fairly sensitive to initial guesses, it does find reproducible optimum values for the various K values and the tube diameters. From the optimum K values and raw data, Equation 5.1 was used to calculate a predicted diameter for each of the data points. Figures 5.1 through 5.3 show the results of this calculation for the three tube diameters. Each graph shows the fractional deviation from the optimum diameter plotted against Reynolds number for each of the three tube lengths. The stated and actual diameters, along with uncertainties and the percentage deviation from the stated diameters, are shown if Table 5.1.

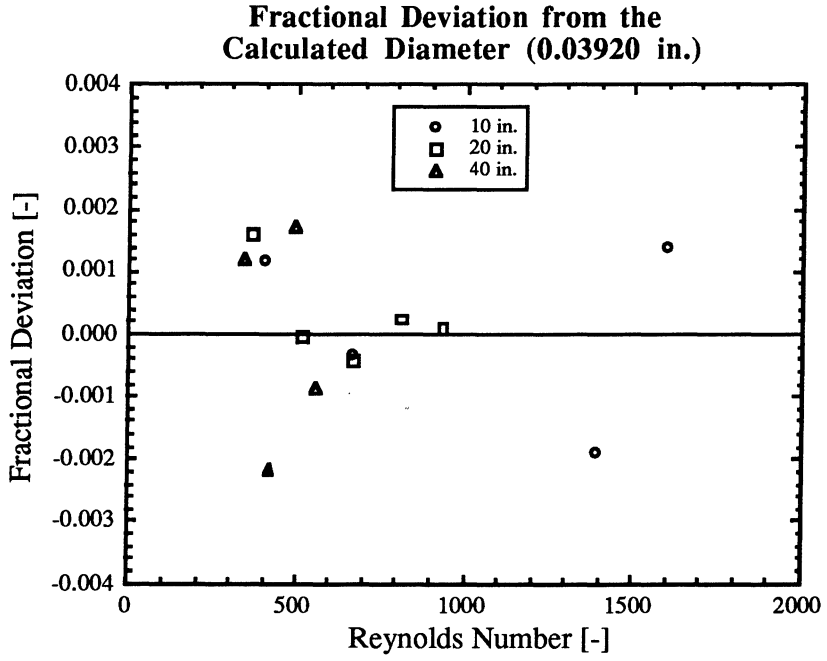

Figure 5.1 Resulting fractional deviations from the calculated best diameter for the 0.039 inch ID capillary tube

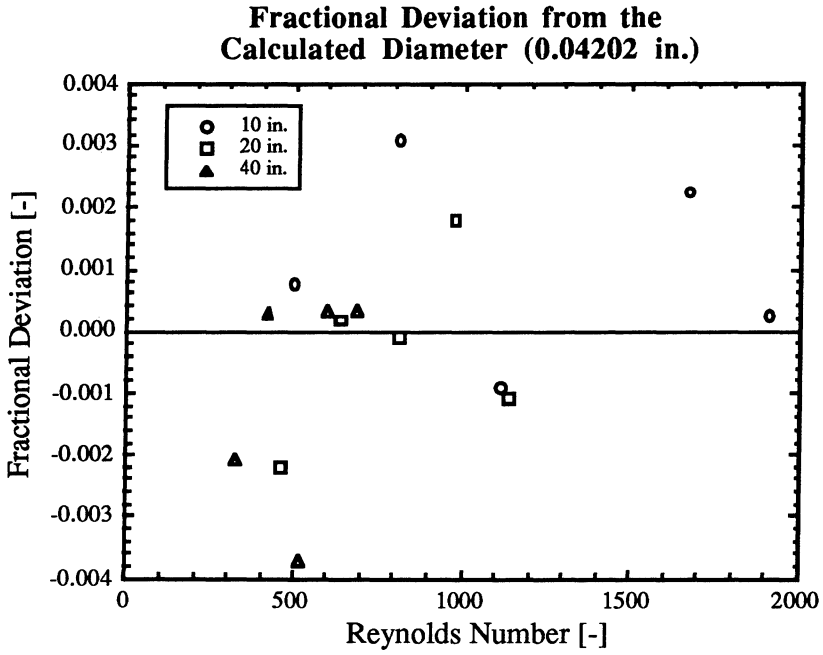

Figure 5.2 Resulting fractional deviations from the calculated best diameter for the 0.042 inch ID capillary tube

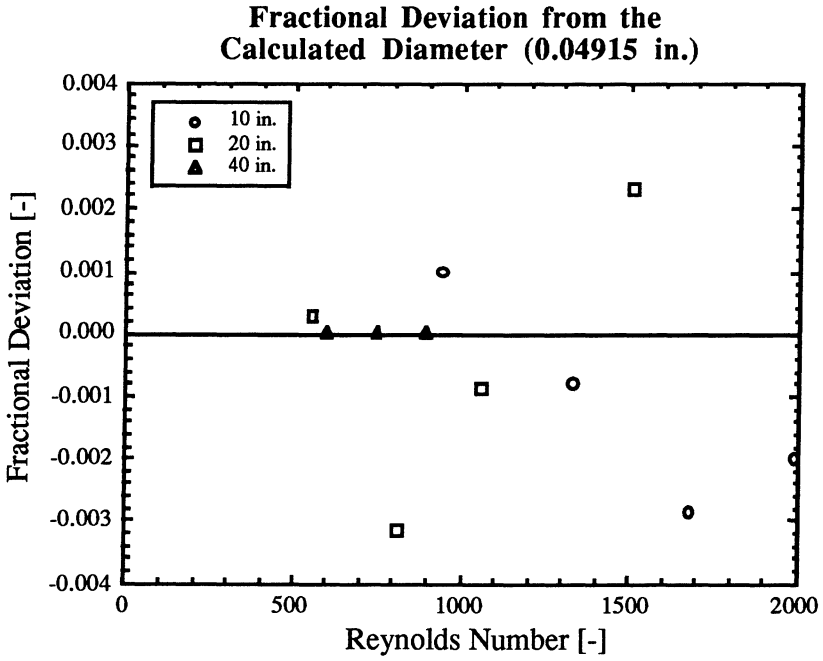

Figure 5.3 Resulting fractional deviations from the calculated best diameter for the 0.049 inch ID capillary tube

Table 5.1 Comparison of stated and determined tube diameters

Stated Diameter	0.039 in.	0.042 in.	0.049 in.
Calculated Diameter	0.03920 ± 0.00012 in.	0.04202 ± 0.00018 in.	0.04915 ± 0.00021 in.
Percentage Difference	0.51	0.05	0.31

5.1.2 Data Reduction

The data are downloaded from the IBM that controls the data acquisition system and converted to Macintosh format. Once loaded into a spreadsheet, a saturation temperature is calculated based on the inlet pressure of the refrigerant. The amount of inlet subcooling is then calculated as the difference between the inlet saturation temperature and the actual inlet temperature. Data recorded during the system warm-up is removed and the remaining data runs are separated form each other so that they may be copied into a graphing routine. Once in the graphing package, the data are plotted to show how the mass flow rate changes with inlet subcooling for each particular inlet pressure and tube combination.

Chapter 6

Capillary Tube Results

This work introduces a new and revealing experimental technique for obtaining capillary tube data. It is believed that with this new approach, much of the "randomness" that has traditionally been associated with capillary tube mass flow rate data will be eliminated.

6.1 Justification and verification of experimental technique

Early data were taken for R-22 flowing through a 0.049-in. capillary tube. The data shown in Figure 6.1 were collected for eight different levels of subcooling with a constant inlet pressure corresponding to a "condensing temperature" of 110 °F. The three data points with the lowest subcooling appear to be on one line whereas the remaining five data points seem to lie on a second distinct line. One can easily visualize a transition of some sort between these two lines at a subcooling of approximately 12 to 13 °F, although the exact nature of such a transition cannot be determined from these data alone. Moreover, one cannot be sure that subcooling is the controlling variable here. Perhaps time plays a role or maybe whether steady state is approached from a starting point of greater or lesser subcooling is important. To address these unresolved issues and answer the perplexing questions inherent in these data, a new experimental technique was developed.

In an attempt to capture more information about these phenomena, all of the data for a given condensing temperature and tube ID are taken in one continuous run. At first, this was accomplished with the following steps: i) the PRT was set to the desired temperature and held constant, ii) the SST was set to a temperature 25 °F cooler than the PRT, thus setting the inlet subcooling at 25 °F, and iii) the SST was heated slowly, reducing the subcooling to zero over the course of about two hours. The resulting data, consisting of 120 (or so) data points, represents 120 different levels of subcooling for the given condensing temperature. When plotted as shown in Figure 6.2, it becomes very clear where jumps occurred, how big they were, and how each state point was reached. Also shown in Figure 6.2 are the data from Figure 6.1.

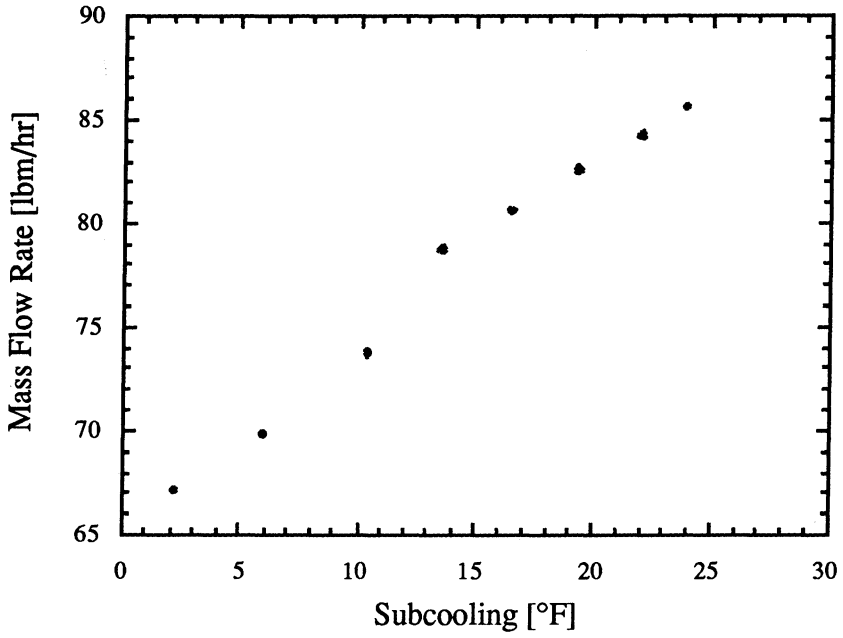

Figure 6.1 Mass flow rate data obtained for discrete levels of subcooling for R-22 flowing through a 46-in. long capillary tube with an inlet pressure of 241 psia

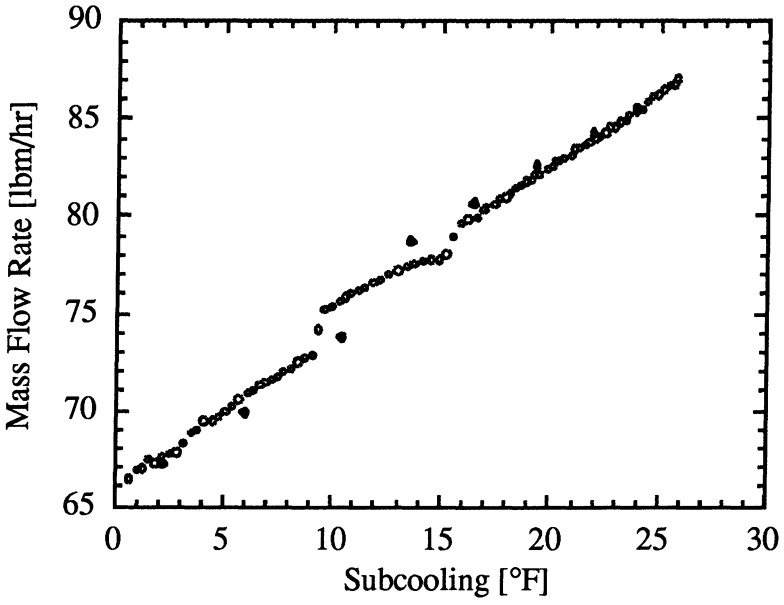

Figure 6.2 Data from Figure 6.1 shown with similiar data obtained from one continuous run

The same data run was repeated several times with R-134a to test for reproducibility. The results are shown in Figure 6.3, where the arrow indicates the direction of changing subcooling as the data were taken. It is clear that there is some variability in where the data starts (high subcooling), and how it proceeds as the subcooling is reduced. How the initial 25 °F of subcooling was reached was slightly different each time, even though a similar procedure was followed. If this accounts for the differences, it seems the mass flow rate for a given condition *is* in fact a function of the path taken to arrive at that state point.

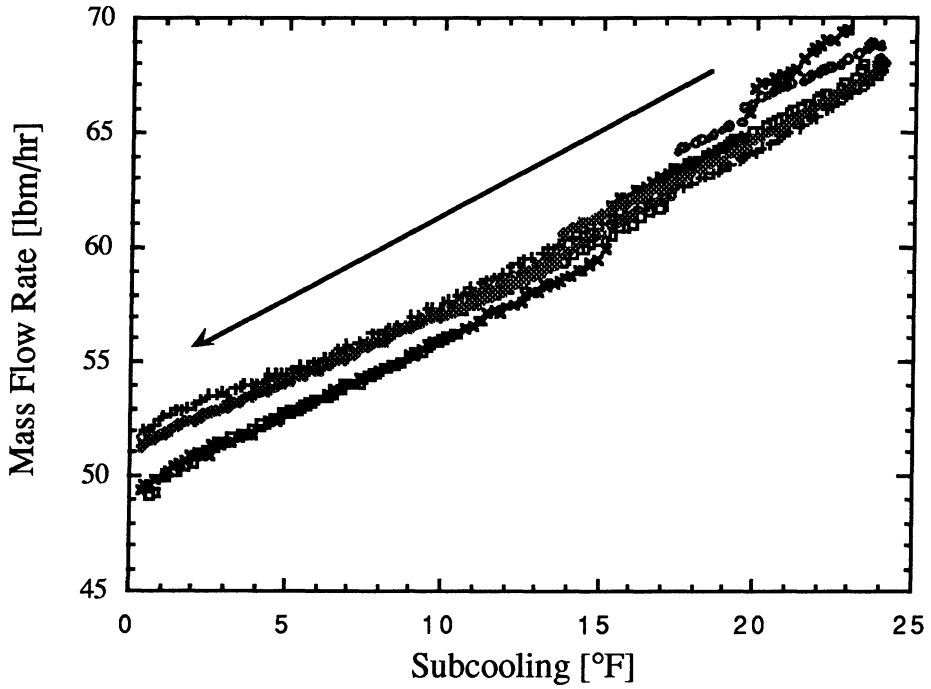

Figure 6.3 Many "identical" trials of R-134a flowing through the 0.049-in. capillary tube

For given condenser and evaporator pressures, the mass flow rate passing through a capillary tube is proportional to the length of the two-phase (or liquid, since the length of the tube is fixed) flow region. If, for example, the flash point moves towards the entrance of the tube (due to an increasing refrigerant inlet temperature decreasing the amount of subcooling at the inlet), the two-phase region will lengthen, resulting in a decreased mass flow rate. As the flash point moves towards the exit of the tube the length of the two-phase region decreases, and the mass flow rate increases. The question, then, is does the length of the liquid region depend on how the particular state point was reached?

To answer this question, we considered a capillary tube operating such that the refrigerant flashes when the pressure falls below the saturation value. In this case, there is no metastable region and the pressure and temperature in the tube will look something like the solid lines in

Figure 6.4. The x-axis represents the distance into the capillary tube and the y-axis is temperature. As a high pressure liquid refrigerant flows through an adiabatic capillary tube, its temperature remains constant while the pressure drops. As the pressure falls below the saturation value, the refrigerant may flash. From this point on, the actual temperature of the refrigerant is the saturation value, and thus the lines on the graph overlap.

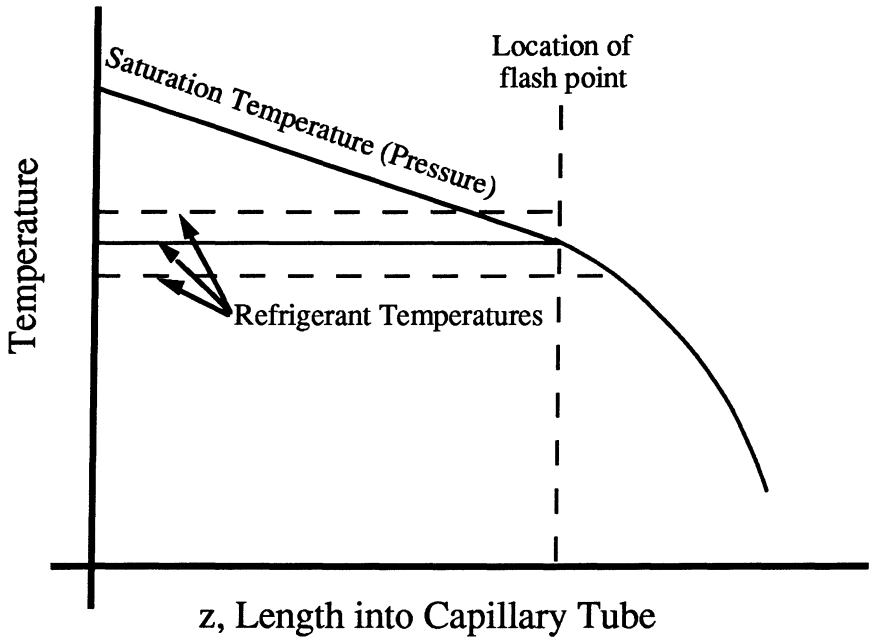

Figure 6.4 Typical temperature and pressure profile in an operating capillary tube

If the inlet refrigerant temperature were raised, reducing the amount of subcooling, the situation may become similar to the horizontal dashed line just above the solid line. In this case, it is possible for the onset of flashing to be delayed until the location of the previous nucleation site. If this occurs, a metastable region will be created, as is indicated on the graph by the dashed horizontal line to the right of the solid saturation temperature line.

If, however, the inlet refrigerant temperature is reduced, increasing the amount of subcooling, the situation may become more like the lower dashed line. In this case, flashing cannot occur at the old flash point because the liquid is sub-cooled at that location. Therefore, the flash point *must* move towards the exit of a capillary tube as the inlet flow is cooled.

If the above two hypotheses concerning heating and cooling the inlet flow of an operating capillary tube are correct, the location of the flash point in a capillary tube, and thus the mass flow rate, may in fact depend on how the particular state point was achieved.

To test this hypothesis, data "loops" were collected with R-134a, where the subcooling started at 25 °F, was reduced to zero (two-phase at the inlet was observed), and then was increased to 25 °F by cooling the SST. The first time this was performed, a double "loop" (25 °F subcooling

to 0 °F subcooling to 25 °F subcooling to 0 °F subcooling) was recorded over about eight hours. As shown in Figure 6.6, several interesting features become evident when the data are plotted. The arrows on the graph indicate the direction in which the subcooling was changing. The data show that the paths corresponding to the subcooling increasing and decreasing do in fact go through very different mass flow rates, forming a hysteresis curve. For this particular refrigerant-tube combination, the mass flow rate for a given state point while the subcooling is decreasing can be as much as 4 lbm/hr (8%) higher than the same conditions while the subcooling is increasing. This result is attributed to the fact that as the subcooling is decreasing, it is possible to create and lengthen a metastable region, in which liquid flow exists where it might otherwise be two phase. Because of the pressure drop resulting from liquid flow is much smaller than that of a two-phase mix, the mass flow rate is increased when a metastable region is present.

To check whether or not this result is an artificial creation due to the fact that the system was never truly at a steady-state condition, the SST was held at a constant temperature for 10-15 minutes during the second loop. If the hysteresis effect is a result of never achieving a steady-state condition, the mass flow rate will change slowly as time is spent at a constant amount of subcooling. As the graph shows, the mass flow rate does not change as a result of holding the SST temperature constant, indicating that steady state is in fact reached for each of the data points recorded. The steady-state check was performed on both the increasing and decreasing subcooling paths of the second loop, and can be seen clearly in Figure 6.5 at about 7 °F subcooling.

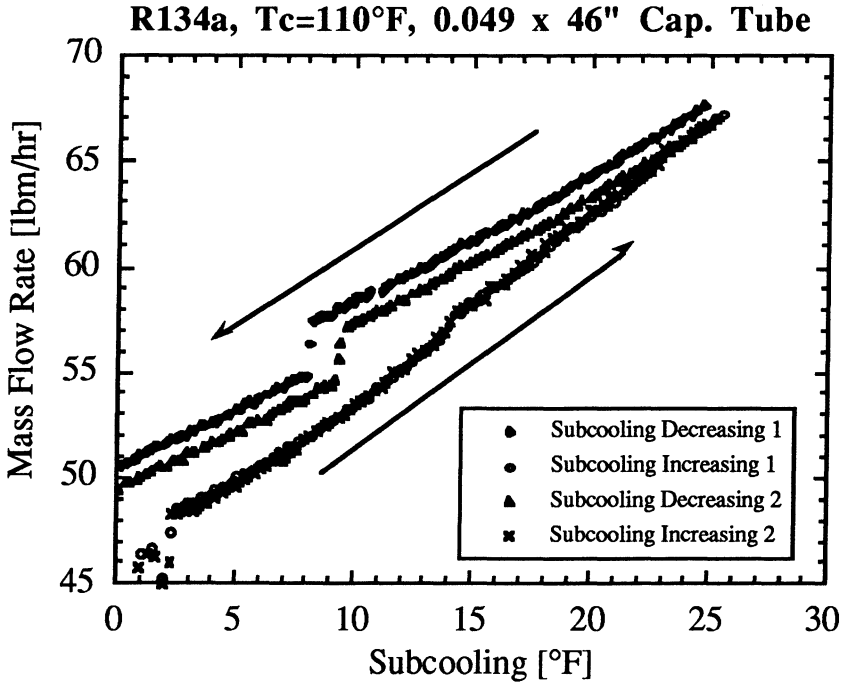

Figure 6.5 A double "loop," showing the hystersis effect resulting from increasing and decreasing the level of inlet subcooling

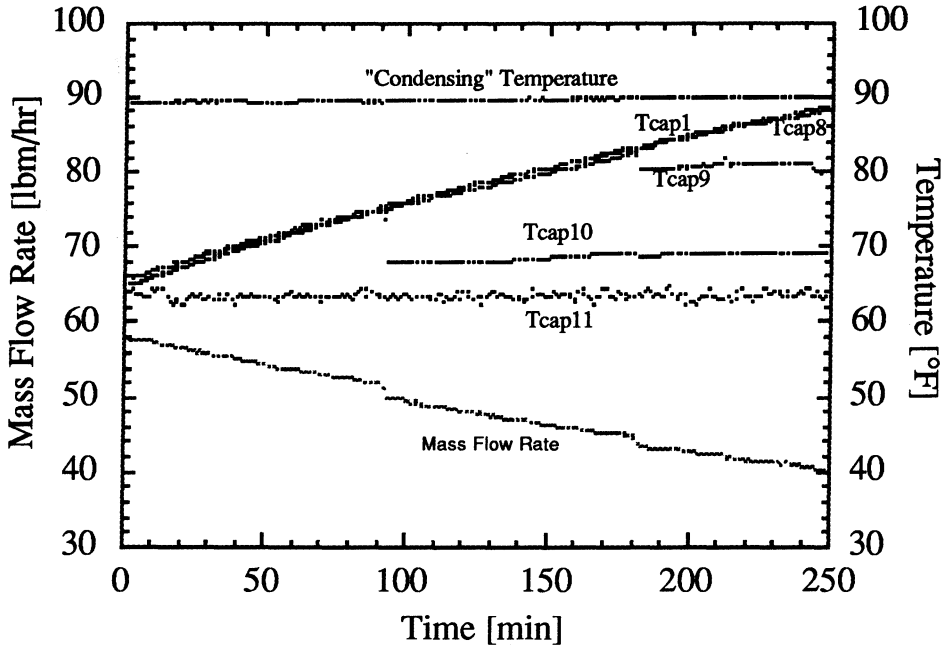

Figure 6.6 Mass flow rate and tube wall temperatures for R-134a flowing through the 0.049-in. capillary tube

Another interesting observation is that the decreasing subcooling lines do not overlap very well, but the increasing subcooling lines do. Because the initial state points for the two decreasing subcooling paths were arrived at differently, the resulting mass flow rates may differ. The increasing subcooling lines, however, overlap extremely well. The good agreement is due to the fact that the starting points were arrived at identically; two-phase at the capillary tube inlet with the subcooling increasing. Also of interest is the slopes of the two different paths. It is clear that the decreasing subcooling path has a much shallower slope that the increasing subcooling lines. This is consistent with the theory that the location of the flash point may not move as the subcooling is decreased, thus having a smaller affect on the change in mass flow rate. The question, then, is which scenario most resembles an actual vapor-compression system?

When a vapor-compression system shuts down, the evaporator is the coldest point in the system and the condenser is among the warmest. Hence, at shut-off, the charge tends to migrate to the evaporator, leaving vapor in the condenser. At start-up, the vapor from the condenser is forced through the capillary tube. As the high-side pressure increases, the condenser begins to liquefy portions the flow. Therefore, at start-up, first vapor, then two-phase, and finally liquid flow is present at the inlet of an operating capillary tube. For this reason all of the data presented here were taken in an increasing subcooling condition, always starting with two-phase at the inlet and

cooling the SST until 25 °F of subcooling was attained. To gather more information on the hysteresis behavior for other refrigerants, "loop" data were obtained for every refrigerant/tube combination at 110 °F. Also, for the case of R-22 flowing through the 0.049-in. capillary tube, "loops" were obtained at all three inlet pressures.

6.1.1 Wall Temperature Measurements

To record the capillary tube's temperature profile, early studies were completed with 36-gage, Type-T thermocouples epoxied to the tube every 4.5 in. A typical graph, including wall temperature measurements, is shown in Figure 6.6. For clarity of presentation, the axes of this graph are different than the axes of earlier ones. During this time the data were still being recorded while decreasing the amount of inlet subcooling. "Tcap1" measured the tube wall at the inlet, "Tcap11" at the exit, "Tcap10" 4.5 in. upstream from the exit, etc. Discontinuities in the mass flow rate occur at about 80, 175, and 245 min. into the run. If these discontinuities are the result of the flash point jumping, and a thermocouple happened to be located in an area that was jumped over, a dramatic temperature drop is expected as the flow at that location goes from single-phase liquid to two-phase. As the graph shows, appropriate thermocouples do in fact drop in temperature.

It was too hard to believe that the thermocouples were placed in exactly the right places to catch each jump. To test this, another thermocouple, "Tcap9.5," was added. The data run was repeated and is shown in Figure 6.7. The new data set has many discontinuities that were not present before the additional thermocouple was added. It looks as though, for example, the flash point oscillated around "Tcap9.5." Both the refrigerant mass flow rate and the temperature of "Tcap9.5" fluctuate with each other perfectly. Might this be more evidence for capturing a metastable jump? Or is the presence of the epoxy bead and/or a thermocouple wire somehow affecting the flow?

To investigate the possibilities further, liquid crystal paint was used to observe the wall temperature of the tube while recording data. All of the epoxy was removed before painting a tube with liquid crystals sensitive to temperatures between 84 °F and 92 °F. When the liquid crystals are in this temperature range, they turn blue, green, white, or red, depending on what temperature they are. Three small epoxy beads, without thermocouple wires, were placed on the tube in an area where the jumps were thought to occur. While the same flow conditions were repeated, the capillary tube was video-taped. The resulting video clearly shows a sharp temperature gradient move upstream as the subcooling was decreased. The color bands, which indicate temperature, seem to get "stuck" just downstream of the epoxy bead. After pausing for a while, the color bands quickly move to the upstream side of the epoxy bead, indicating an abrupt change in the location of the flash point.

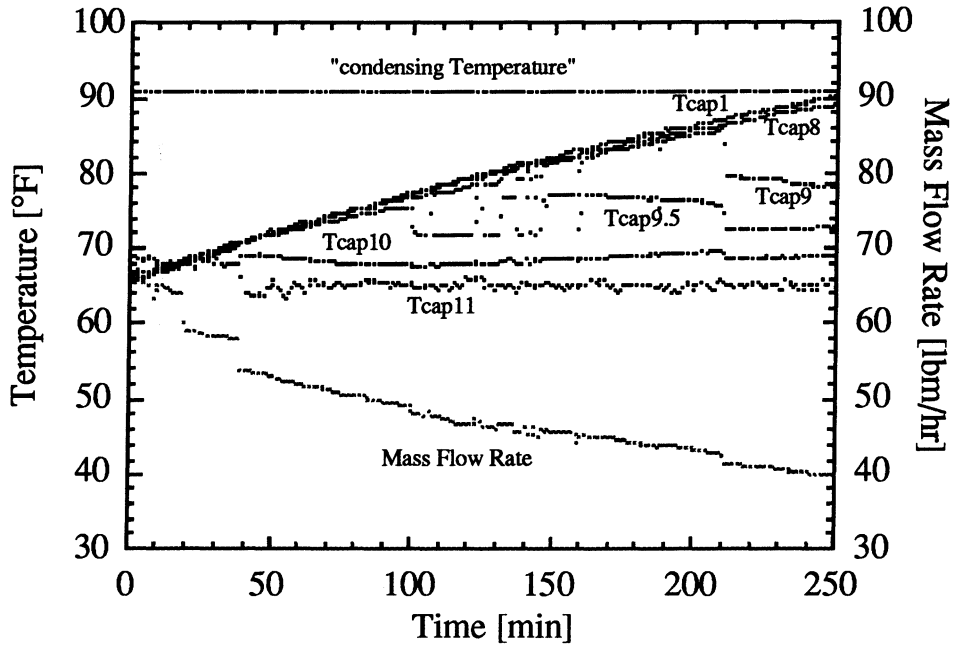

Figure 6.7 The effect on mass flow rate resulting from an additional wall temperature measurement (Tcap9.5)

These results indicate that the placement of epoxy beads does in fact affect the performance of a capillary tube. Due to the thin walls, imbedding the thermocouples in the capillary tube wall is impossible. Because the best possible mass flow rate measurements were of interest, all of the wall thermocouples and residual epoxy were removed before data were collected.

The nature of the relationship between the epoxy beads and the jumps in mass flow rate remains a mystery. It has been speculated that the epoxy may act as a fin, increasing heat transfer with the surroundings and increasing longitudinal conduction. Also, the epoxy may act as a relatively large thermal reservoir, requiring extra cooling as the two-phase regime moves past it. Further studies, involving specific "epoxy bead" tests, will be required to determine the epoxy/mass flow rate interaction.

6.1.2 Pressure Measurements along the Capillary Tube

Because pressure taps also have the ability to affect the mass flow rate, only the pre and post test section pressures were measured. It is believed that pressure taps provide excellent nucleation cites, and therefore may reduces the length of the metastable region, resulting in lower mass flow rates. Melo, *et al.* (1995) examined the effect pressure taps have on the mass flow rate. The same tube was tested before and after having pressure taps installed. They found that the presence of pressure taps reduced the mass flow rate by about 6%. There is a fair amount of scatter in the data, but on average, the capillary tube with pressure taps delivers lower flow rates. With or without

pressure taps, they conclude that "the underpressure of vaporization has a random behavior for the same operating conditions." It is believed that the "random" behavior they, and other capillary tube researchers have observed may be nothing more than a dependence on the path taken to achieve each particular state point. We have found that the mass flow rate as a function of subcooling and tube parameters is very reproducible, as long as the data are obtained in an appropriate manner.

6.2 Length of the Metastable Regions

The capillary tube data are presented on nine graphs, each one representing three condensing temperatures for each refrigerant and tube combination.

When looking at Figures 6.8 through 6.19, it becomes clear that for a given amount of subcooling, a range of possible mass flow rates exists. For example, in Figure 6.10, for the case of 90 °F condensing temperature, there are three different mass flow rates at about 15 °F of subcooling. The lowest one corresponds to no metastable region, the highest one corresponds to the longest metastable region, and the intermediate value results from a collapse of the longest metastable region to a that of a smaller value. It is important to recognize that at a given level of inlet subcooling the mass flow rate may be any value between those corresponding to no metastable region and the maximum possible metastable region.

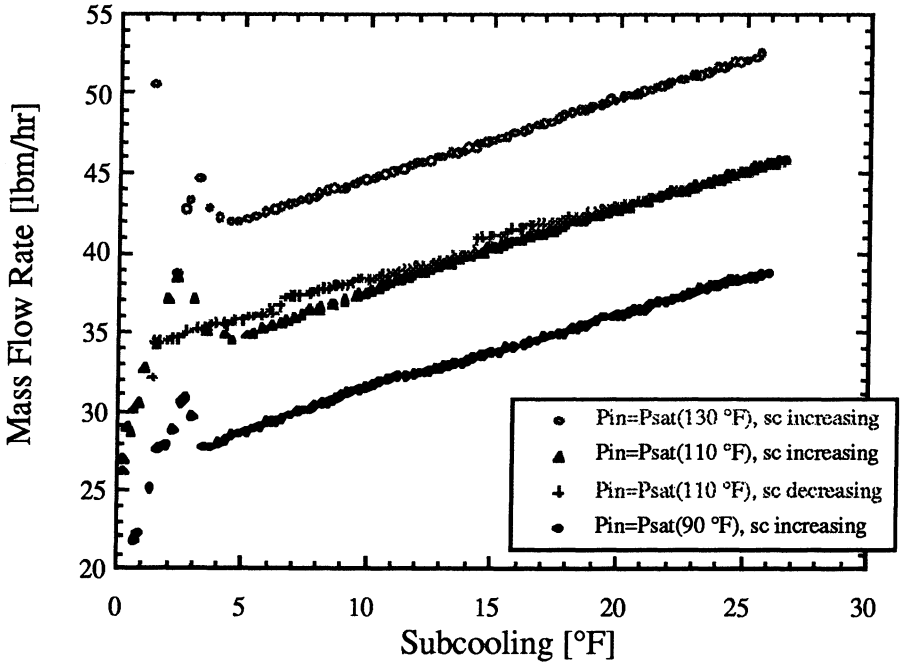

Figure 6.8 R-22 flowing through the 0.039-in. capillary tube

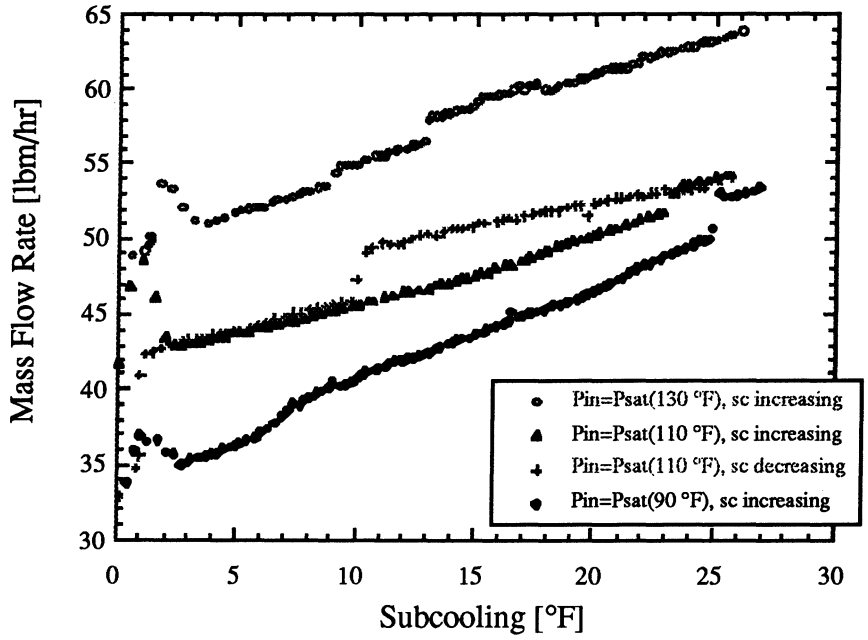

Figure 6.9 R-22 flowing through the 0.042-in. capillary tube

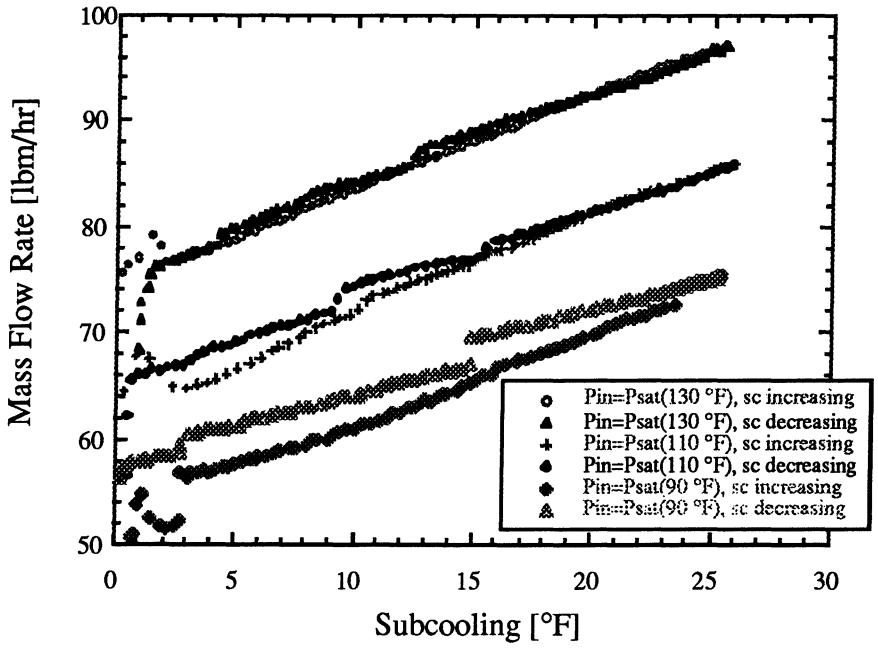

Figure 6.10 R-22 flowing through the 0.049-in. capillary tube

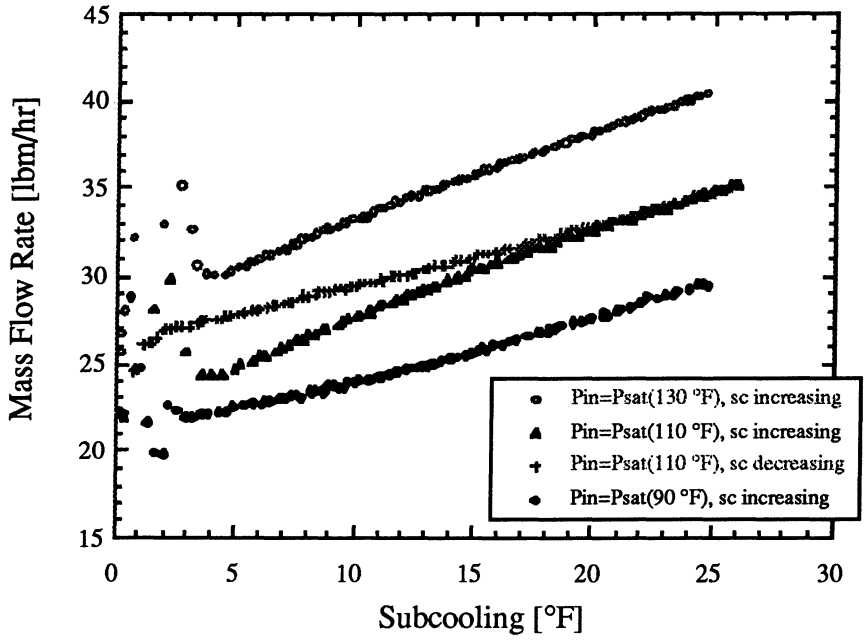

Figure 6.11 R-134a flowing through the 0.039-in. capillary tube

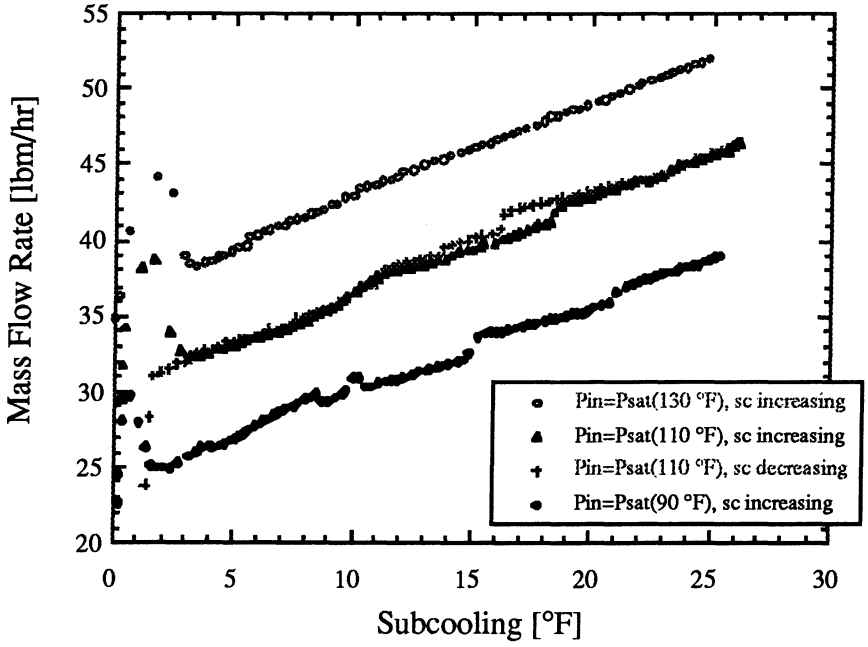

Figure 6.12 R-134a flowing through the 0.042-in. capillary tube

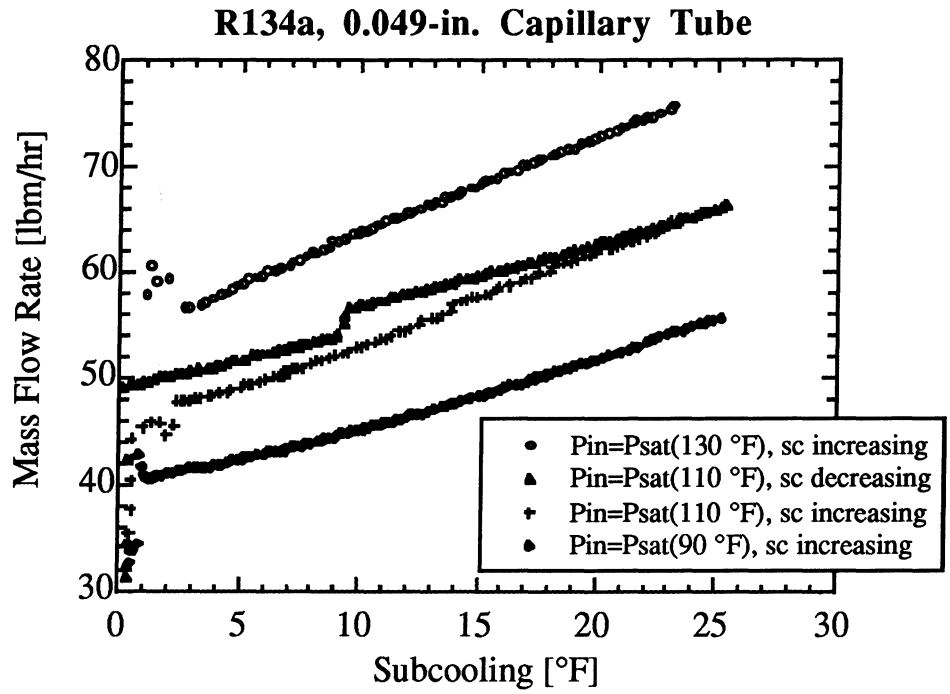

Figure 6.13 R-134a flowing through the 0.049-in. capillary tube

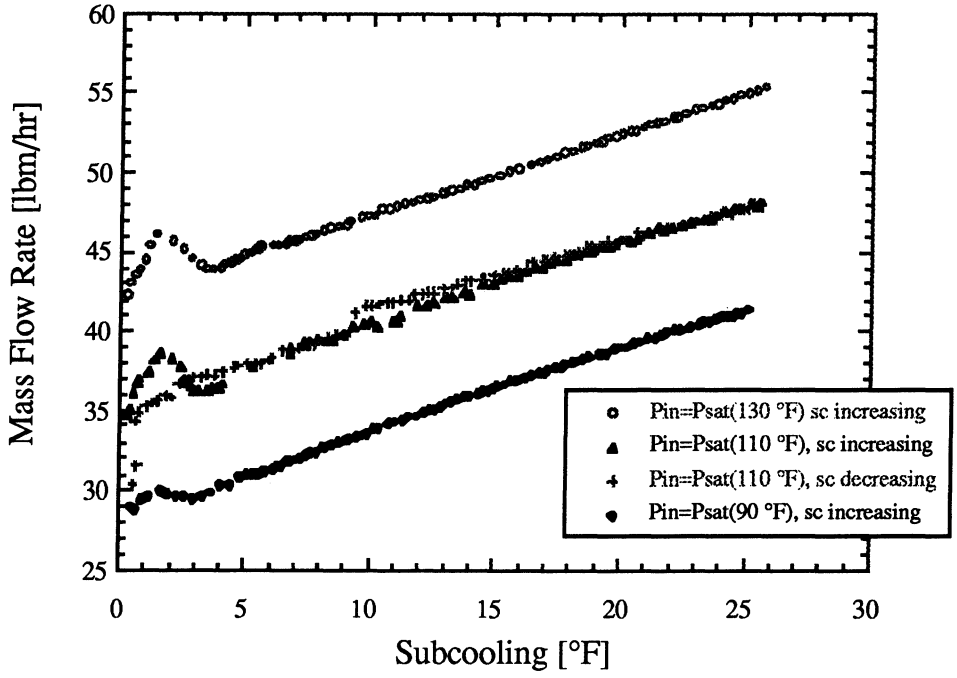

Figure 6.14 R-407C flowing through the 0.039-in. capillary tube

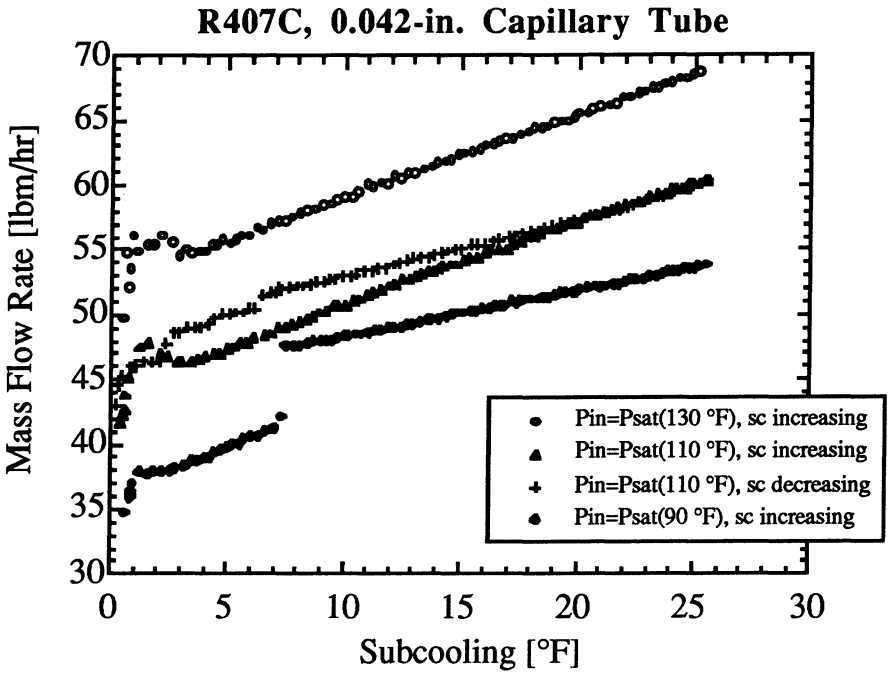

Figure 6.15 R-407C flowing through the 0.042-in. capillary tube

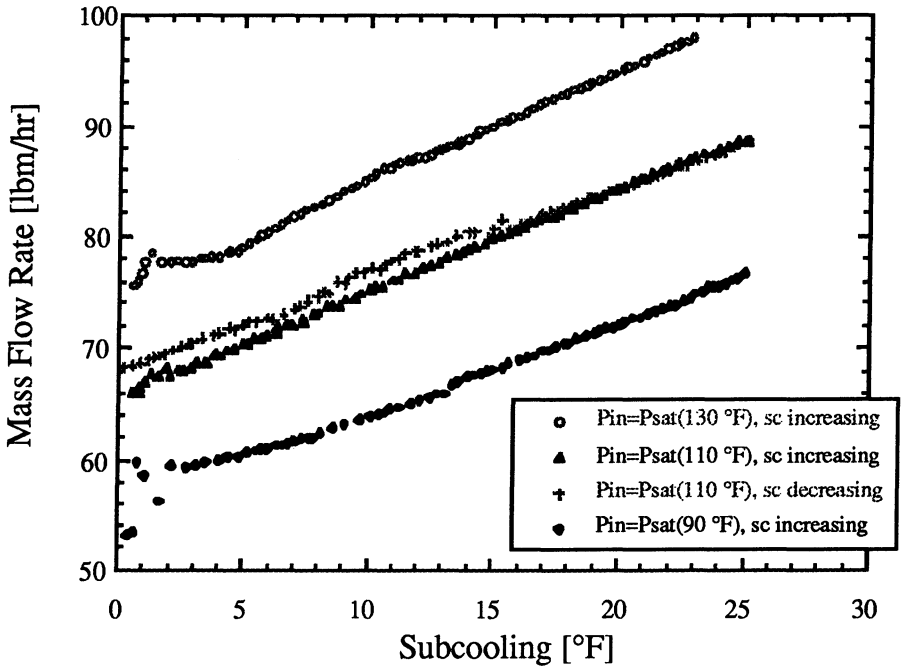

Figure 6.16 R-407C flowing through the 0.049-in. capillary tube

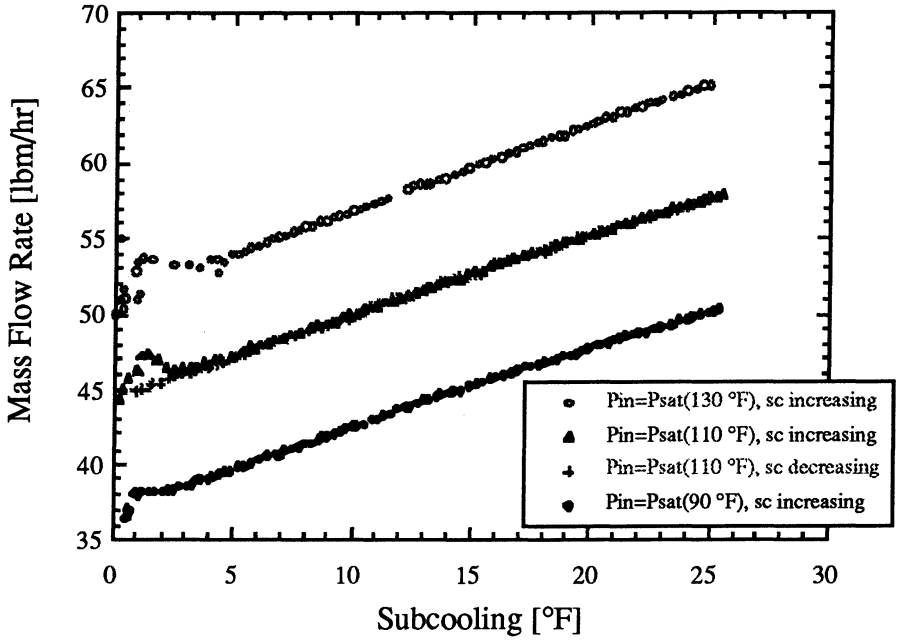

Figure 6.17 R-410A flowing through the 0.039-in. capillary tube

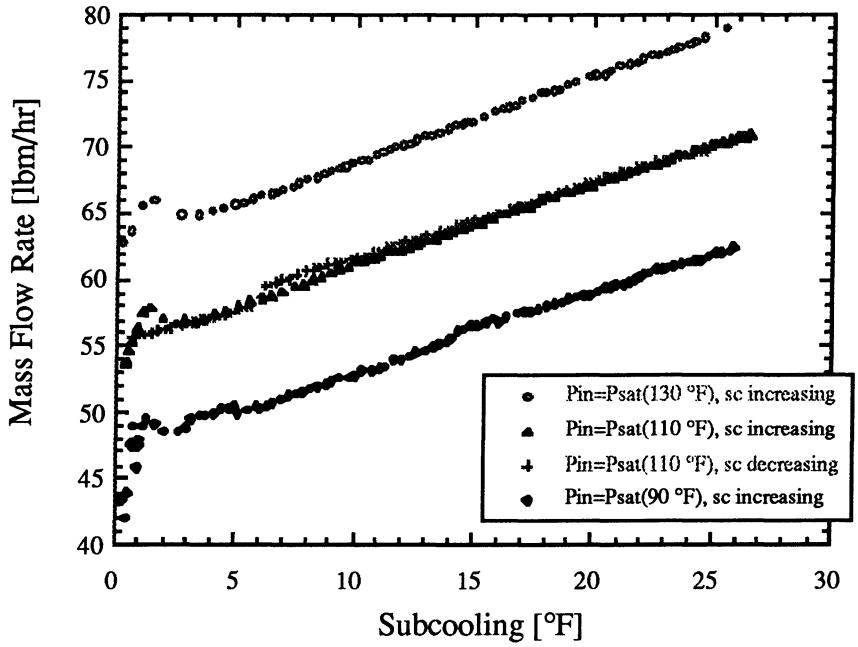

Figure 6.18 R-410A flowing through the 0.042-in. capillary tube

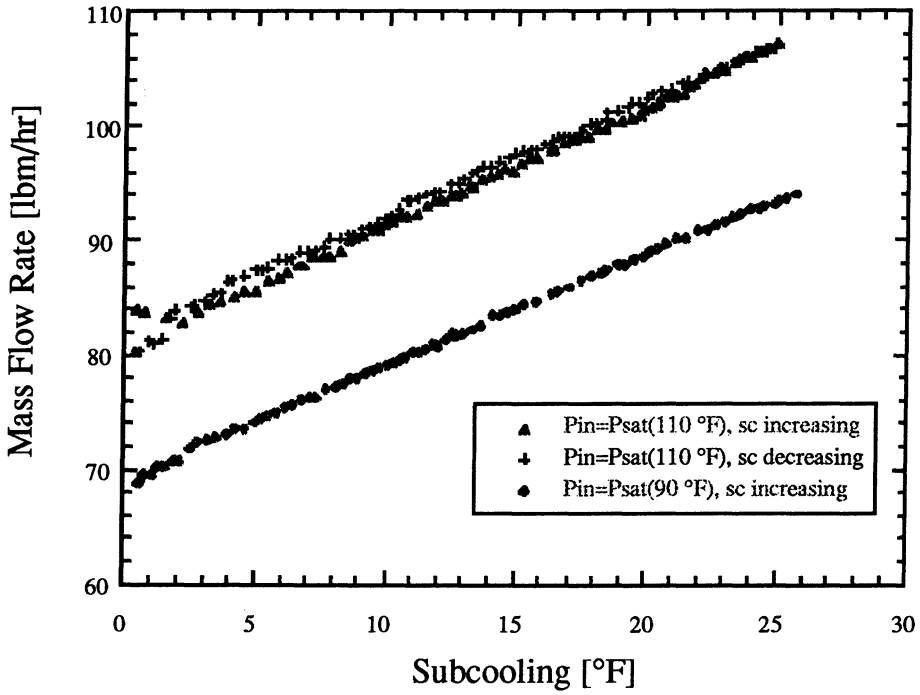

Figure 6.19 R-410A flowing through the 0.049-in. capillary tube

To estimate the lengths of the metastable regions, a capillary tube model developed at the University of Illinois is used to estimate the liquid and two phase lengths under various flow conditions. Because the model does not allow for a metastable region, the length of the metastable region is approximated in the following way: First, the model is used to generate curves that predicted the liquid lengths and mass flow rates as a function of inlet subcooling. Then, from the actual data, the three mass flow rates that occurred at a given amount of subcooling are used to calculate the liquid length of the lowest mass flow rate (no metastable region) and the "equivalent" amount of subcooling required to obtain the two higher mass flow rates. From the equivalent subcooling values, appropriate liquid lengths are calculated. When these three liquid lengths are compared, the difference between the shortest and the longest corresponds to the longest metastable region, and therefore the highest mass flow rate. The length of the metastable region after the collapse is taken to be the difference between the liquid length resulting from the intermediate mass flow rate and the shortest liquid length.

For the case referred to above, R-22 flowing through a 0.049-in. capillary tube, the metastable region was found to collapse from about 8.3 in. to about 5.9 in., causing the mass flow to decrease to 67.3 lbm/hr from 70.3 lbm/hr. The "no metastable region" mass flow rate is 66.0 lbm/hr for 14.9 °F of subcooling. For a similar jump that occurred within the R-134a data set in

the 0.049-in. tube at about 9 °F of subcooling, the metastable region collapsed from about 10.3 in. to about 5.9 in. The effect on mass flow rate was a reduction from 57.2 lbm/hr to 54.7 lbm/hr. The lowest mass flow rate for 9.4 °F of subcooling is 52.9 lbm/hr .

Although there is some randomness surrounding when a jump occurs and how much the metastable region is reduced, an attempt was made to quantify the results. Comparisons are made between the maximum length of the metastable region and the rate of depressurization, dP/dz. Table 6.1 shows the inlet pressures for the four refrigerants, corresponding to the saturation temperatures of 90 °F, 110 °F, and 130 °F. R-410A has the highest saturation pressure at a given temperature, R-134a the lowest. Table 6.2 lists the mass flow rates for 10 °F of inlet subcooling for the various "condensing temperatures." Because the mass flow rate is a function of inlet subcooling, a single level of subcooling (10 °F) was chosen to facilitate comparisons across refrigerants, pressures, and tube diameters. The mass flow rates were obtained from the "no-metastable-region" data sets.

Table 6.1 Capillary tube inlet pressures for the four refrigerants tested

Refrigerant	Psat (90 °F) [psia]	Psat (110 °F) [psia]	Psat (130 °F) [psia]
R-22	183.2	241.1	311.6
R-134a	119.0	161.1	213.4
R-407C	208.5	274.2	353.8
R-410A	288.3	378.0	486.5

Table 6.2 Capillary tube mass flow rates at 10 °F of subcooling for the four refrigerants tested.

Tsat [°F]	ID [in.]	Flow Rate of R-22 [lbm/hr]	Flow Rate of R-134a [lbm/hr]	Flow Rate of R-407C [lbm/hr]	Flow Rate of R-410A [lbm/hr]
90	0.039	32	22	33	42
110	0.039	37	27	39	49
130	0.039	44	33	47	57
90	0.042	40	29	43	52
110	0.042	45	36	51	61
130	0.042	54	43	59	69
90	0.049	60	41	62	78
110	0.049	70	51	74	92
130	0.049	83	63	85	-

Table 6.3 shows the rates of depressurization in the liquid region for the mass flow rates from Table 6.2 These values were obtained form a simple liquid-phase pressure drop equation. As the tables show, the higher the inlet pressure, the higher the mass flow rate and depressurization rate. When looking at both Table 6.3 and Figures 6.8 through 6.19, it becomes apparent that the higher the rate of depressurization, the less the mass flow rate is affected by a metastable region. This trend is found when examining the hysteresis effects of the high and low mass flow rates (corresponding to high and low inlet pressures) for a single tube, as shown in Figure 6.10. This trend also becomes evident when comparing the hysteresis effect resulting from a high and low pressure refrigerant, as shown in Figures 6.19 (high pressure - R407C) and 6.13 (low pressure - R-134a).

Table 6.3 Depressurization rates in the liquid region at 10 °F of subcooling for the four refrigerants tested.

Tsat [°F]	ID [in.]	dP/dz [psi/ft] R-22	dP/dz [psi/ft] R-134a	dP/dz [psi/ft] R-407C	dP/dz [psi/ft] R-410A
90	.039	12.0	6.2	13.0	19.6
110	.039	15.5	9.3	17.5	26.6
130	.039	21.4	13.4	24.6	34.5
90	.042	12.5	7.6	14.8	20.5
110	.042	15.5	11.1	20.1	27.6
130	.042	21.7	15.0	26.3	34.7
90	.049	12.1	6.4	13.4	19.8
110	.049	16.0	9.7	18.3	26.6
130	.049	21.9	14.3	23.7	-

Figure 6.10 shows the only "loop" data taken at temperatures other than 110 °F. The mass flow rates along the increasing and decreasing subcooling lines nearly overlap for the highest inlet pressure. For the lowest inlet pressure, however, a much larger deviation between the mass flow rates at a given level of subcooling exists. Comparing across refrigerants, R-410A has a much higher saturation pressure than R-134a, which leads to higher mass flow rates and a steeper pressure gradient in the liquid region. When comparing the hysteresis curves in figures 6.11 to 10 13 (R-134a) to those in figures 6.17 through 6.19 (R-410A), it is clear that the mass flow rate of R-134a exhibits a much greater hysteresis effect.

In an attempt to quantify the maximum length of the metastable region, the relationship that relates underpressure to critical bubble radius, Equation 6.1, was examined. It is believed that the

wall roughness acts as nucleation sites, and therefore the height of the roughnesses may correspond to the critical bubble radius. From the rate of depressurization and the length of the maximum metastable region, the maximum amount of underpressure ($P_{sat} - P$) at the nucleation

$$P_{sat} - P = \frac{2\sigma}{r_{cr}} \qquad (6.1)$$

point is calculated. Equation 6.1 is then used to calculate the critical bubble radius. The maximum metastable region exists immediately preceding its collapse. This condition is indicated in Figures 6.8 to 6.19 by a sudden jump in the mass flow rate as the level of subcooling is decreasing. Figure 6.10 shows three loops for R-22, each of which contains two jumps, or indications of the metastable region collapsing. These six events were analyzed in an attempt to predict the wall roughness. The results for this analyses are shown in Table 6.4.

Although the roughness values shown in Table 6.4 are somewhat consistent, they are about an order of magnitude higher than accepted values. Part of the problem is due to the approximations associated with determining the liquid lengths corresponding the minimum and maximum metastable regions, but something else is contributing to the error.

Table 6.4 Calculated critical bubble radius and resulting relative roughness from metastable region data for R-22 in a 0.049-in. ID tube

Inlet Pressure [psia]	Critical Radius [ft]	Relative Roughness [-]
183.2	5.93×10^{-6}	.00145
183.2	7.64×10^{-6}	.00187
241.1	3.17×10^{-6}	.00077
241.1	3.54×10^{-6}	.00087
311.6	4.95×10^{-6}	.00121
311.6	6.00×10^{-6}	.00147

Although jumps in the mass flow rate are understandable while the inlet subcooling is decreasing (thus lengthening the metastable region), several jumps, which raised the mass flow rate, were observed while increasing the inlet subcooling. In order for this to occur, a metastable region has to be created where previously two-phase flow existed. The best examples of this are shown in Figures 6.10 and 6.15, for the lowest inlet pressure.

For the lowest inlet pressure in Figure 6.10 the mass flow rate increases sharply from 52 lbm/hr to 57 lbm/hr. After this jump the curve seems to be concave up, whereas for other "increasing subcooling" curves seem to be concave down. It is believed that once the metastable region is created, it is slowly destroyed as the subcooling is increased. This particular configuration was run many times the day after the original data were taken. The results are shown

in Figures 6.20a and 6.20b. Figure 6.20a shows the original data plotted along with two additional data sets, while Figure 6.20b magnifies the same data by changing the axes. Figures 6.21a and 6.21b show similar results for R-407C flowing through a 0.042-in. capillary tube at the lowest inlet pressure. This time, as Figures 6.21a and 6.21b show, three additional re-starts were attempted.

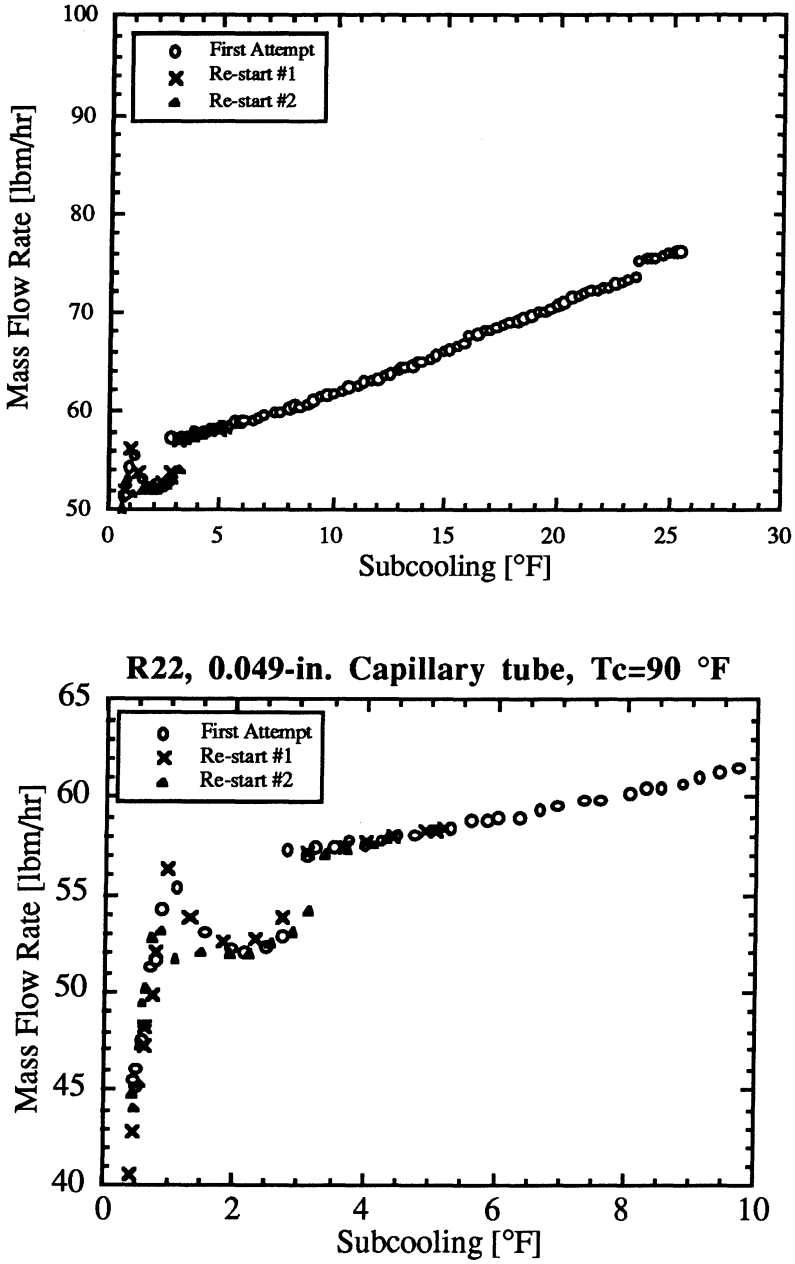

Figure 6.20a&b Mass flow rates from three different attempts to record data for R-22 flowing through the 0.049-in. capillary tube. Figure "b" shows the same data plotted on an expanded scale

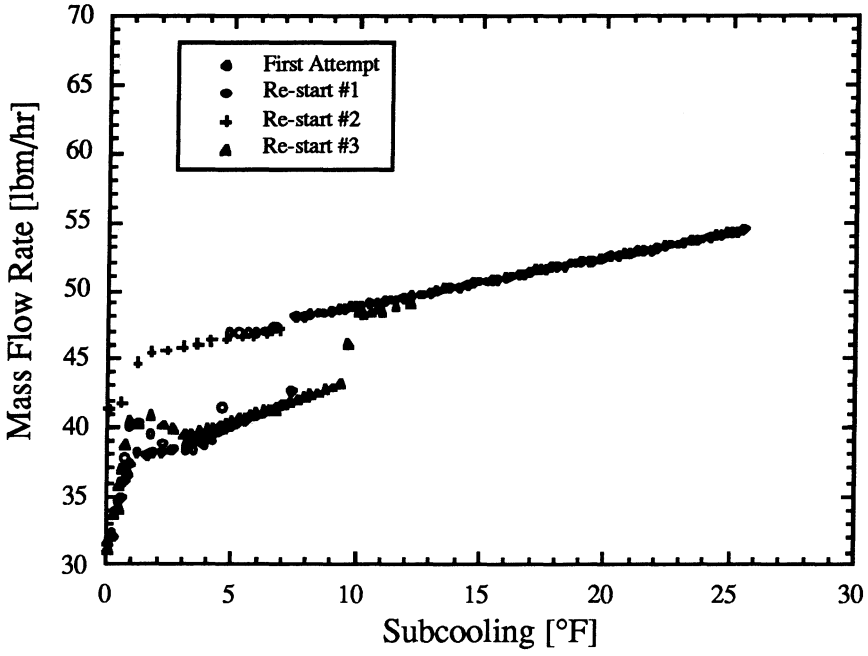

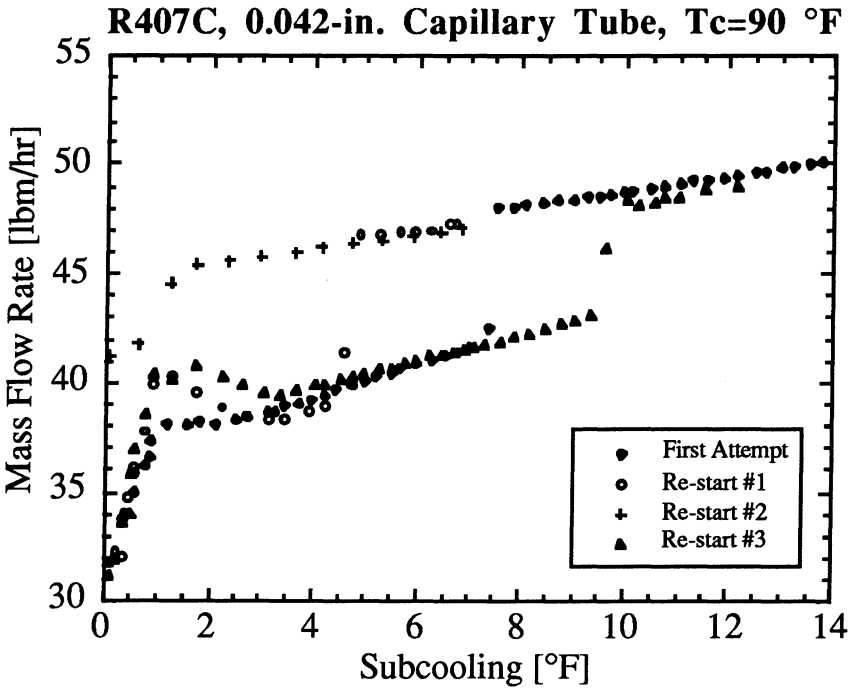

Figure 6.21a&b Mass flow rates from three different attempts to record data for R-407C flowing through the 0.042-in. capillary tube. Figure "b" shows the same data plotted on an expanded scale

But how can a metastable region be created where once two-phase flow existed? If the pressure is at or below the saturation value, and vapor bubbles with large enough diameters exist, the mixture will remain two phase. If no metastable region exists, nucleation begins at the location where the pressure drops below the saturation value. In this instance, the size of the nucleation site may be approximately equal to the critical diameter necessary for bubbles to grow. If a pressure fluctuation increases the local pressure at the nucleation site enough to condense the vapor bubbles, the nucleation cite may be extinguished. The liquid flow will then continue downstream until a suitable nucleation site is found, thus creating a metastable region. The data indicate that this newly formed metastable region is destroyed as the level of subcooling is increased.

The additional re-starts shown Figures 6.20 and 6.21 show that the "random" behavior of capillary tubes, although not well understood, may be much more predictable than many researches believe. Similar increases in mass flow rate can be seen in some of the low inlet pressure data, especially for R-134a, the refrigerant with the lowest rate of depressurization.

Chapter 7

Conclusions and Recommendations

The experimental facility constructed for this work allows data to be taken in a new and informative way. Using well mixed, thermally controlled tanks to set the high side pressure and refrigerant inlet temperature, new insights into the "random" behavior of the metastable region have been revealed for the first time.

7.1 Conclusions and Implications

We found that the refrigerant mass flow rate through a capillary tube is not simply a function of tube dimensions, condensing pressure, and inlet subcooling, but also depends, quite systematically, on the path taken to get to each particular state point. The implications of this finding are far reaching. For a given level of subcooling, there is a *range* of possible mass flow rates, not just one correct value. Therefore, when attempting to correlate mass flow rate data with a single curve, there will always be a tremendous amount of scatter in the data. This scatter, however, is not from noise in the data, but rather represents the range of possible values.

Before mass flow rate data may be evaluated correctly, information concerning how the level of subcooling was attained is necessary. If the level of inlet subcooling was increasing for an appreciable time, there will most likely be little or no metastable region, and a lower mass flow rate will result. If, however, the condition was achieved by decreasing the level of inlet subcooling, an appreciable metastable region may exist, thus increasing the mass flow rate. The length of metastable region depends on many things, including the internal roughness of the tube and rate of depressurization. For this reason, instead of concentrating on defining *the* mass flow rate associated with a level of subcooling, efforts will be better rewarded if the minimum and maximum mass flow rates, corresponding to no metastable region and the longest maintainable metastable region, are investigated, with the understanding that any flow rate between the two is a realistic value.

Future researchers must be aware of the path dependent nature of the mass flow rate. If researchers continue to neglect this effect, the resulting data will continue to show large amounts of scatter. The existing pool of data may be re-analyzed, searching not for a single mass flow rate correlation, but rather for the range of possible mass flow rates. Because wall roughness is responsible for initial nucleation sites, it is believed that the maximum length of a metastable region can be correlated to the roughness of the tube as shown in Equation 6.1.

7.2 Suggestions for Future Research

Although this work offers insights into the nature of the metastable region, further work is necessary to fully understand the metastable phenomena. A study that examines the effect of tube roughness on mass flow rate would be very interesting. If the maximum length of the metastable region is predictable and a function of wall roughness, then the hysteresis effect observed here will decrease as the roughness increases. Rougher walls provide larger nucleation sites, and thus require less underpressure before the bubbles can grow.

If data can be obtained for several accurately-known roughnesses, it would become possible to correlate the maximum length of the metastable region with wall roughness, perhaps as shown in Equation 6.1. If this is proven to be true, a capillary tube with a very rough inner surface will not be able to support a metastable region, and will therefore have no hysteresis effect. The mass flow rate of such a capillary tube will be very predictable, removing much of the uncertainty associated with sizing capillary tubes.

Finally, it is postulated here that the capillary tube in an actual vapor-compression system operates in an increasing subcooling fashion, and thus should have predictable mass flow rates corresponding to minimal metastable lengths. At present, however, no data has been obtained that include these considerations. Checking for mass flow rate hysteresis effects in an operating vapor-compression system is a way to prove or disprove this theory.

References

Battelle Memorial Institute, Ohio 1960 "Analysis of the Potentialities of Using Analog Computers in the Development of Residential Refrigerators (Phase 1)," Report to Whirlpool Corporation by Ungar, Stein, Boyd and Beck.

Bolstad, M.M. and R.C. Jordan. 1948. "Theory and Use of the Capillary Tube Expansion Device." *Journal of the ASRE - Refrigerating Engineering* (December), 519-523.

Bolstad, M.M. and R.C. Jordan. 1949. "Theory and Use of the Capillary Tube Expansion Device." *Journal of the ASRE - Refrigerating Engineering* (June), 577-583.

Chen, S.L., F.M. Gerner, and C.L. Tien. 1987. "General Film Condensation Correlations." *Experimental Heat Transfer* 1: 93-107.

Chen, Z.H. et al. 1990. "A Correlation For Metastable Flow of Refrigerant 12 Through Capillary Tubes." *ASHRAE Transactions*, 96(1), 550-554.

Cooper, L., C.K. Chu, and W.R. Brisken. 1957. "Simple Selection Method for Capillaries Derived from Physical Flow Conditions." *Journal of the ASRE - Refrigerating Engineering* (July), 37-41+.

Erth, R.A., 1970: "Two-Phase Flow in Refrigeration Capillary Tubes: Analysis and Prediction." Ph.D. Thesis, Purdue University.

Fauske, H.K., 1962: "Contribution to the Theory of Two-phase, One-component Critical Flow." ANL-6633, Argonne National Laboratory.

Hirt, C.W., T.A. Oliphant, W.C. Rivard, N.C. Romero, and M.D. Torrey, 1979. "Sola-Loop: A Nonequilibrium, Drift-Flux Code for Two-Phase Flow in Networks." *Report of U.S. Nuclear Regulartory Commision*, NUREG/CR-0626 LA-7659 R-4, pp.1-44.

Hopkins, N.E. 1950. "Rating the Restrictor Tube: Method of Determining Flow Capacities For Freon-12 and Freon-22." *Journal of the ASRE - Refrigerating Engineering* (November), 1087-1094.

Jones, O.C., Jr. 1980. "Flashing Inception in Flowing Liquids." *ASME Transactions - Journal of Heat Transfer*, 102 (August), 439-444.

Koizumi, H. and K. Yokoyama. 1980. "Characteristics of Refrigerant Flow in a Capillary Tube." *ASHRAE Transactions*, 86, 19-27.

Kuijpers, L. J.M. and M.J.P. Janssen. 1990. "Influence of Thermal Non-Equilibrium on Capillary Tube Mass Flow." *IIR Purdue Conference*, 689-698.

Lahey, R.T. and Moody, F.J., 1977: "The Thermal-Hydraulics of a Boiling Water Nuclear Reactor." *American Nuclear Society.*

Levy, S. 1964: "Prediction of Two-phase Critical Flow Rate." *ASME Journal of Heat Transfer*, Vol. 87 (Feb): 53-58

Li, R.Y., S. Lin, and Z.H. Chen. 1990. "Numerical Modeling of Thermodynamic Non-Equilibrium Flow of Refrigerant Through Capillary Tubes." *ASHRAE Transactions*, 96(1), 542-549.

Marcy, G.P. 1949. "Pressure Drop with Change of Phase in a Capillary Tube."*Journal of the ASRE - Refrigerating Engineering*, 53-57.

McAdams, W.H. "Heat Transmissions", NYC, McGraw Hill Book Co., 1933.

Melo, C, R.T.S Ferreira, C. Boabaid Neto, and J.M. Goncalves. 1995. "Measuring Pressure and Temperature Profiles Along Capillary Tubes." *Proceedings of the 19th International Congress of Refrigeration*, 3, 146-153.

Mikol, E.P. 1963. "Adiabatic Single and Two-Phase Flow in Small Bore Tubes" *ASHRAE Journal* (November), 75-86.

Mikol, E.P. and J.C. Dudley. 1964. "A Visual and Photographic Study of the Inception of Vaporization in Adiabatic Flow." *ASME Transactions - Journal of Basic Engineering* (June), 257-264.

Miller, D.S. 1978. "Flow Performance of Piping Systems," Fluid Dynamics Engineering Short Course No. 78-2, Thayer School of Engineering, Dartsmouth College, (Aug. 28-Sept. 1, 1978).

Moody, L.F. 1944. "Friction Factors for Pipe Flow." *ASME Transactions,* 66: 671-684.

Moody, F.J., 1968: "The Pressure Pulse Model for Two-phase Critical Flow and Sonic Velocity." G.R. Rpt. No. APED-5579.

Pate, M.B. 1982. "A Theoretical and Experimental Analysis of Capillary Tube-Suction Line Heat Exchangers." Ph.D. Thesis, Purdue University.

Pate, M.B. and D.R. Tree. 1987. "An Analysis of Choked Flow Conditions in a Capillary Tube-Suction Line Heat Exchanger." *ASHRAE Transactions*, 93(1), 368-380.

Scott, T. C. 1976. "Flashing Refrigerant Flow in Small Bore Tubes." Ph.D. Thesis, The University of Michigan.

Semenov, N.I. and Kosterin, S.I., 1964: "Results of Studying the Speed of Sound in Moving Gas-Liquid Systems." *Thermal Engineering*, Vol. 6, p.59.

Smith, R.V., 1963: Some Idealized Solutions for Choking, Two-phase Flow of Hydrogen, Nitrogen, and Oxygen." Advances in CRYOGENIC ENG. Vol. 8, New York: Plenum.

Sweedyk, J.M. 1981 "Capillary Tubes - Their Standardization and Use." *ASHRAE Transactions,* 87, 1069-1076.

Transport Properties of SUVA® Refrigerants, ART-1. 1992. E.I. du Pont de Nemours and Co. Wilmington, DE.

Wallis, G.B. 1969 "One-Dimensional Two-Phase Flow." New York: McGraw Hill Book Company.

Wallis, G.B. 1980 "Critical Two-Phase Flow." *Int. J. Multiphase Flow*, 6, 97-112.

Wallis, G.B. 1982 "Review - Theoretical Models of Gas-Liquid Flows" *Journal of Fluids Engineering*, September 1982, Vol 104 pp 279-283.

Whitesel, H.A. 1957. "Capillary Two-Phase Flow." *Refrigerating Engineering* (April), 42-44, 98-99.

Whitesel, H.A. 1957. "Capillary Two-Phase Flow, Part II." *Refrigerating Engineering*, 35-40.

APPENDIX A

Mass Flow Rate Data

Table A1.1 Mass flow rate data for R22 in the 0.039-in. capillary tube.

Mdot	Tsat	Tsub	Mdot	Tsat	Tsub	Mdot	Tsat	Tsub	Mdot	Tsat	Tsub
50.62	130.27	1.37	26.14	110.49	0.19	45.80	110.18	26.58	21.77	89.96	0.66
38.74	130.02	2.32	26.98	110.43	0.23	45.68	110.21	26.41	22.30	89.96	0.86
42.67	129.84	2.64	29.01	110.37	0.37	45.58	110.12	26.12	25.15	89.96	1.26
43.30	129.50	2.80	28.70	110.31	0.51	45.38	110.15	25.85	27.56	89.96	1.56
44.74	129.47	3.17	30.09	110.21	0.61	45.31	110.15	25.55	27.86	89.96	1.86
42.75	129.55	3.55	30.44	110.15	0.85	45.14	110.12	25.22	28.76	89.96	2.16
42.23	129.71	4.01	32.67	110.09	1.09	45.01	110.15	25.05	30.61	89.96	2.46
41.97	129.76	4.46	34.26	109.93	1.53	44.90	110.09	24.69	30.85	89.96	2.66
42.01	129.86	4.76	37.04	109.78	1.98	44.77	110.09	24.39	29.57	89.96	2.96
42.09	129.91	5.11	38.50	109.62	2.32	44.58	110.09	24.09	27.74	89.96	3.36
42.27	129.91	5.41	37.05	109.81	3.01	44.39	110.09	23.79	27.75	89.96	3.66
42.54	129.99	5.79	35.11	109.87	3.47	44.35	110.09	23.49	28.01	89.96	3.96
42.70	130.07	6.17	34.82	110.12	4.22	44.16	110.06	23.16	28.23	89.96	4.26
42.92	130.07	6.47	34.55	110.06	4.56	44.07	110.03	22.83	28.40	89.96	4.56
42.99	130.07	6.77	34.82	110.25	5.15	43.97	110.09	22.59	28.52	89.96	4.86
43.13	130.09	6.99	34.99	110.15	5.35	43.84	110.00	22.30	28.68	89.96	5.16
43.25	130.07	7.27	35.18	110.25	5.75	43.78	110.06	22.06	28.90	89.96	5.46
43.44	130.02	7.52	35.46	110.21	6.11	43.63	110.06	21.76	28.99	89.96	5.66
43.55	130.02	7.82	35.57	110.25	6.45	43.53	110.00	21.50	29.26	89.96	5.96
43.69	129.99	7.99	35.78	110.28	6.68	43.38	110.00	21.20	29.36	89.96	6.16
43.85	129.99	8.29	35.87	110.28	6.98	43.28	110.03	20.93	29.43	89.96	6.36
44.04	129.99	8.59	36.17	110.31	7.31	43.26	110.03	20.73	29.50	89.96	6.56
44.00	129.99	8.89	36.36	110.28	7.58	43.09	110.03	20.43	29.79	89.96	6.86
44.16	129.96	9.06	36.45	110.37	7.97	43.01	110.03	20.23	29.98	89.96	7.16
44.33	129.99	9.39	36.64	110.25	8.05	42.88	110.00	19.90	30.11	89.96	7.46
44.48	129.96	9.56	36.79	110.40	8.50	42.87	110.03	19.73	30.14	89.96	7.66
44.54	129.96	9.86	36.91	110.31	8.61	42.74	110.00	19.40	30.31	89.96	7.86
44.68	129.94	10.14	37.03	110.43	9.03	42.71	110.03	19.23	30.42	89.96	8.16
44.80	129.94	10.34	37.14	110.28	9.08	42.52	110.00	19.00	30.56	89.96	8.36
44.89	129.91	10.61	37.34	110.43	9.53	42.50	110.00	18.70	30.66	89.96	8.56
45.06	129.91	10.91	37.50	110.28	9.58	42.36	110.00	18.50	30.82	89.96	8.76
45.21	129.89	11.09	37.49	110.40	9.90	42.26	110.03	18.23	31.03	89.96	8.96
45.27	129.91	11.41	37.71	110.28	10.08	42.26	110.00	18.00	31.18	89.96	9.16
45.47	129.89	11.69	37.83	110.40	10.40	42.13	110.00	17.80	31.29	89.96	9.36
45.63	129.89	11.89	37.99	110.31	10.61	41.98	110.03	17.53	31.44	89.96	9.66

Table A1.1 (cont.) Mass flow rate data for R22 in the 0.039-in. capillary tube.

Mdot	Tsat	Tsub	Mdot	Tsat	Tsub	Mdot	Tsat	Tsub	Mdot	Tsat	Tsub
45.69	129.86	12.16	38.14	110.31	10.81	41.95	110.00	17.30	31.49	89.96	9.96
45.82	129.86	12.46	38.23	110.37	11.07	41.84	110.03	17.03	31.77	89.96	10.26
46.05	129.84	12.74	38.30	110.28	11.28	41.81	110.03	16.83	31.86	89.96	10.46
46.05	129.81	12.91	38.54	110.31	11.51	41.67	110.00	16.60	31.99	89.96	10.76
46.22	129.84	13.24	38.66	110.31	11.71	41.70	110.03	16.43	32.08	89.96	10.96
46.29	129.78	13.48	38.70	110.34	12.04	41.59	110.03	16.13	32.21	89.96	11.16
46.38	129.81	13.71	38.88	110.28	12.18	41.50	110.06	15.96	32.25	89.96	11.56
46.61	129.76	13.96	38.97	110.21	12.41	41.43	110.03	15.73	32.29	89.96	11.86
46.63	129.76	14.26	39.13	110.31	12.71	41.27	110.03	15.43	32.42	89.96	12.06
46.80	129.73	14.43	39.31	110.25	12.85	41.17	110.00	15.20	32.45	89.96	12.26
46.95	129.73	14.73	39.39	110.15	13.05	41.10	110.03	15.03	32.58	89.96	12.46
47.07	129.71	14.91	39.39	110.18	13.28	40.98	110.03	14.83	32.66	89.96	12.76
47.22	129.73	15.23	39.58	110.25	13.55	41.00	110.06	14.56	32.72	89.96	12.86
47.25	129.73	15.53	39.77	110.15	13.75	40.87	110.03	14.33	32.83	89.96	13.06
47.60	129.78	15.78	39.86	110.21	14.01	40.18	110.06	14.16	32.92	89.96	13.26
47.69	129.81	16.11	40.02	110.21	14.21	39.93	110.03	13.93	33.02	89.96	13.46
47.82	129.89	16.39	39.99	110.18	14.38	39.78	110.06	13.66	33.08	89.96	13.76
48.05	129.94	16.74	40.12	110.12	14.52	39.76	110.06	13.46	33.24	89.96	13.96
48.14	129.94	16.94	40.26	110.12	14.72	39.79	110.12	13.32	33.42	89.96	14.26
48.26	129.99	17.29	40.28	110.18	14.98	39.54	110.09	13.09	33.49	89.96	14.46
48.47	130.07	17.57	40.40	110.09	15.09	39.43	110.15	12.85	33.57	89.96	14.66
48.66	130.12	17.82	40.55	110.09	15.29	39.39	110.12	12.62	33.72	89.96	14.96
48.79	130.09	18.09	40.63	110.15	15.55	39.29	110.12	12.42	33.82	89.96	15.26
48.93	130.12	18.42	40.80	110.06	15.66	39.29	110.12	12.22	33.96	89.96	15.56
49.00	130.12	18.62	40.79	110.03	15.93	39.10	110.09	11.89	34.13	89.96	15.86
49.10	130.04	18.74	40.84	110.06	16.16	39.08	110.12	11.82	34.23	89.96	16.26
49.15	130.04	18.94	40.96	110.03	16.33	39.02	110.18	11.58	34.37	89.96	16.46
49.36	130.09	19.29	41.02	109.96	16.46	38.95	110.21	11.41	34.52	89.96	16.76
49.47	130.04	19.44	41.22	110.03	16.73	38.85	110.18	11.18	34.73	89.96	17.06
49.63	130.07	19.67	41.25	110.06	16.96	38.80	110.18	10.98	34.84	89.96	17.36
49.59	130.04	19.84	41.37	109.96	17.16	38.67	110.18	10.78	34.98	89.96	17.66
49.85	130.04	20.14	41.40	109.93	17.33	38.64	110.18	10.58	35.01	89.96	17.86
49.91	129.99	20.29	41.54	110.00	17.50	38.57	110.21	10.41	35.18	89.96	18.16
49.94	129.99	20.59	41.67	110.00	17.70	38.46	110.21	10.21	35.33	89.96	18.36
50.04	129.96	20.76	41.88	110.00	17.90	38.33	110.25	10.05	35.43	89.96	18.56

Table A1.1 (cont.) Mass flow rate data for R22 in the 0.039-in. capillary tube.

Mdot	Tsat	Tsub	Mdot	Tsat	Tsub	Mdot	Tsat	Tsub	Mdot	Tsat	Tsub
50.15	129.99	20.99	42.00	110.03	18.13	38.38	110.25	9.75	35.48	89.96	18.76
50.26	129.94	21.24	42.03	110.00	18.30	38.37	110.25	9.55	35.64	89.96	18.96
50.40	129.94	21.44	42.02	110.06	18.56	38.16	110.25	9.35	35.80	89.96	19.16
50.52	129.91	21.71	42.18	110.00	18.70	38.08	110.21	9.21	35.98	89.96	19.36
50.66	129.94	21.94	42.32	110.06	18.96	38.00	110.21	8.91	36.05	89.96	19.46
50.69	129.84	22.04	42.42	110.12	19.22	37.96	110.25	8.75	36.02	89.96	19.76
50.93	129.94	22.44	42.53	110.09	19.39	37.88	110.31	8.61	36.13	89.96	19.97
51.04	129.86	22.56	42.57	110.03	19.53	37.79	110.25	8.35	36.20	89.96	20.22
51.21	129.89	22.89	42.71	110.06	19.76	37.78	110.21	8.11	36.25	89.96	20.43
51.23	129.86	23.06	42.81	110.06	19.96	37.64	110.25	7.95	36.46	89.96	20.68
51.24	129.78	23.18	42.86	110.06	20.16	37.52	110.21	7.71	36.43	89.96	20.87
51.29	129.84	23.54	42.97	110.12	20.42	37.50	110.28	7.58	36.56	89.96	21.07
51.49	129.76	23.66	43.10	110.06	20.56	37.37	110.25	7.25	36.76	89.96	21.29
51.69	129.81	23.91	43.18	110.03	20.73	37.30	110.18	6.98	36.83	89.96	21.46
51.73	129.76	24.16	43.30	110.09	21.09	37.36	110.25	6.85	36.92	89.96	21.67
51.77	129.73	24.33	43.47	110.12	21.32	37.22	110.25	6.65	37.01	89.96	21.90
52.02	129.78	24.58	43.58	110.12	21.62	36.61	110.18	6.38	37.14	89.96	22.14
52.10	129.78	24.78	43.74	110.12	21.92	36.29	110.21	6.21	37.23	89.96	22.38
52.21	129.81	25.11	43.85	110.12	22.12	36.34	110.25	6.05	37.33	89.96	22.60
52.34	129.84	25.44	43.96	110.15	22.45	36.08	110.15	5.75	37.45	89.96	22.84
52.52	129.84	25.64	44.02	110.15	22.65	36.10	110.25	5.65	37.59	89.96	23.07
			44.10	110.12	22.82	36.04	110.25	5.35	37.84	89.96	23.29
			44.23	110.15	23.05	36.01	110.21	5.11	37.82	89.96	23.48
			44.34	110.15	23.35	35.81	110.21	4.91	37.94	89.96	23.70
			44.46	110.18	23.58	35.75	110.21	4.71	38.02	89.96	23.90
			44.52	110.21	23.81	35.65	110.21	4.51	38.02	89.96	24.08
			44.61	110.21	24.01	35.45	110.21	4.31	38.17	89.96	24.26
			44.71	110.18	24.18	35.56	110.21	4.11	38.23	89.96	24.43
			44.88	110.18	24.28	35.55	110.31	3.91	38.26	89.96	24.61
			44.94	110.18	24.48	35.49	110.21	3.61	38.33	89.96	24.82
			45.04	110.25	24.85	35.29	110.25	3.45	38.45	89.96	25.02
			45.14	110.28	25.08	35.19	110.18	3.18	38.54	89.96	25.31
			45.32	110.34	25.34	35.18	110.28	3.08	38.52	89.96	25.48
			45.37	110.21	25.41	35.06	110.21	2.71	38.65	89.96	25.69
			45.43	110.21	25.61	34.85	110.28	2.58	38.75	89.96	25.99

Table A1.1 (cont.) Mass flow rate data for R22 in the 0.039-in. capillary tube.

Mdot	Tsat	Tsub	Mdot	Tsat	Tsub	Mdot	Tsat	Tsub	Mdot	Tsat	Tsub
			45.61	110.25	25.95	34.66	110.25	2.35			
			45.67	110.21	26.11	34.56	110.25	2.15			
			45.86	110.28	26.38	34.54	110.25	1.95			
			45.93	110.21	26.61	34.40	110.21	1.61			
			45.86	110.21	26.71	34.31	110.21	1.41			
						32.06	110.37	1.37			

Table A1.2 Mass flow rate data for R22 in the 0.042-in. capillary tube.

Mdot	Tsat	Tsub	Mdot	Tsat	Tsub	Mdot	Tsat	Tsub	Mdot	Tsat	Tsub
48.93	130.87	0.57	41.75	110.09	0.09	54.13	110.05	25.65	33.77	89.78	0.48
49.11	130.70	1.10	46.82	109.99	0.49	54.17	110.09	25.59	35.95	89.74	0.74
49.62	130.26	1.26	48.62	109.99	1.09	54.03	110.05	25.25	36.92	89.78	0.98
50.10	129.85	1.35	46.16	110.05	1.55	53.91	110.09	25.09	36.49	89.89	1.29
49.79	129.56	1.46	43.49	110.12	2.02	53.84	110.05	24.75	36.64	90.01	1.71
53.59	129.38	1.78	42.99	110.12	2.42	53.40	110.09	24.49	35.86	90.08	2.08
53.27	129.35	2.25	42.99	110.09	2.69	53.34	110.15	24.35	35.66	90.20	2.40
52.12	129.51	2.71	43.03	110.09	2.99	53.23	110.05	23.95	35.05	90.20	2.70
51.17	129.64	3.24	43.11	110.05	3.35	53.17	110.09	23.69	35.07	90.23	2.93
51.05	129.74	3.74	43.10	109.99	3.49	53.15	110.15	23.45	35.30	90.20	3.10
51.17	129.77	4.07	43.29	109.99	3.79	52.98	110.09	23.09	35.45	90.20	3.40
51.41	129.82	4.42	43.38	109.99	4.09	53.23	110.18	22.88	35.49	90.16	3.56
51.75	129.87	4.87	43.58	109.99	4.29	53.02	110.05	22.55	35.63	90.16	3.76
51.83	129.85	5.15	43.60	110.02	4.52	53.02	110.09	22.29	35.68	90.16	3.96
51.94	129.82	5.42	43.73	110.02	4.82	52.81	110.12	22.02	35.73	90.16	4.16
52.10	129.82	5.72	43.74	110.02	5.02	52.93	110.15	21.75	35.86	90.12	4.32
52.12	129.74	5.94	43.75	109.99	5.29	52.77	110.12	21.42	36.02	90.08	4.48
52.07	129.64	6.14	43.83	110.02	5.52	52.66	110.12	21.12	36.21	90.08	4.78
52.39	129.67	6.47	44.15	110.02	5.82	52.66	110.18	20.88	36.32	90.04	4.94
52.60	129.56	6.66	44.23	110.02	6.22	52.52	110.09	20.49	36.43	90.04	5.14
52.51	129.59	6.99	44.39	110.02	6.52	52.39	110.09	20.19	36.62	90.04	5.44
52.77	129.59	7.29	44.39	109.99	6.79	52.34	110.15	19.95	36.82	90.08	5.78
52.94	129.59	7.59	44.58	110.09	7.19	51.44	110.15	19.65	37.08	90.12	6.02
53.16	129.59	7.79	44.59	110.09	7.49	52.21	110.15	19.35	37.38	90.12	6.32
53.14	129.56	7.96	44.77	110.15	7.85	52.16	110.21	19.11	37.75	90.12	6.62
53.39	129.64	8.34	44.98	110.18	8.18	52.03	110.18	18.78	38.15	90.16	6.96
53.52	129.69	8.59	45.04	110.18	8.48	51.80	110.15	18.45	38.56	90.16	7.16
53.53	129.67	8.77	45.21	110.21	8.81	51.80	110.15	18.15	38.98	90.08	7.38
54.32	129.69	9.09	45.30	110.21	9.11	51.84	110.21	17.91	38.96	90.16	7.66
54.86	129.69	9.29	45.39	110.21	9.41	51.69	110.21	17.61	39.21	90.12	7.82
54.95	129.74	9.54	45.57	110.24	9.84	51.63	110.21	17.31	39.34	90.12	8.02
54.90	129.72	9.82	45.62	110.21	10.11	51.51	110.24	17.04	39.56	90.12	8.22
54.95	129.72	10.02	45.87	110.24	10.44	51.29	110.18	16.68	39.69	90.08	8.38
55.25	129.74	10.24	45.92	110.24	10.74	51.32	110.24	16.34	39.84	90.08	8.58
55.29	129.72	10.42	46.18	110.24	11.14	51.20	110.21	16.11	40.13	90.08	8.88

Table A1.2 (cont.) Mass flow rate data for R22 in the 0.042-in. capillary tube.

Mdot	Tsat	Tsub	Mdot	Tsat	Tsub	Mdot	Tsat	Tsub	Mdot	Tsat	Tsub
55.50	129.77	10.77	46.27	110.27	11.57	51.13	110.27	15.87	40.61	90.04	9.04
55.53	129.77	10.97	46.46	110.27	11.97	51.02	110.21	15.41	40.23	90.08	9.38
55.57	129.79	11.19	46.54	110.21	12.21	50.96	110.27	15.17	40.31	90.04	9.64
55.77	129.74	11.34	46.64	110.21	12.61	50.74	110.27	14.87	40.46	90.01	9.91
55.92	129.79	11.59	46.73	110.21	13.01	50.67	110.21	14.51	40.80	89.97	10.07
55.94	129.79	11.79	46.97	110.21	13.31	50.64	110.24	14.24	41.03	90.01	10.31
55.98	129.74	12.04	47.05	110.18	13.58	50.62	110.34	14.04	41.18	89.93	10.43
56.28	129.77	12.27	47.11	110.18	13.88	50.40	110.24	13.64	41.31	89.97	10.77
56.24	129.77	12.47	47.18	110.15	14.15	50.22	110.21	13.31	41.35	89.93	10.93
56.39	129.77	12.67	47.42	110.12	14.42	50.28	110.24	12.94	41.55	90.01	11.21
56.42	129.72	12.82	47.50	110.15	14.65	50.17	110.21	12.61	41.73	90.01	11.41
57.88	129.69	12.99	47.56	110.18	14.98	49.92	110.18	12.28	41.83	90.01	11.61
58.08	129.64	13.14	47.77	110.15	15.25	49.68	110.21	12.01	41.98	90.01	11.81
58.19	129.67	13.37	47.85	110.15	15.55	49.61	110.18	11.68	41.92	90.01	12.01
58.17	129.64	13.54	48.07	110.15	15.85	49.59	110.18	11.38	42.10	90.04	12.24
58.41	129.64	13.74	48.22	110.15	16.25	49.73	110.21	11.11	42.16	90.01	12.41
58.33	129.59	13.89	48.33	110.12	16.52	49.34	110.15	10.65	42.28	90.04	12.64
58.49	129.59	14.09	48.56	110.15	16.85	49.15	110.21	10.41	42.40	90.04	12.84
58.57	129.59	14.29	48.61	110.12	17.12	47.33	110.15	10.05	42.46	90.04	13.04
58.62	129.56	14.46	48.73	110.09	17.29	45.87	110.21	9.81	42.52	90.04	13.14
58.64	129.51	14.71	48.97	110.12	17.62	45.81	110.15	9.45	42.71	90.04	13.34
58.76	129.48	14.88	49.12	110.12	17.92	45.68	110.18	9.08	42.77	90.01	13.51
59.11	129.48	15.08	49.22	110.05	18.05	45.50	110.18	8.78	43.04	90.08	13.88
59.47	129.46	15.26	49.47	110.09	18.39	45.43	110.09	8.39	43.13	90.08	14.08
59.42	129.46	15.46	49.56	110.05	18.55	45.27	110.15	8.05	43.31	90.08	14.28
59.44	129.48	15.68	49.70	110.05	18.75	45.13	110.09	7.69	43.48	90.08	14.48
59.55	129.51	15.91	49.82	110.05	19.05	45.03	110.12	7.32	43.43	90.04	14.74
59.66	129.51	16.11	49.91	110.09	19.39	44.88	110.09	6.99	43.62	90.08	14.98
59.64	129.56	16.36	50.04	110.09	19.69	44.71	110.05	6.55	43.78	90.08	15.18
59.94	129.54	16.54	50.23	110.09	19.99	44.51	110.09	6.29	43.83	90.04	15.34
60.13	129.56	16.76	50.40	110.05	20.15	44.20	110.09	5.89	43.98	90.04	15.44
59.97	129.54	16.94	50.53	110.09	20.59	44.11	110.09	5.59	44.13	90.08	15.68
60.12	129.56	17.16	50.66	110.09	20.89	43.89	110.05	5.15	44.20	90.08	15.88
60.19	129.51	17.31	50.88	110.05	21.25	43.94	110.12	4.82	44.25	90.04	15.94
60.29	129.61	17.51	51.06	110.12	21.62	43.82	110.12	4.52	44.41	90.08	16.18

Table A1.2 (cont.) Mass flow rate data for R22 in the 0.042-in. capillary tube.

Mdot	Tsat	Tsub	Mdot	Tsat	Tsub	Mdot	Tsat	Tsub	Mdot	Tsat	Tsub
59.94	129.67	17.87	51.20	110.09	21.89	43.73	110.18	4.28	44.47	90.08	16.28
59.78	129.67	18.07	51.48	110.12	22.22	43.66	110.12	3.92	44.61	90.12	16.42
60.04	129.64	18.24	51.57	110.09	22.59	43.47	110.18	3.58	45.19	90.04	16.54
60.16	129.61	18.41	51.76	110.05	22.85	43.26	110.18	3.28	44.81	90.12	16.82
60.33	129.67	18.67	53.05	110.09	23.29	43.34	110.24	3.04	44.93	90.08	16.98
60.37	129.64	18.84	53.62	110.09	23.59	43.18	110.27	2.77	45.09	90.08	17.18
60.43	129.67	19.07	53.66	109.99	23.89	42.90	110.21	2.41	45.11	90.04	17.34
60.67	129.67	19.27	53.81	110.05	24.25	43.01	110.30	2.20	45.22	90.08	17.58
60.65	129.64	19.44	53.87	110.05	24.65	42.71	110.24	1.84	45.32	90.04	17.84
60.71	129.61	19.61	54.04	110.02	25.02	42.52	110.24	1.54	45.50	90.08	18.08
60.81	129.67	19.87	54.16	110.09	25.39	42.32	110.21	1.21	45.63	90.04	18.24
60.95	129.59	19.99	54.24	110.05	25.65	40.88	110.30	1.00	45.72	90.04	18.54
61.04	129.61	20.21				35.64	110.55	0.95	45.85	90.04	18.74
61.23	129.56	20.36				34.77	110.65	0.85	45.90	90.01	18.91
61.28	129.56	20.66				32.89	110.43	0.13	46.06	90.08	19.28
61.28	129.54	20.84							46.15	90.01	19.41
61.35	129.51	21.01							46.43	90.01	19.71
61.38	129.46	21.26							46.49	90.01	19.91
61.53	129.46	21.46							46.73	90.01	20.20
61.65	129.46	21.76							46.89	90.01	20.45
62.12	129.43	21.93							47.14	89.97	20.68
62.01	129.43	22.23							47.36	89.97	20.93
62.22	129.46	22.46							47.49	89.97	21.17
62.36	129.41	22.71							47.68	89.97	21.41
62.38	129.41	23.01							47.88	90.01	21.69
62.51	129.41	23.21							48.08	89.93	21.82
62.59	129.41	23.51							48.22	89.97	22.09
62.72	129.43	23.83							48.29	89.97	22.32
62.80	129.41	24.01							48.51	89.93	22.49
62.98	129.41	24.31							48.67	89.97	22.77
63.07	129.43	24.53							48.82	89.89	22.90
63.12	129.46	24.76							48.94	89.97	23.21
63.25	129.43	25.03							49.06	89.89	23.34
63.31	129.46	25.36							49.23	89.97	23.62
63.61	129.48	25.58							49.40	89.89	23.74

Table A1.2 (cont.) Mass flow rate data for R22 in the 0.042-in. capillary tube.

Mdot	Tsat	Tsub	Mdot	Tsat	Tsub	Mdot	Tsat	Tsub	Mdot	Tsat	Tsub
63.60	129.43	25.73							49.47	89.97	24.02
63.81	129.51	26.11							49.69	89.89	24.13
									49.78	89.93	24.36
									49.86	89.93	24.54
									50.00	89.93	24.71
									50.61	89.89	24.85
									52.97	89.97	25.15
									52.81	89.93	25.36
									52.78	89.97	25.61
									52.82	89.89	25.72
									52.87	89.89	25.94
									53.00	89.93	26.25
									53.19	89.97	26.61
									53.34	89.89	26.87

Table A1.3 Mass flow rate data for R22 in the 0.049-in. capillary tube.

Mdot	Tsat	Tsub	Mdot	Tsat	Tsub	Mdot	Tsat	Tsub	Mdot	Tsat	Tsub
75.56	129.63	0.33	97.09	129.55	25.55	64.35	109.60	0.40	85.88	109.73	25.83
76.25	129.71	0.51	96.69	129.55	25.25	67.83	109.54	0.84	85.69	109.76	25.66
77.04	129.78	0.98	96.50	129.53	24.93	67.58	109.66	1.46	85.59	109.76	25.46
79.10	129.78	1.48	96.20	129.50	24.60	64.95	109.98	2.38	85.39	109.76	25.16
78.12	129.91	1.91	95.81	129.47	24.27	64.84	110.10	3.00	85.10	109.76	24.96
76.84	130.02	2.42	95.61	129.50	24.00	65.02	110.07	3.47	85.00	109.79	24.69
76.94	130.04	2.74	95.32	129.47	23.67	65.31	109.91	3.81	84.70	109.82	24.42
77.14	130.07	3.17	95.02	129.45	23.35	65.61	109.85	4.25	84.41	109.76	24.16
77.43	130.02	3.42	94.73	129.50	23.00	66.12	109.91	4.71	84.31	109.82	23.92
77.63	129.99	3.69	94.53	129.50	22.70	66.65	109.94	5.14	84.11	109.82	23.62
77.73	129.91	3.91	94.33	129.53	22.43	67.11	109.98	5.68	83.82	109.85	23.45
78.12	129.91	4.21	94.04	129.55	22.15	67.67	110.01	6.11	83.72	109.88	23.18
78.32	129.86	4.46	93.84	129.55	21.85	68.31	110.04	6.54	83.43	109.85	22.95
78.51	129.78	4.68	93.65	129.60	21.60	68.63	110.07	6.87	83.43	109.91	22.71
78.71	129.78	4.98	93.45	129.60	21.30	69.01	110.07	7.27	83.23	109.91	22.51
79.00	129.73	5.23	93.25	129.60	21.00	69.47	110.13	7.73	83.03	109.91	22.21
79.30	129.73	5.53	93.15	129.63	20.73	69.96	110.10	8.00	82.93	109.94	22.04
79.49	129.71	5.81	92.96	129.68	20.48	70.55	110.13	8.43	82.74	109.98	21.78
79.89	129.73	6.03	92.76	129.68	20.28	70.85	110.16	8.76	82.54	109.98	21.58
80.18	129.78	6.38	92.56	129.73	20.03	71.14	110.16	9.16	82.44	110.04	21.34
80.28	129.73	6.63	92.47	129.76	19.86	71.44	110.13	9.43	82.34	110.04	21.14
80.48	129.73	6.83	92.37	129.81	19.61	71.73	110.13	9.83	82.05	110.04	20.94
80.77	129.71	7.11	92.17	129.81	19.41	72.22	110.16	10.16	81.95	110.04	20.64
81.07	129.68	7.38	92.07	129.84	19.24	73.11	110.16	10.46	81.75	109.94	20.34
81.36	129.71	7.61	91.88	129.89	18.99	73.60	110.16	10.76	81.75	110.10	20.30
81.66	129.73	7.93	91.68	129.91	18.81	73.79	110.16	11.16	81.46	110.07	20.07
81.85	129.68	8.18	91.58	129.91	18.51	73.99	110.16	11.46	81.36	110.07	19.87
82.15	129.71	8.41	91.48	129.99	18.39	74.29	110.16	11.76	81.07	110.01	19.51
82.34	129.68	8.68	91.29	129.99	18.19	74.48	110.13	12.03	81.07	109.98	19.28
82.64	129.71	8.91	91.29	130.02	18.02	74.68	110.16	12.36	80.87	110.01	19.11
82.93	129.73	9.23	90.99	130.02	17.72	74.88	110.13	12.63	80.77	109.98	18.88
83.13	129.71	9.51	90.80	130.02	17.52	75.17	110.13	12.93	80.58	109.94	18.64
83.33	129.71	9.81	90.80	130.02	17.32	75.27	110.13	13.23	80.38	109.98	18.38
83.62	129.73	10.03	90.50	129.99	16.99	75.47	110.10	13.50	80.08	109.91	18.11
83.82	129.71	10.31	90.40	129.99	16.79	75.56	110.01	13.61	79.89	109.91	17.91

Table A1.3 (cont.) Mass flow rate data for R22 in the 0.049-in. capillary tube.

Mdot	Tsat	Tsub	Mdot	Tsat	Tsub	Mdot	Tsat	Tsub	Mdot	Tsat	Tsub
84.11	129.68	10.48	90.30	129.96	16.56	75.76	110.01	13.91	79.79	109.91	17.61
84.21	129.68	10.78	90.11	129.91	16.31	75.96	109.94	14.14	79.59	109.91	17.41
84.70	129.73	11.03	89.91	129.89	16.09	76.06	109.88	14.38	79.40	109.85	17.05
84.80	129.73	11.33	89.81	129.89	15.89	76.25	109.88	14.58	79.30	109.88	16.88
85.10	129.73	11.53	89.52	129.84	15.64	76.35	109.85	14.85	78.91	109.88	16.58
85.19	129.73	11.83	89.42	129.81	15.41	76.94	109.88	15.18	78.81	109.88	16.18
85.49	129.71	12.01	89.22	129.81	15.21	77.23	109.82	15.42	78.61	109.88	15.88
85.78	129.76	12.36	89.03	129.78	14.98	77.43	109.82	15.62	77.92	109.85	15.55
85.88	129.71	12.51	88.93	129.76	14.76	77.63	109.85	15.95	77.14	109.91	15.21
86.18	129.73	12.83	88.73	129.73	14.43	77.82	109.82	16.22	76.84	109.98	14.88
86.37	129.71	13.01	88.54	129.71	14.21	78.02	109.85	16.55	76.84	109.94	14.54
86.67	129.73	13.33	88.34	129.71	14.01	78.22	109.82	16.72	76.74	109.91	14.11
86.87	129.71	13.51	88.24	129.71	13.81	78.51	109.85	17.05	76.64	109.94	13.74
87.06	129.71	13.81	88.04	129.71	13.61	78.81	109.85	17.25	76.45	109.98	13.38
87.26	129.73	14.03	87.85	129.71	13.31	78.91	109.85	17.55	76.25	109.94	12.94
87.45	129.71	14.21	87.75	129.68	13.08	79.20	109.88	17.78	76.06	109.94	12.54
87.65	129.68	14.48	87.55	129.68	12.88	79.49	109.88	18.08	75.86	109.94	12.24
87.95	129.71	14.71	87.36	129.68	12.68	79.69	109.88	18.28	75.66	109.98	11.88
88.14	129.73	15.03	86.77	129.68	12.48	79.99	109.94	18.64	75.37	109.98	11.48
88.24	129.71	15.21	85.78	129.71	12.21	80.18	109.94	18.84	75.27	109.98	11.18
88.54	129.73	15.43	85.59	129.68	11.98	80.48	109.94	19.14	75.07	110.01	10.81
88.73	129.71	15.71	85.39	129.68	11.78	80.87	109.94	19.54	74.88	110.04	10.54
88.83	129.65	15.85	85.29	129.73	11.63	81.17	109.98	19.88	74.78	110.07	10.27
89.13	129.68	16.08	85.29	129.76	11.46	81.56	109.98	20.28	74.48	110.04	9.94
89.32	129.68	16.28	85.10	129.78	11.28	81.95	110.01	20.61	74.29	110.04	9.64
89.42	129.65	16.55	85.00	129.84	11.14	82.34	109.98	20.98	73.30	110.10	9.30
89.71	129.71	16.81	85.00	129.89	10.89	82.64	110.01	21.31	72.03	110.13	9.03
89.81	129.65	16.95	84.80	129.91	10.71	82.74	109.98	21.58	71.83	110.13	8.73
90.11	129.68	17.18	84.70	129.94	10.54	83.03	109.94	21.84	71.63	110.16	8.36
90.30	129.71	17.51	84.51	129.96	10.36	83.23	109.94	22.14	71.24	110.13	8.03
90.50	129.71	17.71	84.51	130.02	10.22	83.33	109.91	22.41	71.14	110.13	7.73
90.80	129.76	17.96	84.31	130.07	9.97	83.52	109.88	22.68	70.95	110.16	7.46
90.99	129.76	18.16	84.31	130.09	9.79	83.62	109.85	22.85	70.75	110.20	7.20
91.09	129.76	18.36	84.11	130.09	9.59	83.82	109.82	23.12	70.65	110.20	6.90
91.48	129.78	18.68	84.02	130.07	9.27	84.02	109.85	23.45	70.45	110.23	6.63

Table A1.3 (cont.) Mass flow rate data for R22 in the 0.049-in. capillary tube.

Mdot	Tsat	Tsub	Mdot	Tsat	Tsub	Mdot	Tsat	Tsub	Mdot	Tsat	Tsub
91.58	129.81	18.91	83.82	130.12	9.12	84.11	109.79	23.59	70.16	110.20	6.30
91.78	129.78	19.08	83.72	130.12	8.92	84.41	109.82	23.92	70.06	110.26	6.06
91.98	129.81	19.31	83.52	130.09	8.69	84.51	109.79	24.19	69.77	110.23	5.63
92.17	129.81	19.51	83.43	130.07	8.47	84.80	109.79	24.39	69.37	110.26	5.36
92.47	129.78	19.68	83.13	130.07	8.17	85.00	109.79	24.69	69.10	110.26	5.06
92.47	129.81	20.01	82.74	130.02	7.92	85.19	109.76	24.86	68.81	110.26	4.76
92.76	129.78	20.18	82.34	129.99	7.69	85.39	109.79	25.09	68.63	110.26	4.46
92.96	129.81	20.41	82.05	130.02	7.52	85.59	109.76	25.36	68.62	110.29	4.09
93.15	129.81	20.61	81.85	129.99	7.19	85.69	109.73	25.53	68.21	110.23	3.73
93.35	129.81	20.81	81.75	129.99	6.99	85.78	109.73	25.73	68.02	110.29	3.49
93.55	129.81	21.01	81.46	129.91	6.71	85.88	109.69	25.89	67.43	110.23	3.13
93.65	129.73	21.23	81.36	129.91	6.51	85.98	109.76	25.96	67.01	110.23	2.83
93.84	129.81	21.51	81.07	129.89	6.29				66.89	110.23	2.53
94.04	129.78	21.68	80.87	129.86	6.06				66.74	110.20	2.20
94.24	129.78	21.88	80.58	129.86	5.76				66.46	110.16	1.86
94.43	129.78	22.18	80.38	129.86	5.56				66.62	110.20	1.50
94.63	129.78	22.38	80.18	129.86	5.36				66.15	110.16	1.26
94.82	129.78	22.58	79.89	129.81	5.01				66.08	110.16	0.96
95.02	129.76	22.76	79.79	129.86	4.86				65.63	110.20	0.70
95.22	129.78	23.08	79.40	129.81	4.51				62.24	110.35	0.55
95.41	129.76	23.26	79.30	129.84	4.34				56.65	110.63	0.63
95.51	129.73	23.53	78.12	129.84	4.14				56.24	110.41	0.41
95.71	129.73	23.73	77.92	129.84	3.84						
95.91	129.73	23.93	77.63	129.81	3.61						
96.00	129.71	24.21	77.53	129.84	3.34						
96.20	129.68	24.38	77.43	129.89	3.19						
96.40	129.71	24.61	77.23	129.89	2.99						
96.50	129.65	24.75	77.04	129.91	2.71						
96.79	129.68	24.98	76.84	129.89	2.49						
96.89	129.63	25.13	76.64	129.96	2.36						
96.99	129.60	25.40	76.64	129.96	2.06						
97.18	129.58	25.58	76.35	129.94	1.84						
			76.35	129.99	1.69						
			75.47	129.91	1.41						
			74.19	130.04	1.34						

Table A1.3 (cont.) Mass flow rate data for R22 in the 0.049-in. capillary tube.

Mdot	Tsat	Tsub	Mdot	Tsat	Tsub	Mdot	Tsat	Tsub	Mdot	Tsat	Tsub
			72.91	130.09	1.09						
			71.24	130.22	1.02						
			68.49	130.48	0.98						

Table A1.3 (cont.) Mass flow rate data for R22 in the 0.049-in. capillary tube.

Mdot	Tsat	Tsub	Mdot	Tsat	Tsub	Mdot	Tsat	Tsub	Mdot	Tsat	Tsub
50.81	89.71	0.71	75.17	89.71	25.34						
51.07	89.71	0.81	75.17	89.71	25.25						
53.73	89.68	0.88	75.07	89.68	25.12						
54.85	89.71	1.11	74.88	89.64	24.95						
52.49	89.83	1.53	74.88	89.68	24.84						
51.71	89.94	1.94	74.88	89.68	24.70						
51.53	89.87	2.17	74.68	89.64	24.52						
51.84	89.98	2.48	74.68	89.64	24.36						
52.34	89.94	2.74	74.58	89.68	24.25						
56.72	89.79	2.79	74.58	89.64	24.07						
56.49	89.79	3.09	74.48	89.71	23.98						
56.77	89.75	3.25	74.38	89.71	23.83						
56.85	89.71	3.51	74.38	89.71	23.67						
57.21	89.75	3.75	74.29	89.79	23.60						
56.98	89.68	3.98	74.09	89.71	23.35						
57.22	89.64	4.24	73.99	89.75	23.22						
57.49	89.60	4.50	73.89	89.75	23.02						
57.46	89.56	4.76	73.79	89.75	22.80						
57.72	89.56	5.06	73.60	89.75	22.55						
57.85	89.52	5.32	73.50	89.75	22.32						
58.15	89.52	5.62	73.30	89.75	22.07						
58.20	89.48	5.88	73.21	89.75	21.83						
58.33	89.45	6.05	73.11	89.75	21.59						
58.38	89.48	6.38	73.01	89.79	21.38						
58.70	89.48	6.68	72.91	89.83	21.16						
58.88	89.45	6.95	72.62	89.71	20.76						
59.22	89.48	7.38	72.52	89.79	20.54						
59.22	89.41	7.61	72.32	89.79	20.23						
59.50	89.45	8.05	72.22	89.83	19.96						
59.83	89.41	8.31	72.03	89.75	19.55						
59.77	89.33	8.53	71.83	89.75	19.25						
60.04	89.37	8.87	71.63	89.71	18.91						
60.33	89.41	9.11	71.53	89.75	18.65						
60.63	89.41	9.41	71.24	89.64	18.24						
60.79	89.41	9.71	71.14	89.68	17.98						

Table A1.3 (cont.) Mass flow rate data for R22 in the 0.049-in. capillary tube.

Mdot	Tsat	Tsub	Mdot	Tsat	Tsub	Mdot	Tsat	Tsub	Mdot	Tsat	Tsub
61.03	89.41	10.01	70.95	89.68	17.68						
61.34	89.41	10.41	70.75	89.60	17.30						
61.62	89.41	10.71	70.55	89.56	16.96						
61.80	89.45	11.05	70.45	89.64	16.84						
62.12	89.45	11.35	70.45	89.60	16.50						
62.37	89.48	11.68	70.36	89.64	16.34						
62.59	89.45	11.95	70.16	89.64	16.14						
62.85	89.56	12.26	69.86	89.52	15.72						
63.05	89.52	12.52	69.77	89.56	15.56						
63.34	89.56	12.86	69.77	89.56	15.36						
63.66	89.52	13.02	69.67	89.60	15.20						
63.64	89.52	13.22	69.47	89.56	14.96						
63.89	89.56	13.56	67.07	89.71	14.91						
64.21	89.56	13.76	66.55	89.68	14.58						
64.25	89.52	13.92	66.48	89.64	14.34						
64.59	89.60	14.30	66.29	89.64	14.14						
64.86	89.56	14.56	66.39	89.75	13.95						
65.21	89.60	14.90	66.29	89.79	13.79						
65.39	89.52	15.12	66.02	89.71	13.51						
65.89	89.56	15.56	66.16	89.79	13.39						
66.05	89.56	15.86	66.00	89.83	13.13						
66.79	89.48	16.08	65.71	89.87	12.87						
67.03	89.52	16.42	65.52	89.87	12.57						
67.39	89.60	16.80	65.38	89.87	12.27						
67.42	89.48	16.98	65.37	89.91	12.11						
67.62	89.45	17.25	65.27	89.98	11.88						
67.81	89.45	17.55	65.20	90.02	11.62						
68.14	89.48	17.88	64.85	89.98	11.38						
68.37	89.56	18.26	64.88	90.10	11.20						
68.50	89.48	18.48	64.67	90.10	10.90						
68.82	89.56	18.86	64.62	90.10	10.60						
69.17	89.56	19.16	64.32	90.10	10.30						
69.27	89.52	19.42	64.14	90.14	10.14						
69.47	89.56	19.70	64.03	90.06	9.76						
69.86	89.64	20.04	63.90	90.06	9.46						

Table A1.3 (cont.) Mass flow rate data for R22 in the 0.049-in. capillary tube.

Mdot	Tsat	Tsub	Mdot	Tsat	Tsub	Mdot	Tsat	Tsub	Mdot	Tsat	Tsub
70.16	89.64	20.30	63.73	90.02	9.12						
70.65	89.71	20.63	63.61	90.06	8.96						
70.85	89.75	20.92	63.30	89.98	8.58						
71.04	89.79	21.19	63.10	89.94	8.24						
71.34	89.83	21.47	63.02	89.94	8.04						
71.44	89.87	21.78	62.87	89.87	7.67						
71.63	89.83	22.00	62.56	89.87	7.37						
71.73	89.79	22.24	62.39	89.83	7.13						
72.03	89.83	22.57	62.38	89.87	6.87						
72.12	89.79	22.81	62.16	89.83	6.53						
72.32	89.79	23.08	61.96	89.75	6.25						
72.62	89.87	23.44	61.93	89.75	5.95						
74.19	89.75	23.58	61.81	89.79	5.79						
74.48	89.79	23.89	61.71	89.75	5.45						
74.58	89.75	24.09	61.24	89.68	5.18						
74.58	89.71	24.29	61.25	89.64	4.84						
74.88	89.79	24.62	61.05	89.56	4.56						
74.97	89.75	24.85	61.08	89.64	4.34						
75.07	89.75	25.07	60.89	89.56	3.96						
75.27	89.71	25.22	60.90	89.64	3.84						
75.17	89.68	25.32	60.71	89.64	3.54						
75.27	89.71	25.38	60.53	89.68	3.38						
			60.44	89.60	3.10						
			59.57	89.60	2.80						
			58.59	89.68	2.68						
			58.54	89.64	2.34						
			58.26	89.64	2.14						
			58.35	89.71	1.91						
			58.24	89.75	1.75						
			58.04	89.75	1.45						
			58.13	89.87	1.27						
			57.88	89.83	1.03						
			57.83	89.79	0.69						
			57.71	89.87	0.57						
			57.53	89.94	0.34						

Table A1.4 Mass flow rate data for R134a in the 0.039-in. capillary tube.

Mdot	Tsat	Tsub	Mdot	Tsat	Tsub	Mdot	Tsat	Tsub	Mdot	Tsat	Tsub
22.36	129.02	0.12	21.96	109.99	0.39	35.12	110.03	25.93	11.66	89.38	0.18
25.73	129.13	0.23	24.70	109.86	0.86	35.23	110.03	25.83	22.16	89.27	0.27
26.70	129.26	0.26	28.15	109.69	1.59	34.99	110.03	25.63	28.83	89.49	0.59
28.04	129.26	0.36	29.84	109.73	2.23	34.91	109.99	25.39	24.81	89.75	1.05
32.16	129.19	0.79	25.66	109.95	2.95	34.86	110.03	25.23	21.61	89.75	1.35
32.86	129.09	1.99	24.37	110.12	3.62	34.62	110.03	25.03	19.91	89.65	1.65
35.18	129.09	2.69	24.33	110.12	4.02	34.61	110.03	24.83	19.78	89.65	2.05
32.62	128.95	3.15	24.35	110.16	4.46	34.54	110.07	24.67	22.64	89.49	2.19
30.53	128.78	3.38	24.68	110.25	4.95	34.58	110.03	24.33	22.31	89.49	2.59
30.15	128.78	3.78	24.98	110.20	5.20	34.53	110.03	24.13	21.97	89.54	2.94
30.05	128.78	4.08	25.23	110.33	5.73	34.27	110.03	23.93	21.97	89.43	3.23
30.10	128.95	4.55	25.47	110.33	6.03	34.21	110.07	23.77	22.15	89.54	3.64
30.26	128.92	4.72	25.50	110.29	6.29	34.08	110.07	23.57	22.09	89.38	3.88
30.47	128.99	5.09	25.68	110.42	6.72	34.10	110.07	23.27	22.25	89.49	4.29
30.53	129.02	5.42	25.92	110.33	6.93	33.95	110.07	23.07	22.20	89.49	4.59
30.81	128.95	5.55	26.08	110.37	7.27	34.00	110.07	22.87	22.50	89.49	4.89
30.72	128.99	5.79	26.36	110.37	7.57	33.87	110.07	22.57	22.62	89.54	5.34
31.02	128.99	5.99	26.45	110.37	7.87	33.69	110.12	22.42	22.63	89.43	5.43
31.21	129.02	6.22	26.69	110.37	8.07	33.66	110.16	22.26	22.73	89.43	5.73
31.21	129.02	6.52	26.75	110.37	8.37	33.65	110.12	21.92	22.67	89.54	6.14
31.39	129.09	6.79	26.97	110.37	8.67	33.41	110.03	21.63	22.85	89.43	6.23
31.55	129.13	7.03	27.00	110.25	8.85	33.42	110.07	21.47	22.89	89.49	6.49
31.53	129.09	7.19	27.19	110.42	9.32	33.11	110.12	21.32	22.98	89.49	6.79
31.81	129.09	7.39	27.45	110.37	9.47	33.18	110.12	21.12	23.00	89.43	6.93
31.79	129.06	7.56	27.65	110.29	9.69	33.11	110.07	20.77	23.05	89.49	7.19
32.12	129.06	7.76	27.74	110.42	10.12	33.09	110.07	20.57	23.14	89.38	7.28
32.16	129.02	7.92	27.81	110.25	10.15	32.84	110.12	20.42	23.24	89.43	7.53
32.23	129.06	8.16	27.94	110.42	10.62	32.94	110.12	20.22	23.08	89.38	7.78
32.39	129.09	8.39	28.15	110.25	10.65	32.91	110.16	20.06	23.40	89.54	8.14
32.59	129.06	8.66	28.30	110.33	11.03	32.68	110.07	19.67	23.39	89.38	8.18
32.66	129.02	8.82	28.47	110.29	11.19	32.72	110.07	19.47	23.47	89.38	8.38
32.63	128.95	8.95	28.46	110.33	11.53	32.63	110.12	19.32	23.51	89.49	8.69
32.78	128.95	9.25	28.65	110.25	11.65	32.57	110.16	19.06	23.37	89.38	8.78
32.99	128.99	9.49	28.60	110.29	11.99	32.39	110.12	18.82	23.71	89.32	8.92
33.06	128.88	9.58	28.94	110.25	12.15	32.35	110.12	18.52	23.71	89.43	9.23

Table A1.4 (cont.) Mass flow rate data for R134a in the 0.039-in. capillary tube.

Mdot	Tsat	Tsub	Mdot	Tsat	Tsub	Mdot	Tsat	Tsub	Mdot	Tsat	Tsub
33.20	128.88	9.88	28.94	110.25	12.35	32.22	110.12	18.32	23.70	89.38	9.38
33.26	128.85	10.15	29.13	110.25	12.65	32.00	110.16	18.16	23.70	89.38	9.58
33.36	128.85	10.35	29.23	110.20	12.80	32.17	110.12	17.92	23.93	89.32	9.72
33.37	128.81	10.51	29.25	110.25	13.05	32.07	110.12	17.62	23.99	89.32	10.02
33.57	128.81	10.71	29.45	110.25	13.25	31.86	110.07	17.37	24.04	89.27	10.17
33.80	128.81	11.01	29.47	110.20	13.40	31.77	110.03	17.13	24.06	89.32	10.52
33.80	128.78	11.18	29.68	110.33	13.83	31.72	110.12	17.02	24.09	89.22	10.62
34.04	128.78	11.48	29.85	110.20	13.90	31.61	110.12	16.72	24.22	89.38	10.98
34.22	128.74	11.64	29.82	110.33	14.23	31.54	110.07	16.47	24.27	89.32	11.12
34.14	128.74	11.84	30.02	110.20	14.30	31.60	110.07	16.27	24.34	89.43	11.43
34.46	128.74	12.14	30.03	110.29	14.59	31.30	110.07	16.07	24.49	89.27	11.47
34.56	128.71	12.31	30.30	110.25	14.75	31.35	110.07	15.87	24.45	89.27	11.67
34.50	128.74	12.64	30.47	110.25	14.95	31.25	110.07	15.57	24.53	89.16	11.76
34.86	128.78	12.88	30.42	110.33	15.23	31.30	110.03	15.33	24.60	89.11	11.81
34.88	128.71	13.01	30.50	110.25	15.35	31.28	110.03	15.13	24.64	89.27	12.17
34.93	128.74	13.34	30.66	110.29	15.69	30.98	110.07	14.97	24.77	89.27	12.37
34.97	128.60	13.40	30.80	110.29	15.89	30.99	110.07	14.77	24.82	89.32	12.62
35.17	128.64	13.64	30.79	110.20	16.00	30.88	109.99	14.49	24.87	89.32	12.82
35.23	128.60	13.80	30.99	110.33	16.43	30.85	110.07	14.27	24.91	89.32	13.02
35.40	128.60	14.10	31.05	110.25	16.55	30.77	110.07	14.07	25.04	89.38	13.28
35.49	128.60	14.30	31.19	110.33	16.83	30.56	110.03	13.83	25.02	89.27	13.37
35.59	128.60	14.50	31.28	110.25	16.95	30.61	110.07	13.67	25.23	89.32	13.62
35.54	128.57	14.67	31.37	110.25	17.15	30.58	110.07	13.37	25.33	89.32	13.92
35.76	128.60	15.00	31.55	110.29	17.39	30.49	110.03	13.13	25.29	89.27	14.07
35.89	128.57	15.17	31.54	110.25	17.55	30.32	110.07	12.97	25.38	89.22	14.32
36.02	128.57	15.37	31.69	110.25	17.75	30.41	110.12	12.82	25.49	89.27	14.67
36.10	128.60	15.60	31.73	110.25	18.05	30.19	110.03	12.53	25.63	89.32	14.92
36.18	128.57	15.87	31.71	110.25	18.25	30.14	110.03	12.33	25.82	89.32	15.22
36.33	128.57	16.07	31.93	110.16	18.36	30.06	110.12	12.12	25.85	89.27	15.37
36.48	128.53	16.23	32.15	110.25	18.65	30.05	110.03	11.83	25.77	89.16	15.56
36.57	128.50	16.50	32.26	110.25	18.85	30.04	110.03	11.63	26.05	89.22	15.82
36.63	128.50	16.80	32.20	110.12	19.02	29.94	110.07	11.47	26.12	89.32	16.22
36.79	128.46	16.96	32.29	110.25	19.35	29.78	110.03	11.13	26.05	89.11	16.21
36.86	128.50	17.30	32.45	110.20	19.60	29.81	110.12	11.02	26.35	89.22	16.52
37.04	128.46	17.46	32.65	110.16	19.76	29.64	110.07	10.77	26.45	89.27	16.77

Table A1.4 (cont.) Mass flow rate data for R134a in the 0.039-in. capillary tube.

Mdot	Tsat	Tsub	Mdot	Tsat	Tsub	Mdot	Tsat	Tsub	Mdot	Tsat	Tsub
37.11	128.50	17.80	32.64	110.20	20.00	29.65	110.07	10.57	26.38	89.05	16.75
37.17	128.46	17.96	32.76	110.20	20.30	29.69	110.12	10.42	26.57	89.32	17.32
37.39	128.50	18.30	32.91	110.20	20.60	29.59	110.03	10.13	26.59	89.00	17.20
37.53	128.46	18.46	33.08	110.16	20.76	29.45	110.16	10.06	26.77	89.27	17.77
37.59	128.46	18.76	33.15	110.20	21.00	29.44	110.07	9.77	26.82	89.05	17.75
37.79	128.46	18.96	33.23	110.20	21.20	29.29	110.20	9.60	26.85	89.22	18.12
37.77	128.50	19.30	33.25	110.16	21.46	29.35	110.12	9.32	27.02	89.05	18.15
37.97	128.46	19.46	33.25	110.16	21.66	29.25	110.16	9.16	26.97	89.11	18.41
37.98	128.50	19.80	33.56	110.20	21.90	29.17	110.20	9.00	27.17	89.05	18.55
38.30	128.50	20.00	33.65	110.20	22.10	29.15	110.07	8.67	27.17	89.00	18.70
38.28	128.53	20.23	33.60	110.16	22.26	29.17	110.16	8.46	27.35	89.11	19.11
38.42	128.53	20.53	33.80	110.16	22.46	28.95	110.25	8.35	27.42	88.95	19.18
38.61	128.53	20.73	33.81	110.16	22.76	28.88	110.12	8.02	27.42	89.11	19.56
38.74	128.57	20.97	33.86	110.16	22.96	28.94	110.12	7.82	27.41	88.89	19.56
38.76	128.57	21.27	34.08	110.16	23.26	28.74	110.25	7.75	27.59	89.05	19.92
38.92	128.57	21.47	34.06	110.16	23.46	28.51	110.12	7.42	27.66	88.78	19.88
39.02	128.53	21.73	34.28	110.16	23.76	28.56	110.12	7.22	27.75	89.11	20.43
39.11	128.57	21.97	34.39	110.16	24.06	28.41	110.20	7.00	27.94	88.89	20.41
39.28	128.57	22.17	34.54	110.12	24.32	28.36	110.07	6.67	27.69	88.89	20.60
39.39	128.53	22.33	34.71	110.12	24.52	28.32	110.16	6.56	28.04	89.00	20.96
39.47	128.57	22.67	34.70	110.16	24.86	28.21	110.16	6.36	28.00	88.84	21.01
39.56	128.57	22.87	34.90	110.12	25.02	28.15	110.07	5.97	28.15	88.84	21.18
39.61	128.57	23.07	34.81	110.12	25.32	28.02	110.20	5.90	28.25	89.00	21.53
39.73	128.60	23.30	34.99	110.07	25.47	28.02	110.12	5.62	28.24	88.84	21.54
39.90	128.57	23.57	35.18	110.07	25.67	27.85	109.99	5.29	28.45	89.00	21.90
40.08	128.60	23.80	35.24	110.03	25.83	27.88	110.16	5.26	28.49	88.89	22.00
40.07	128.57	23.97	35.18	110.07	25.97	27.77	110.12	5.02	28.82	88.89	22.23
40.23	128.60	24.20				27.76	110.03	4.73	28.79	89.11	22.67
40.25	128.57	24.37				27.76	110.12	4.52	28.71	88.89	22.67
40.47	127.98	24.68				27.53	110.16	4.46	28.94	88.95	22.96
						27.51	110.12	4.12	28.96	89.05	23.30
						27.56	109.99	3.79	29.14	88.89	23.43
						27.41	110.03	3.63	29.34	89.16	23.98
						27.38	110.16	3.56	29.25	88.89	23.94
						27.28	110.16	3.36	29.53	89.05	24.38

Table A1.4 (cont.) Mass flow rate data for R134a in the 0.039-in. capillary tube.

Mdot	Tsat	Tsub	Mdot	Tsat	Tsub	Mdot	Tsat	Tsub	Mdot	Tsat	Tsub
						27.14	110.12	3.12	29.50	88.95	24.54
						27.14	110.03	2.73	29.44	88.84	24.69
						27.16	109.99	2.49			
						27.01	110.07	2.37			
						26.99	110.12	2.12			
						26.90	110.16	1.96			
						26.51	110.12	1.72			
						26.23	110.12	1.52			
						26.15	110.12	1.32			
						26.07	110.12	1.12			
						24.60	110.07	0.77			

Table A1.5 Mass flow rate data for R134a in the 0.042-in. capillary tube.

Mdot	Tsat	Tsub	Mdot	Tsat	Tsub	Mdot	Tsat	Tsub	Mdot	Tsat	Tsub
34.88	129.75	0.05	29.46	110.00	0.30	46.26	109.91	26.01	22.67	89.72	0.22
36.35	129.61	0.21	31.80	109.91	0.41	46.20	109.87	25.77	24.48	89.66	0.26
40.51	129.58	0.58	34.20	109.74	0.44	46.02	109.91	25.61	28.07	89.56	0.36
44.09	129.72	1.72	38.21	109.70	1.10	45.91	109.96	25.36	29.72	89.56	0.46
43.08	129.89	2.39	38.77	109.79	1.69	45.81	109.91	25.11	29.78	89.66	0.66
38.95	129.92	2.92	34.03	109.91	2.31	45.59	109.96	24.86	28.01	89.77	1.07
38.44	129.79	3.19	32.72	110.00	2.80	45.42	109.96	24.56	26.31	89.82	1.32
38.32	129.79	3.49	32.38	110.04	3.24	45.24	109.96	24.26	25.06	89.88	1.58
38.52	129.79	3.79	32.34	110.09	3.59	45.09	109.96	23.96	24.97	89.88	1.78
38.63	129.79	4.09	32.62	110.13	3.93	44.90	110.00	23.80	25.01	89.88	2.08
38.89	129.75	4.35	32.77	110.13	4.23	44.76	110.04	23.54	24.93	89.88	2.38
39.03	129.75	4.55	32.86	110.13	4.53	44.59	110.04	23.24	25.29	89.93	2.73
39.22	129.79	4.89	33.01	110.13	4.83	44.35	110.09	23.09	25.74	89.93	3.13
39.48	129.79	5.19	33.12	110.13	5.03	44.31	110.13	22.83	25.94	89.93	3.43
39.62	129.79	5.49	33.19	110.13	5.33	44.16	110.13	22.53	26.29	89.93	3.73
40.17	129.75	5.65	33.38	110.13	5.53	43.98	110.13	22.23	26.41	89.88	3.98
40.29	129.75	5.95	33.50	110.13	5.73	43.98	110.13	22.03	26.24	89.88	4.18
40.55	129.79	6.29	33.63	110.13	6.03	43.88	110.13	21.73	26.43	89.88	4.48
40.61	129.75	6.45	33.72	110.13	6.23	43.71	110.17	21.47	26.49	89.88	4.68
40.84	129.75	6.75	33.76	110.13	6.43	43.68	110.17	21.17	26.77	89.88	4.88
40.89	129.75	7.05	33.84	110.13	6.63	43.57	110.17	20.97	26.90	89.93	5.13
41.22	129.79	7.29	33.95	110.13	6.83	43.46	110.17	20.67	27.07	89.88	5.28
41.39	129.82	7.62	34.07	110.09	6.99	43.35	110.17	20.37	27.30	89.88	5.48
41.52	129.79	7.89	34.17	110.09	7.19	43.22	110.13	20.03	27.51	89.88	5.68
41.68	129.79	8.19	34.34	110.09	7.49	43.12	110.13	19.73	27.68	89.88	5.88
41.82	129.82	8.42	34.55	110.04	7.74	43.08	110.13	19.43	27.89	89.88	6.08
41.93	129.82	8.72	34.76	110.04	8.04	42.93	110.13	19.13	28.11	89.88	6.28
42.26	129.82	9.02	34.96	110.00	8.30	42.80	110.09	18.79	28.24	89.88	6.48
42.35	129.79	9.29	35.21	110.00	8.60	42.64	110.09	18.49	28.45	89.82	6.72
42.80	129.75	9.65	35.40	109.96	8.86	42.54	110.04	18.14	28.63	89.82	6.92
42.95	129.82	10.02	35.61	110.00	9.10	42.44	110.04	17.84	28.82	89.77	7.07
43.42	129.75	10.25	35.77	109.96	9.36	42.35	110.00	17.50	28.90	89.77	7.27
43.49	129.75	10.55	36.08	109.96	9.56	42.22	110.00	17.20	29.05	89.77	7.57
43.59	129.75	10.95	36.31	109.96	9.76	42.05	110.00	16.90	29.22	89.72	7.72
43.82	129.72	11.22	36.67	110.00	10.10	41.98	110.00	16.60	29.45	89.72	8.02

Table A1.5 (cont.) Mass flow rate data for R134a in the 0.042-in. capillary tube.

Mdot	Tsat	Tsub	Mdot	Tsat	Tsub	Mdot	Tsat	Tsub	Mdot	Tsat	Tsub
44.00	129.72	11.52	36.94	109.96	10.36	41.74	110.00	16.30	29.64	89.72	8.22
44.11	129.72	11.82	37.38	110.00	10.70	40.75	110.00	16.10	29.88	89.66	8.46
44.43	129.68	12.08	37.64	110.00	11.00	40.43	110.00	15.80	29.42	89.66	8.66
44.59	129.72	12.52	37.87	110.00	11.30	40.25	109.96	15.36	29.41	89.66	8.96
44.90	129.75	12.95	37.96	110.00	11.50	40.13	110.00	15.10	29.63	89.66	9.26
45.14	129.75	13.35	37.99	110.04	11.84	39.97	110.00	14.80	29.83	89.66	9.56
45.28	129.79	13.69	38.12	110.04	12.04	39.87	110.00	14.50	30.04	89.61	9.71
45.56	129.75	14.05	38.18	110.04	12.34	39.74	110.00	14.10	30.92	89.61	10.01
45.71	129.79	14.49	38.31	110.09	12.59	39.43	110.00	13.80	30.97	89.56	10.26
45.90	129.79	14.79	38.43	110.13	12.93	39.05	110.00	13.50	30.34	89.56	10.56
46.08	129.75	15.05	38.53	110.13	13.23	38.94	110.00	13.20	30.35	89.61	10.81
46.27	129.75	15.35	38.69	110.13	13.53	38.79	110.00	12.80	30.58	89.61	11.11
46.39	129.75	15.65	38.81	110.17	13.87	38.66	110.00	12.50	30.70	89.56	11.36
46.63	129.75	15.95	38.99	110.13	14.13	38.61	110.00	12.20	30.79	89.56	11.66
46.81	129.75	16.25	39.19	110.13	14.43	38.44	110.00	11.90	30.84	89.50	11.90
46.92	129.75	16.55	39.34	110.17	14.77	38.27	110.00	11.60	30.97	89.50	12.10
47.14	129.72	16.82	39.41	110.17	14.97	38.01	110.00	11.30	31.05	89.50	12.40
47.33	129.72	17.22	39.58	110.17	15.27	37.18	110.04	11.04	31.15	89.50	12.60
47.60	129.75	17.65	39.77	110.17	15.47	37.06	110.04	10.74	31.37	89.50	12.80
47.78	129.72	17.92	39.83	110.17	15.87	36.92	110.04	10.44	31.43	89.50	13.10
48.08	129.72	18.22	40.04	110.17	16.17	36.67	110.09	10.19	31.50	89.45	13.25
48.17	129.72	18.52	40.21	110.13	16.43	36.44	110.09	9.89	31.65	89.45	13.55
48.34	129.68	18.88	40.33	110.13	16.73	36.16	110.09	9.59	31.75	89.45	13.75
48.60	129.68	19.18	40.53	110.09	16.99	35.85	110.13	9.33	31.92	89.45	14.05
48.66	129.68	19.48	40.66	110.09	17.29	35.61	110.13	9.03	32.03	89.50	14.40
48.83	129.68	19.78	40.85	110.09	17.59	35.40	110.13	8.73	32.17	89.45	14.65
49.06	129.68	20.18	40.97	110.04	17.74	35.28	110.17	8.47	32.61	89.45	14.85
49.23	129.68	20.48	41.04	110.04	18.04	35.05	110.13	8.13	33.71	89.50	15.20
49.47	129.68	20.78	41.20	110.04	18.24	34.95	110.21	7.91	33.88	89.50	15.50
49.67	129.68	21.08	41.86	110.00	18.40	34.84	110.21	7.61	33.96	89.45	15.75
49.90	129.68	21.48	42.37	109.96	18.66	34.36	110.21	7.31	34.00	89.50	16.00
50.10	129.79	21.89	42.55	109.96	18.96	34.25	110.26	7.06	34.05	89.50	16.30
50.35	129.61	22.01	42.62	109.91	19.21	34.05	110.26	6.76	34.14	89.50	16.50
50.48	129.65	22.35	42.66	109.87	19.37	34.10	110.30	6.50	34.27	89.50	16.80
50.69	129.65	22.75	42.77	109.87	19.67	33.81	110.30	6.20	34.40	89.50	17.10

Table A1.5 (cont.) Mass flow rate data for R134a in the 0.042-in. capillary tube.

Mdot	Tsat	Tsub	Mdot	Tsat	Tsub	Mdot	Tsat	Tsub	Mdot	Tsat	Tsub
50.91	129.65	23.05	42.80	109.87	19.87	33.67	110.30	5.90	34.50	89.50	17.30
51.10	129.61	23.31	43.05	109.87	20.17	33.52	110.30	5.60	34.52	89.50	17.60
51.21	129.61	23.61	43.20	109.83	20.33	33.46	110.30	5.30	34.59	89.45	17.75
51.36	129.58	23.88	43.30	109.83	20.63	33.26	110.30	5.00	34.72	89.50	18.10
51.55	129.58	24.18	43.37	109.83	20.93	33.26	110.30	4.70	34.81	89.50	18.30
51.66	129.58	24.48	43.59	109.83	21.23	32.94	110.30	4.40	34.88	89.50	18.50
51.92	129.61	24.81	43.69	109.79	21.49	32.85	110.30	4.10	34.92	89.50	18.80
			43.84	109.74	21.74	32.77	110.26	3.76	35.05	89.50	19.00
			43.93	109.74	22.04	32.57	110.26	3.46	35.15	89.50	19.20
			43.90	109.74	22.34	32.13	110.26	3.16	35.24	89.50	19.40
			43.95	109.74	22.54	32.05	110.21	2.91	35.22	89.50	19.65
			44.21	109.74	22.84	31.85	110.21	2.61	35.40	89.50	19.87
			44.58	109.79	23.19	31.56	110.21	2.31	35.62	89.45	20.16
			44.73	109.83	23.43	31.30	110.17	1.97	35.77	89.45	20.40
			44.87	109.79	23.59	31.05	110.13	1.63	35.87	89.45	20.74
			45.04	109.83	23.93	28.30	110.21	1.51	36.63	89.39	21.02
			45.20	109.83	24.23	23.79	110.38	1.38	37.02	89.45	21.40
			45.30	109.83	24.53	19.70	110.72	1.12	37.21	89.39	21.72
			45.43	109.83	24.83	15.77	110.68	0.18	37.32	89.39	21.95
			45.62	109.83	25.13	14.84	110.68	0.08	37.50	89.39	22.18
			45.78	109.83	25.33	11.48	110.55	0.05	37.59	89.39	22.45
			45.90	109.83	25.63				37.68	89.34	22.69
			46.14	109.83	25.83				37.85	89.34	22.94
			46.43	109.83	26.03				37.93	89.34	23.15
			46.40	109.83	26.13				37.97	89.34	23.34
									38.08	89.34	23.56
									38.12	89.29	23.69
									38.26	89.29	23.87
									38.33	89.29	24.06
									38.42	89.29	24.25
									38.44	89.23	24.41
									38.63	89.29	24.70
									38.77	89.29	24.92
									38.84	89.23	25.07
									39.01	89.29	25.35

Table A1.6 Mass flow rate data for R134a in the 0.049-in. capillary tube.

Mdot	Tsat	Tsub	Mdot	Tsat	Tsub	Mdot	Tsat	Tsub	Mdot	Tsat	Tsub
57.74	129.22	1.12	66.24	109.30	25.30	35.44	110.20	0.40	32.61	88.84	0.44
60.57	129.26	1.26	66.14	109.34	25.14	35.67	110.16	0.36	33.78	88.79	0.49
59.03	129.22	1.52	65.92	109.34	24.94	37.54	110.16	0.46	34.00	88.79	0.59
59.23	129.33	2.03	65.79	109.34	24.64	40.34	110.16	0.46	34.53	88.84	0.74
56.56	129.54	2.64	65.60	109.39	24.39	42.49	110.03	0.53	42.87	88.73	0.73
56.51	129.57	2.87	65.39	109.39	24.19	44.28	109.94	0.54	41.67	88.73	0.93
56.81	129.60	3.30	65.25	109.39	23.89	45.31	109.90	0.90	40.94	88.62	1.02
57.01	129.57	3.47	65.09	109.39	23.69	45.92	109.86	1.26	40.62	88.57	1.17
57.46	129.67	3.87	64.95	109.43	23.43	45.81	109.99	1.69	40.53	88.51	1.31
57.71	129.67	4.17	64.68	109.43	23.23	44.66	110.03	1.93	40.91	88.51	1.51
58.05	129.71	4.41	64.63	109.47	22.97	45.53	110.03	2.23	41.00	88.51	1.71
58.33	129.67	4.67	64.40	109.47	22.67	47.84	110.03	2.33	41.19	88.51	2.01
58.67	129.64	4.84	64.34	109.56	22.56	47.85	109.94	2.54	41.08	88.46	2.26
58.82	129.60	5.10	64.13	109.52	22.22	47.88	109.86	2.66	41.24	88.41	2.41
59.19	129.67	5.37	63.99	109.52	22.02	47.88	109.86	2.86	41.38	88.41	2.61
59.49	129.67	5.67	63.86	109.56	21.76	47.98	109.69	2.89	41.49	88.41	2.81
59.59	129.60	5.90	63.70	109.60	21.60	47.94	109.77	3.17	41.53	88.46	3.06
59.94	129.60	6.10	63.56	109.60	21.30	48.13	109.60	3.10	41.51	88.41	3.21
60.11	129.64	6.44	63.42	109.64	21.14	48.09	109.64	3.34	41.73	88.41	3.41
60.24	129.57	6.57	63.30	109.73	21.03	48.19	109.47	3.37	41.74	88.41	3.61
60.40	129.50	6.70	63.12	109.73	20.73	48.36	109.56	3.66	41.73	88.30	3.60
60.66	129.57	7.07	63.02	109.73	20.53	48.39	109.47	3.77	41.71	88.30	3.80
60.92	129.47	7.17	62.86	109.77	20.27	48.59	109.56	4.06	41.92	88.24	3.94
61.04	129.50	7.50	62.74	109.82	20.12	48.69	109.47	4.17	41.95	88.24	4.14
61.52	129.54	7.74	62.57	109.82	19.92	48.79	109.56	4.46	41.91	88.19	4.29
61.84	129.54	8.04	62.44	109.77	19.57	48.95	109.47	4.57	42.08	88.24	4.54
61.63	129.43	8.13	62.23	109.73	19.33	49.10	109.56	4.96	42.32	88.19	4.69
62.05	129.47	8.47	62.04	109.69	18.99	49.34	109.56	5.16	42.29	88.19	4.89
62.26	129.43	8.63	61.82	109.64	18.74	49.46	109.56	5.36	42.48	88.24	5.14
62.89	129.43	8.83	61.61	109.60	18.50	49.55	109.52	5.52	42.57	88.19	5.19
62.74	129.40	9.10	61.46	109.60	18.20	49.72	109.64	5.84	42.52	88.13	5.33
63.25	129.47	9.37	61.34	109.56	17.96	49.89	109.60	6.10	42.62	88.13	5.53
63.22	129.33	9.43	61.27	109.56	17.76	49.97	109.60	6.30	42.84	88.13	5.73
63.45	129.33	9.73	61.10	109.60	17.60	50.25	109.60	6.60	42.89	88.19	5.99
63.62	129.33	9.93	60.93	109.56	17.26	50.48	109.64	6.84	42.94	88.13	6.13

Table A1.6 (cont.) Mass flow rate data for R134a in the 0.049-in. capillary tube.

Mdot	Tsat	Tsub	Mdot	Tsat	Tsub	Mdot	Tsat	Tsub	Mdot	Tsat	Tsub
63.87	129.26	10.06	60.82	109.56	17.06	50.59	109.64	7.04	43.21	88.08	6.28
63.86	129.26	10.26	60.66	109.56	16.86	50.77	109.60	7.30	43.04	88.13	6.53
64.09	129.16	10.46	60.58	109.60	16.60	50.79	109.64	7.44	43.24	88.08	6.68
64.40	129.22	10.72	60.39	109.60	16.40	50.80	109.64	7.34	43.22	88.08	6.88
64.41	129.16	10.86	60.36	109.60	16.20	50.45	109.60	7.10	43.33	88.03	6.93
64.75	129.16	11.06	60.18	109.60	16.00	50.38	109.64	6.94	43.49	88.08	7.18
65.05	129.19	11.39	60.06	109.64	15.84	50.25	109.64	6.84	43.60	88.03	7.23
65.08	129.12	11.52	59.98	109.64	15.54	50.39	109.64	6.74	43.65	88.03	7.43
65.18	129.16	11.76	59.87	109.60	15.30	50.28	109.60	6.60	43.55	87.97	7.57
65.59	129.16	11.96	59.64	109.64	15.14	50.30	109.73	6.73	43.87	87.97	7.77
65.60	129.09	12.09	59.59	109.60	14.90	50.28	109.60	6.70	43.90	88.03	8.03
65.81	129.09	12.29	59.46	109.64	14.74	50.32	109.69	6.79	44.15	88.03	8.23
65.89	129.02	12.52	59.40	109.60	14.50	50.47	109.64	6.84	44.16	88.03	8.43
66.43	129.16	12.86	59.29	109.60	14.20	50.42	109.64	6.84	44.23	88.03	8.53
66.39	129.09	12.99	59.02	109.60	14.00	50.38	109.69	6.79	44.53	88.03	8.73
66.66	129.09	13.19	58.99	109.64	13.84	50.38	109.73	6.83	44.47	88.08	8.98
66.61	129.02	13.42	58.82	109.60	13.60	50.35	109.64	6.74	44.61	88.08	9.08
66.97	128.98	13.58	58.72	109.60	13.40	50.53	109.73	6.93	44.75	88.08	9.28
67.06	128.91	13.71	58.60	109.60	13.20	50.54	109.60	6.90	44.76	88.03	9.33
67.22	128.95	13.95	58.34	109.60	13.00	50.69	109.69	7.19	44.85	88.08	9.58
67.39	128.91	14.11	58.30	109.52	12.72	50.87	109.69	7.39	44.94	88.08	9.68
67.56	128.84	14.24	58.17	109.56	12.56	51.00	109.60	7.60	45.09	88.08	9.88
68.07	128.98	14.68	58.10	109.56	12.36	51.26	109.69	7.89	45.15	88.08	9.98
67.98	128.91	14.81	57.86	109.52	12.12	51.43	109.64	8.14	45.23	88.08	10.18
68.27	128.88	15.08	57.90	109.56	11.96	51.66	109.64	8.44	45.31	88.03	10.23
68.50	128.84	15.24	57.82	109.56	11.76	51.89	109.69	8.79	45.34	88.03	10.43
68.63	128.88	15.48	57.60	109.47	11.47	52.03	109.60	8.90	45.53	88.08	10.58
68.97	128.91	15.71	57.53	109.52	11.32	52.33	109.73	9.33	45.60	88.08	10.78
69.20	128.91	16.01	57.29	109.52	11.12	52.35	109.64	9.54	45.54	88.08	10.88
69.47	128.91	16.21	57.30	109.47	10.87	52.76	109.60	9.80	45.82	88.08	10.98
69.68	129.02	16.62	57.25	109.52	10.72	52.89	109.69	10.09	45.72	88.03	11.13
69.97	129.05	16.85	57.04	109.52	10.52	53.10	109.60	10.30	45.84	88.03	11.23
70.10	129.02	17.02	56.94	109.52	10.32	53.32	109.64	10.64	46.01	88.08	11.48
70.40	128.98	17.28	56.82	109.52	10.12	53.58	109.56	10.86	46.04	88.08	11.58
70.60	128.98	17.48	56.88	109.56	9.96	53.75	109.64	11.14	46.21	88.08	11.78

Table A1.6 (cont.) Mass flow rate data for R134a in the 0.049-in. capillary tube.

Mdot	Tsat	Tsub	Mdot	Tsat	Tsub	Mdot	Tsat	Tsub	Mdot	Tsat	Tsub
70.80	128.98	17.68	56.70	109.60	9.80	53.91	109.52	11.32	46.12	88.03	11.83
70.90	128.98	17.98	56.60	109.60	9.60	54.40	109.56	11.66	46.28	88.08	11.98
71.10	128.98	18.18	55.88	109.52	9.42	54.52	109.60	11.90	46.44	88.08	12.08
71.40	129.02	18.42	55.14	109.64	9.34	54.61	109.52	12.12	46.62	88.08	12.28
71.60	129.09	18.69	54.11	109.60	9.10	54.99	109.60	12.50	46.48	88.08	12.38
71.60	128.98	18.78	53.85	109.69	8.99	55.30	109.52	12.62	46.72	88.03	12.53
71.70	128.98	18.98	53.80	109.64	8.74	55.49	109.56	12.96	46.66	88.08	12.68
72.10	129.05	19.25	53.74	109.77	8.67	55.62	109.56	13.26	46.91	88.08	12.88
72.20	128.95	19.45	53.64	109.73	8.43	56.04	109.60	13.50	47.03	88.08	13.18
72.40	128.91	19.61	53.41	109.73	8.23	56.35	109.60	13.80	47.20	88.08	13.48
72.30	128.77	19.67	53.35	109.82	8.12	56.81	109.52	13.92	47.38	88.08	13.68
72.60	128.70	19.80	53.23	109.77	7.87	57.28	109.56	14.26	47.61	88.13	13.93
72.80	128.77	20.07	53.12	109.82	7.72	57.46	109.52	14.52	47.56	88.08	14.08
73.10	128.88	20.38	53.14	109.86	7.56	57.55	109.56	14.76	47.73	88.13	14.23
73.40	129.02	20.72	53.04	109.90	7.40	57.63	109.52	14.92	47.94	88.19	14.49
73.50	128.98	20.88	52.99	109.86	7.26	57.88	109.52	15.22	47.91	88.19	14.59
73.70	129.09	21.19	52.99	109.90	7.30	57.90	109.52	15.52	48.16	88.19	14.69
74.00	129.12	21.42	52.99	109.90	7.30	58.42	109.52	15.72	48.33	88.24	15.04
74.20	129.19	21.59	53.05	109.90	7.40	58.51	109.47	15.87	48.38	88.24	15.24
74.30	129.22	21.82	53.05	109.90	7.50	58.63	109.56	16.26	48.67	88.30	15.50
74.70	129.33	22.03	53.14	109.94	7.54	58.83	109.47	16.37	48.66	88.24	15.64
74.70	129.29	22.29	53.08	109.94	7.54	59.06	109.56	16.76	48.89	88.35	15.95
75.00	129.36	22.56	53.12	109.90	7.50	59.38	109.52	16.92	49.08	88.30	16.10
75.40	129.47	22.97	53.05	109.90	7.40	59.48	109.56	17.26	49.28	88.35	16.35
75.80	129.47	23.17	53.03	109.94	7.44	59.93	109.56	17.46	49.34	88.30	16.60
			52.99	109.94	7.34	59.90	109.52	17.62	49.52	88.35	16.85
			52.99	109.90	7.30	60.09	109.60	18.00	49.65	88.35	17.05
			52.92	109.90	7.20	60.44	109.47	18.07	49.77	88.35	17.15
			52.79	109.94	7.04	60.69	109.56	18.36	49.92	88.41	17.41
			52.68	109.90	6.80	60.78	109.47	18.57	49.98	88.35	17.45
			52.53	109.90	6.60	60.91	109.52	18.82	50.16	88.35	17.65
			52.44	109.94	6.44	61.23	109.47	18.97	50.29	88.35	17.85
			52.23	109.90	6.20	61.22	109.47	19.17	50.37	88.30	17.90
			52.20	109.90	5.90	61.53	109.47	19.47	50.36	88.35	18.05
			52.08	109.86	5.66	61.48	109.43	19.63	50.57	88.35	18.25

Table A1.6 (cont.) Mass flow rate data for R134a in the 0.049-in. capillary tube.

Mdot	Tsat	Tsub	Mdot	Tsat	Tsub	Mdot	Tsat	Tsub	Mdot	Tsat	Tsub
			52.04	109.90	5.50	61.94	109.52	19.92	50.64	88.30	18.45
			51.72	109.86	5.26	61.97	109.43	20.03	50.81	88.30	18.66
			51.62	109.90	5.10	62.16	109.52	20.42	50.99	88.30	18.82
			51.59	109.86	4.76	62.19	109.47	20.57	51.08	88.35	19.02
			51.50	109.94	4.64	62.50	109.43	20.73	51.12	88.24	19.09
			51.40	109.94	4.44	62.59	109.47	20.97	51.39	88.24	19.31
			51.21	109.90	4.20	62.71	109.39	21.09	51.39	88.24	19.55
			51.19	109.90	4.00	62.99	109.47	21.37	51.62	88.30	19.83
			51.01	109.94	3.84	63.03	109.39	21.49	51.73	88.19	20.01
			50.90	109.94	3.64	63.21	109.34	21.64	51.94	88.19	20.25
			50.70	109.86	3.26	63.44	109.43	22.03	52.08	88.24	20.51
			50.64	109.99	3.19	63.51	109.34	22.14	52.32	88.19	20.72
			50.60	109.90	2.90	63.80	109.43	22.43	52.50	88.13	20.99
			50.36	109.94	2.74	63.85	109.26	22.46	52.62	88.19	21.37
			50.32	109.94	2.54	64.05	109.34	22.74	52.88	88.19	21.53
			50.30	109.94	2.34	64.44	109.30	22.90	53.07	88.13	21.78
			50.03	109.99	2.09	64.77	109.26	23.06	53.35	88.19	22.08
			50.11	109.94	1.84	64.88	109.34	23.34	53.54	88.13	22.24
			49.96	109.99	1.69	64.92	109.30	23.50	53.66	88.13	22.40
			49.85	109.94	1.44	65.20	109.34	23.74	53.87	88.13	22.60
			49.71	109.94	1.14	65.28	109.39	23.99	54.05	88.13	22.91
			49.58	109.90	0.90	65.48	109.30	24.10	54.29	88.13	23.16
			49.43	109.99	0.79	65.51	109.26	24.26	54.39	88.13	23.37
			49.38	109.90	0.50	65.75	109.34	24.54	54.52	88.13	23.57
			49.30	109.99	0.39	65.84	109.26	24.56	54.74	88.13	23.77
			49.01	109.90	0.10	66.00	109.30	24.80	54.75	88.08	23.89
			42.42	110.37	0.37				55.03	88.08	24.22
			34.38	110.54	0.44				55.10	88.03	24.46
			27.56	110.41	0.31				55.36	88.08	24.63
			32.23	110.46	0.36				55.46	87.97	24.82
			31.26	110.20	0.30				55.66	88.03	25.13
			34.53	110.16	0.36						

Table A1.7 Mass flow rate data for R407C in the 0.039-in. capillary tube.

Mdot	Tsat	Tsub	Mdot	Tsat	Tsub	Mdot	Tsat	Tsub	Mdot	Tsat	Tsub
42.38	130.48	0.28	34.72	110.03	0.23	48.13	110.20	25.50	29.04	90.48	0.48
43.05	130.50	0.40	34.99	110.11	0.41	48.04	110.22	25.32	28.87	90.38	0.58
43.50	130.48	0.58	36.04	110.20	0.50	47.99	110.14	25.14	29.38	90.48	0.88
43.92	130.43	0.73	36.66	110.17	0.67	47.85	110.25	25.05	29.67	90.54	1.14
44.42	130.46	0.96	37.05	110.06	0.76	47.63	110.17	24.77	30.02	90.74	1.64
45.42	130.46	1.16	37.52	110.00	1.10	47.75	110.25	24.65	29.81	90.80	1.90
46.07	130.46	1.46	38.21	109.97	1.37	47.39	110.20	24.40	29.59	90.93	2.23
45.60	130.46	2.06	38.60	109.92	1.62	47.55	110.25	24.15	29.67	90.96	2.56
45.16	130.46	2.46	38.36	110.00	2.00	47.43	110.28	23.98	29.48	91.03	2.93
44.59	130.46	2.76	37.67	110.09	2.39	47.13	110.22	23.72	29.69	91.09	3.29
44.06	130.48	3.18	37.01	109.83	2.53	47.26	110.31	23.51	29.92	91.09	3.59
43.87	130.48	3.38	36.82	109.61	2.61	47.02	110.34	23.34	30.36	91.19	3.99
43.92	130.48	3.68	36.47	109.39	2.79	47.00	110.34	23.04	30.40	91.19	4.39
44.04	130.48	3.98	36.30	109.25	2.95	46.92	110.34	22.84	30.79	91.22	4.72
44.20	130.48	4.18	36.26	109.11	3.11	46.76	110.34	22.44	30.82	91.12	4.82
44.32	130.48	4.38	36.27	109.05	3.45	46.50	110.25	22.05	30.91	91.06	5.06
44.47	130.48	4.58	36.37	108.97	3.67	46.55	110.31	21.81	30.98	90.99	5.29
44.61	130.48	4.78	36.41	108.83	3.73	46.33	110.25	21.45	31.04	90.86	5.36
44.79	130.46	4.86	36.44	108.74	3.94	46.12	110.22	21.12	30.95	90.74	5.54
44.92	130.46	5.16	36.66	108.57	4.07	46.04	110.28	20.88	31.15	90.70	5.70
45.09	130.46	5.36	37.74	109.56	5.26	46.22	110.34	20.64	31.17	90.64	5.84
45.19	130.46	5.46	38.91	110.92	6.82	45.68	110.25	20.25	31.34	90.61	6.11
45.28	130.48	5.58	39.22	111.11	7.31	45.80	110.36	20.06	31.45	90.54	6.24
45.37	130.50	6.00	38.96	111.00	7.40	45.44	110.31	19.71	31.51	90.51	6.41
45.44	130.52	6.22	38.67	110.11	6.81	45.60	110.39	19.49	31.75	90.51	6.61
45.54	130.52	6.52	39.38	110.67	7.57	45.37	110.34	19.14	31.78	90.51	6.81
45.65	130.54	6.75	39.43	110.64	7.84	45.37	110.36	18.86	31.87	90.51	7.01
45.69	130.54	6.95	39.36	110.67	8.07	45.30	110.42	18.62	32.00	90.54	7.24
45.81	130.52	7.12	39.52	110.75	8.45	45.01	110.31	18.21	32.09	90.51	7.41
45.93	130.52	7.32	39.80	110.81	8.91	44.93	110.36	17.96	32.35	90.64	7.64
46.06	130.52	7.62	40.28	110.89	9.29	44.81	110.39	17.69	32.38	90.51	7.81
46.17	130.50	7.80	40.38	110.89	9.69	44.72	110.34	17.34	32.60	90.57	8.07
46.32	130.48	8.08	40.62	110.86	9.96	44.48	110.34	17.04	32.72	90.54	8.24
46.45	130.48	8.38	40.35	110.78	10.28	44.46	110.45	16.85	32.85	90.57	8.47
46.63	130.46	8.66	40.70	111.03	10.83	44.40	110.45	16.45	32.96	90.51	8.71

Table A1.7 (cont.) Mass flow rate data for R407C in the 0.039-in. capillary tube.

Mdot	Tsat	Tsub	Mdot	Tsat	Tsub	Mdot	Tsat	Tsub	Mdot	Tsat	Tsub
46.76	130.46	8.96	40.62	110.78	10.98	44.02	110.39	16.19	33.05	90.61	9.01
46.96	130.46	9.16	40.97	110.64	11.14	43.82	110.45	15.85	33.22	90.54	9.14
47.23	130.50	9.60	41.61	110.92	11.82	43.76	110.39	15.49	33.36	90.51	9.41
47.34	130.50	9.90	41.62	110.83	12.23	43.66	110.45	15.25	33.49	90.54	9.64
47.34	130.43	10.13	41.92	110.72	12.52	43.55	110.42	14.92	33.61	90.48	9.88
47.65	130.41	10.41	42.19	110.75	12.95	43.31	110.36	14.56	33.78	90.48	10.08
47.64	130.39	10.69	42.22	110.59	13.29	43.34	110.47	14.37	33.93	90.44	10.34
47.91	130.39	10.99	42.42	110.50	13.70	43.13	110.45	14.05	34.14	90.48	10.68
48.00	130.41	11.31	42.39	110.31	13.91	43.15	110.47	13.77	34.21	90.41	10.91
48.18	130.39	11.59	42.92	110.39	14.49	42.92	110.53	13.53	34.41	90.48	11.28
48.30	130.39	11.89	43.07	110.39	14.89	42.68	110.50	13.20	34.59	90.44	11.54
48.34	130.39	12.19	43.26	110.36	15.26	42.66	110.47	12.87	34.66	90.44	11.84
48.50	130.41	12.41	43.57	110.34	15.54	42.48	110.39	12.49	34.90	90.44	12.14
48.69	130.41	12.81	43.56	110.34	15.94	42.48	110.47	12.27	35.04	90.48	12.38
48.72	130.32	12.92	43.73	110.34	16.24	42.32	110.45	12.05	35.10	90.41	12.61
48.88	130.30	13.20	43.98	110.39	16.59	42.29	110.45	11.75	35.21	90.44	12.84
48.96	130.28	13.48	44.00	110.36	16.86	42.01	110.47	11.47	35.40	90.41	13.01
49.17	130.28	13.78	44.35	110.36	17.16	42.02	110.56	11.26	35.53	90.38	13.28
49.23	130.28	14.08	44.41	110.34	17.44	41.86	110.47	10.87	35.68	90.41	13.51
49.50	130.26	14.36	44.41	110.39	17.79	41.84	110.53	10.63	35.87	90.41	13.81
49.72	130.28	14.68	44.78	110.42	18.02	41.79	110.53	10.33	35.93	90.38	13.98
49.85	130.23	15.13	44.79	110.36	18.26	41.61	110.50	10.00	36.09	90.41	14.31
50.10	130.26	15.56	45.04	110.42	18.62	41.65	110.59	9.79	36.19	90.41	14.51
50.33	130.23	15.93	44.91	110.34	18.74	41.12	110.47	9.37	36.30	90.41	14.71
50.48	130.23	16.33	45.16	110.34	18.94	39.97	110.53	9.13	36.43	90.41	14.91
50.69	130.23	16.73	45.32	110.31	19.21	39.83	110.47	8.87	36.54	90.41	15.11
50.89	130.23	17.03	45.36	110.31	19.51	39.75	110.50	8.60	36.66	90.41	15.41
51.04	130.21	17.41	45.52	110.28	19.78	39.63	110.50	8.30	36.84	90.41	15.61
51.24	130.21	17.71	45.75	110.25	19.95	39.33	110.47	7.97	36.84	90.44	15.84
51.39	130.21	18.01	45.80	110.28	20.28	39.13	110.50	7.70	37.00	90.41	16.01
51.56	130.21	18.41	45.68	110.14	20.34	39.16	110.50	7.40	37.17	90.44	16.24
51.70	130.19	18.59	45.92	110.17	20.67	38.95	110.47	7.07	37.28	90.44	16.44
51.84	130.19	18.99	46.11	110.25	21.05	38.81	110.47	6.77	37.32	90.41	16.71
51.98	130.19	19.19	46.24	110.09	21.09	38.80	110.50	6.50	37.42	90.44	16.94
52.19	130.17	19.47	46.44	110.20	21.50	38.27	110.45	6.05	37.57	90.41	17.11

Table A1.7 (cont.) Mass flow rate data for R407C in the 0.039-in. capillary tube.

Mdot	Tsat	Tsub	Mdot	Tsat	Tsub	Mdot	Tsat	Tsub	Mdot	Tsat	Tsub
52.33	130.17	19.77	46.38	110.14	21.74	38.22	110.50	5.90	37.72	90.44	17.44
52.39	130.15	20.05	46.55	110.14	22.04	37.92	110.45	5.55	37.76	90.41	17.61
52.60	130.17	20.37	46.73	110.14	22.44	37.97	110.53	5.33	37.94	90.41	17.81
52.69	130.17	20.57	46.86	110.14	22.74	37.92	110.56	5.06	38.02	90.41	18.11
52.91	130.19	20.89	47.01	110.11	23.01	37.83	110.50	4.70	38.18	90.38	18.28
53.02	130.19	21.19	47.10	110.09	23.29	37.68	110.59	4.49	38.27	90.38	18.58
53.09	130.21	21.41	47.06	110.03	23.53	37.45	110.50	4.10	38.39	90.38	18.78
53.28	130.23	21.73	47.36	109.97	23.77	37.26	110.50	3.80	38.53	90.41	19.11
53.46	130.26	22.06	47.56	110.03	24.13	37.24	110.45	3.45	38.66	90.35	19.25
53.53	130.26	22.26	47.65	110.11	24.51	37.12	110.56	3.26	38.62	90.38	19.48
53.73	130.26	22.56	47.83	110.03	24.73	37.10	110.53	2.93	38.86	90.35	19.75
53.91	130.28	22.88	48.11	110.11	25.21	36.94	110.53	2.63	38.97	90.35	19.95
54.02	130.28	23.18	47.90	110.09	25.49	36.65	110.50	2.30	39.07	90.38	20.28
54.18	130.28	23.58	48.17	110.14	25.54	35.83	110.45	2.05	39.21	90.38	20.54
54.36	130.30	23.80				35.89	110.50	1.80	39.39	90.41	20.83
54.51	130.32	24.12				35.52	110.47	1.47	39.55	90.41	21.08
54.69	130.35	24.45				35.44	110.50	1.30	39.63	90.44	21.37
54.86	130.35	24.75				35.17	110.53	1.03	39.75	90.44	21.63
55.03	130.37	25.07				34.90	110.59	0.79	39.92	90.44	21.89
55.14	130.37	25.37				34.31	110.72	0.62	40.09	90.44	22.13
55.42	130.50	25.70				31.57	110.95	0.65	40.08	90.44	22.36
						30.37	111.25	0.55	40.23	90.48	22.66
									40.29	90.44	22.86
									40.42	90.48	23.14
									40.63	90.41	23.32
									40.72	90.41	23.59
									40.77	90.41	23.81
									40.98	90.41	24.03
									40.97	90.41	24.27
									41.08	90.41	24.46
									41.18	90.41	24.68
									41.17	90.35	24.82
									41.39	90.38	25.07

Table A1.8 Mass flow rate data for R407C in the 0.042-in. capillary tube.

Mdot	Tsat	Tsub	Mdot	Tsat	Tsub	Mdot	Tsat	Tsub	Mdot	Tsat	Tsub
49.78	130.49	0.49	41.63	110.29	0.39	60.31	110.09	25.49	34.73	89.90	0.60
54.75	130.49	0.69	42.35	110.26	0.46	60.09	110.07	25.27	35.92	90.29	0.79
52.08	130.46	0.76	42.69	110.26	0.56	60.03	110.07	24.97	36.31	90.45	0.85
53.62	130.40	0.80	43.77	110.21	0.61	59.67	110.04	24.74	36.27	90.45	0.85
56.04	130.35	0.95	45.18	110.21	0.71	59.81	110.01	24.41	37.02	90.49	0.89
54.98	130.40	1.10	46.08	110.15	0.95	59.50	110.01	24.11	37.86	90.62	1.22
55.33	130.42	1.62	47.44	110.07	1.27	59.36	109.98	23.88	37.79	90.68	1.58
55.31	130.33	1.83	47.83	110.04	1.54	59.19	110.01	23.61	37.91	90.71	1.81
56.06	130.33	2.13	46.96	110.15	2.05	59.01	110.01	23.41	37.83	90.75	2.15
55.64	130.46	2.56	46.73	110.18	2.38	58.93	110.01	23.11	38.02	90.84	2.54
54.61	130.49	2.89	46.47	110.23	2.83	58.73	110.01	22.81	38.10	90.84	2.74
55.03	130.46	3.16	46.45	110.23	3.03	58.65	110.01	22.61	38.37	90.94	3.14
54.81	130.44	3.44	46.33	110.23	3.43	58.51	110.04	22.34	38.39	90.84	3.24
54.94	130.51	3.71	46.65	110.21	3.71	58.27	110.07	22.07	38.71	90.87	3.47
54.89	130.49	3.99	46.74	110.21	4.01	58.23	110.07	21.77	38.73	90.84	3.74
55.33	130.49	4.29	46.90	110.21	4.41	58.08	110.07	21.47	38.95	90.87	3.97
55.28	130.42	4.52	47.12	110.15	4.65	57.87	110.09	21.19	39.11	90.84	4.24
55.73	130.40	4.70	47.39	110.15	4.95	57.75	110.12	20.82	39.35	90.84	4.44
55.50	130.40	5.10	47.53	110.12	5.22	57.67	110.12	20.52	39.62	90.87	4.77
55.85	130.42	5.32	47.85	110.12	5.52	57.46	110.15	20.25	39.80	90.81	5.01
56.08	130.33	5.53	47.83	110.09	5.79	57.30	110.18	19.88	40.02	90.81	5.21
56.14	130.37	5.87	48.23	110.09	6.09	57.18	110.18	19.58	40.16	90.81	5.51
56.64	130.46	6.26	48.40	110.15	6.55	57.04	110.18	19.28	40.39	90.78	5.68
56.59	130.40	6.50	48.57	110.15	6.85	56.87	110.21	18.91	40.58	90.78	5.98
57.04	130.44	6.84	48.95	110.15	7.15	56.67	110.21	18.61	40.73	90.78	6.28
57.30	130.49	7.19	49.13	110.18	7.48	56.53	110.21	18.31	40.92	90.75	6.55
57.34	130.46	7.46	49.34	110.15	7.75	56.44	110.21	17.91	41.13	90.78	6.78
57.54	130.40	7.70	49.49	110.18	8.08	56.27	110.21	17.61	41.28	90.71	7.01
57.87	130.44	8.04	49.77	110.21	8.41	56.11	110.21	17.31	42.23	90.75	7.35
58.08	130.46	8.36	49.90	110.18	8.68	55.92	110.21	17.01	47.61	90.62	7.52
58.14	130.46	8.76	50.22	110.21	8.91	55.82	110.23	16.63	47.62	90.65	7.85
58.45	130.46	9.06	50.28	110.23	9.23	55.65	110.23	16.33	47.69	90.58	8.08
58.57	130.46	9.36	50.56	110.23	9.53	55.40	110.23	16.03	47.84	90.62	8.42
58.88	130.46	9.66	50.66	110.23	9.73	55.39	110.23	15.73	47.92	90.58	8.68
59.11	130.49	9.99	50.78	110.26	10.06	55.28	110.23	15.43	47.94	90.58	8.98

Table A1.8 (cont.) Mass flow rate data for R407C in the 0.042-in. capillary tube.

Mdot	Tsat	Tsub	Mdot	Tsat	Tsub	Mdot	Tsat	Tsub	Mdot	Tsat	Tsub
59.12	130.49	10.29	51.04	110.26	10.36	55.09	110.26	15.06	48.11	90.55	9.25
59.52	130.46	10.56	51.27	110.26	10.66	55.02	110.26	14.76	48.14	90.49	9.49
60.04	130.49	10.99	51.49	110.26	10.96	54.85	110.26	14.46	48.21	90.49	9.69
59.90	130.46	11.26	51.74	110.26	11.26	54.69	110.26	14.16	48.31	90.45	9.95
60.24	130.49	11.59	51.94	110.29	11.59	54.64	110.26	13.86	48.36	90.42	10.12
60.15	130.42	11.82	52.17	110.26	11.86	54.42	110.26	13.56	48.47	90.49	10.49
60.66	130.44	12.14	52.44	110.26	12.16	54.41	110.26	13.26	48.52	90.45	10.75
60.60	130.40	12.40	52.69	110.26	12.46	54.28	110.26	12.96	48.65	90.45	11.05
61.04	130.44	12.74	52.80	110.26	12.76	54.12	110.23	12.63	48.83	90.49	11.29
60.97	130.37	12.97	52.93	110.26	13.06	53.96	110.23	12.33	48.82	90.45	11.55
61.23	130.40	13.40	53.13	110.23	13.33	53.81	110.23	12.03	48.93	90.45	11.85
61.47	130.40	13.70	53.31	110.21	13.51	53.63	110.23	11.73	49.04	90.45	12.15
61.71	130.37	13.97	53.46	110.21	13.81	53.53	110.21	11.41	49.17	90.49	12.49
61.92	130.37	14.27	53.56	110.18	14.08	53.48	110.21	11.11	49.23	90.49	12.69
62.07	130.33	14.53	53.69	110.15	14.25	53.35	110.21	10.81	49.33	90.49	12.99
62.35	130.35	14.85	53.88	110.15	14.55	53.19	110.21	10.51	49.47	90.52	13.22
62.45	130.33	15.13	53.91	110.12	14.82	53.02	110.21	10.21	49.55	90.52	13.52
62.55	130.35	15.45	54.18	110.09	15.09	52.91	110.18	9.88	49.67	90.55	13.75
62.77	130.35	15.75	54.28	110.09	15.39	52.83	110.18	9.58	49.79	90.58	14.08
63.04	130.31	16.01	54.50	110.09	15.69	52.75	110.18	9.38	49.85	90.58	14.38
63.23	130.35	16.35	54.69	110.12	16.02	52.60	110.18	9.08	50.02	90.62	14.62
63.37	130.35	16.65	54.86	110.12	16.32	52.51	110.18	8.78	50.11	90.65	14.85
63.65	130.31	16.91	55.07	110.12	16.62	52.34	110.18	8.48	50.20	90.65	15.15
63.66	130.33	17.23	55.12	110.12	16.92	52.25	110.21	8.21	50.32	90.68	15.48
64.01	130.35	17.55	55.44	110.12	17.22	52.19	110.21	7.91	50.32	90.62	15.62
64.06	130.35	17.85	55.64	110.12	17.52	52.06	110.23	7.63	50.46	90.68	15.98
64.37	130.31	18.11	55.87	110.15	17.85	51.93	110.23	7.33	50.50	90.68	16.18
64.45	130.31	18.41	56.01	110.15	18.15	52.02	110.26	7.16	50.63	90.68	16.48
64.59	130.26	18.66	56.27	110.18	18.48	52.01	110.26	7.16	50.67	90.68	16.68
64.90	130.26	18.96	56.48	110.15	18.75	52.00	110.26	7.26	50.80	90.68	16.88
64.93	130.26	19.26	56.65	110.18	19.08	51.83	110.29	7.09	51.00	90.68	17.18
65.03	130.24	19.54	56.84	110.18	19.38	51.66	110.29	6.79	50.94	90.65	17.35
65.29	130.22	19.82	57.02	110.18	19.68	51.44	110.29	6.49	51.04	90.65	17.55
65.56	130.26	20.06	57.18	110.21	20.01	50.49	110.29	6.19	51.15	90.68	17.78
65.58	130.22	20.42	57.44	110.21	20.31	50.41	110.29	5.89	51.14	90.62	18.02

Table A1.8 (cont.) Mass flow rate data for R407C in the 0.042-in. capillary tube.

Mdot	Tsat	Tsub	Mdot	Tsat	Tsub	Mdot	Tsat	Tsub	Mdot	Tsat	Tsub
65.82	130.24	20.64	57.64	110.21	20.51	50.23	110.32	5.62	51.26	90.62	18.32
65.99	130.22	20.92	57.73	110.21	20.81	50.20	110.34	5.34	51.41	90.62	18.52
66.14	130.22	21.32	57.92	110.23	21.13	50.08	110.34	5.04	51.41	90.58	18.78
66.38	130.22	21.62	58.12	110.23	21.43	49.94	110.34	4.74	51.57	90.62	19.02
66.69	130.24	21.94	58.30	110.23	21.73	49.70	110.34	4.44	51.61	90.58	19.28
66.79	130.22	22.22	58.44	110.23	22.03	49.26	110.34	4.14	51.65	90.55	19.45
67.06	130.29	22.59	58.63	110.23	22.33	49.19	110.34	3.84	51.78	90.58	19.78
67.20	130.24	22.84	58.83	110.23	22.63	48.93	110.34	3.54	51.80	90.55	19.95
67.44	130.26	23.16	58.96	110.23	22.93	48.93	110.34	3.24	51.94	90.55	20.15
67.49	130.24	23.44	59.17	110.23	23.13	48.76	110.32	2.92	52.04	90.55	20.45
67.79	130.22	23.72	59.36	110.23	23.43	48.68	110.34	2.64	52.19	90.55	20.74
67.96	130.22	24.02	59.42	110.23	23.73	47.76	110.34	2.34	52.16	90.52	20.98
68.16	130.22	24.32	59.70	110.21	24.01	46.49	110.34	2.04	52.22	90.49	21.19
68.28	130.18	24.58	59.76	110.21	24.21	46.36	110.37	1.77	52.44	90.52	21.50
68.49	130.24	24.94	59.80	110.18	24.48	46.41	110.37	1.37	52.40	90.49	21.75
68.63	130.20	25.20	60.05	110.15	24.75	46.16	110.37	1.07	52.54	90.49	22.02
			60.15	110.15	24.95	46.07	110.40	0.80	52.65	90.52	22.31
			60.25	110.15	25.25	45.25	110.37	0.47	52.75	90.49	22.52
			60.38	110.12	25.42	44.57	110.40	0.30	52.84	90.52	22.82
			60.35	110.09	25.59	43.12	110.46	0.26	52.91	90.52	23.08
									53.02	90.52	23.33
									53.13	90.52	23.58
									53.22	90.52	23.84
									53.33	90.52	24.11
									53.40	90.52	24.35
									53.53	90.55	24.61
									53.62	90.52	24.79
									53.59	90.52	24.98
									53.70	90.52	25.19
									53.84	90.58	25.49

Table A1.9 Mass flow rate data for R407C in the 0.049-in. capillary tube.

Mdot	Tsat	Tsub	Mdot	Tsat	Tsub	Mdot	Tsat	Tsub	Mdot	Tsat	Tsub
75.66	129.29	0.59	66.07	110.19	0.49	88.63	109.69	25.09	53.24	89.79	0.39
75.96	129.25	0.75	66.20	110.22	0.82	88.34	109.69	24.79	53.45	89.69	0.59
76.64	129.18	0.88	66.60	110.05	0.85	88.04	109.66	24.46	59.87	89.56	0.76
77.63	129.07	1.07	66.96	109.94	1.04	87.65	109.69	24.19	58.72	89.46	1.06
78.41	129.00	1.30	67.76	110.00	1.30	87.36	109.69	23.79	56.26	89.76	1.66
77.63	129.07	1.67	67.54	110.00	1.60	87.06	109.63	23.43	59.50	89.79	2.09
77.63	129.14	2.04	68.28	110.05	1.85	86.87	109.75	23.15	59.35	89.89	2.69
77.82	129.14	2.34	67.54	109.97	2.07	86.37	109.61	22.71	59.46	89.82	3.12
77.73	129.14	2.64	68.22	110.08	2.38	86.37	109.75	22.45	59.90	89.79	3.49
77.73	129.11	2.91	67.94	109.97	2.57	85.98	109.69	22.09	60.00	89.76	3.96
77.92	129.11	3.21	68.34	110.00	2.90	85.59	109.66	21.76	60.31	89.76	4.36
78.02	129.11	3.41	68.63	110.02	3.12	85.49	109.69	21.49	60.39	89.69	4.79
78.12	129.09	3.69	68.84	110.05	3.45	85.10	109.69	21.19	60.64	89.66	5.16
78.22	129.07	3.97	69.57	110.11	3.81	84.90	109.66	20.76	60.80	89.62	5.52
78.51	129.07	4.27	69.27	110.02	4.02	84.70	109.75	20.55	60.97	89.66	5.76
78.61	129.05	4.45	69.77	110.00	4.30	84.60	109.75	20.25	61.11	89.59	5.99
78.71	129.02	4.72	69.96	110.02	4.62	84.21	109.75	19.95	61.29	89.66	6.36
79.00	129.00	4.90	70.55	110.11	5.01	84.02	109.69	19.59	61.43	89.66	6.56
79.30	128.98	5.18	70.45	109.94	5.14	83.82	109.75	19.35	61.60	89.69	6.79
79.69	128.98	5.48	70.85	110.02	5.42	83.62	109.77	18.97	61.74	89.69	6.99
79.99	128.96	5.66	70.85	109.97	5.67	83.43	109.83	18.73	61.88	89.69	7.29
80.38	128.96	5.96	71.24	109.91	5.91	83.13	109.75	18.35	62.05	89.79	7.59
80.67	128.98	6.18	71.93	110.00	6.30	82.93	109.77	18.07	62.13	89.76	7.76
80.97	128.96	6.46	71.44	109.80	6.30	82.64	109.72	17.72	62.38	89.76	8.06
81.36	128.98	6.68	72.22	109.94	6.74	82.44	109.75	17.45	62.82	89.79	8.59
81.75	128.93	6.93	72.12	109.86	6.96	82.25	109.77	17.17	63.23	89.85	9.05
82.05	128.96	7.26	72.71	109.94	7.34	82.05	109.75	16.85	63.52	89.82	9.62
82.34	128.98	7.48	72.42	109.80	7.40	81.36	109.72	16.52	63.84	89.79	10.09
82.64	128.98	7.78	73.11	109.86	7.76	81.26	109.75	16.25	64.15	89.82	10.42
82.93	129.00	8.10	73.21	109.80	7.90	81.07	109.77	15.97	64.26	89.82	10.62
83.23	128.98	8.38	73.70	109.89	8.29	80.77	109.80	15.60	64.60	89.82	10.82
83.62	129.00	8.70	73.89	109.83	8.53	81.46	109.83	15.33	64.81	89.82	11.22
84.02	128.98	8.98	73.89	109.83	8.83	80.67	109.80	15.00	65.05	89.79	11.69
84.31	129.00	9.30	74.38	109.83	9.03	79.89	109.86	14.76	65.36	89.79	12.09
84.60	128.98	9.48	74.58	109.89	9.39	80.28	109.77	14.27	65.63	89.76	12.46

Table A1.9 (cont.) Mass flow rate data for R407C in the 0.049-in. capillary tube.

Mdot	Tsat	Tsub	Mdot	Tsat	Tsub	Mdot	Tsat	Tsub	Mdot	Tsat	Tsub
84.90	128.98	9.78	74.88	109.86	9.66	80.28	109.86	13.96	65.92	89.72	12.72
85.29	128.98	10.08	75.27	109.91	10.01	79.99	109.83	13.53	66.00	89.72	13.02
85.59	128.98	10.28	75.37	109.83	10.23	79.59	109.83	13.13	66.83	89.72	13.32
86.08	128.96	10.56	75.66	109.89	10.59	79.30	109.86	12.76	67.06	89.69	13.59
86.18	128.96	10.86	76.06	109.94	10.94	79.20	109.94	12.54	67.40	89.66	13.96
86.37	128.93	11.03	76.15	109.86	11.16	78.71	109.77	11.97	67.70	89.62	14.22
86.57	128.91	11.21	76.64	109.89	11.49	78.61	109.91	11.81	67.77	89.56	14.56
86.77	128.91	11.51	76.74	109.83	11.83	78.51	109.89	11.49	67.93	89.56	14.76
86.87	128.91	11.71	77.14	109.83	12.13	78.02	109.86	11.16	68.22	89.53	15.03
87.06	128.91	11.91	77.53	109.86	12.46	77.82	109.86	10.86	68.34	89.56	15.36
87.16	128.91	12.21	77.73	109.83	12.83	77.53	110.00	10.70	68.72	89.53	15.63
87.36	128.91	12.41	78.12	109.83	13.13	77.04	109.97	10.37	68.92	89.53	16.03
87.65	128.89	12.59	78.51	109.89	13.49	77.14	110.00	10.10	69.13	89.53	16.33
87.85	128.89	12.79	78.61	109.80	13.70	76.74	110.00	9.80	69.37	89.56	16.66
88.04	128.89	12.99	78.91	109.75	13.95	76.74	109.97	9.47	69.77	89.53	16.93
88.14	128.89	13.19	79.10	109.77	14.27	76.35	110.00	9.20	69.77	89.53	17.23
88.34	128.89	13.49	79.40	109.80	14.60	75.86	110.02	9.02	70.16	89.49	17.49
88.54	128.87	13.67	79.79	109.86	14.96	75.96	110.05	8.75	70.45	89.53	17.83
88.83	128.84	13.94	80.08	109.86	15.26	74.88	110.00	8.40	70.55	89.49	17.99
89.22	128.84	14.24	80.38	109.83	15.63	75.07	110.05	8.15	70.85	89.49	18.29
89.52	128.82	14.42	80.58	109.83	15.93	74.58	110.08	7.88	71.04	89.49	18.59
89.62	128.82	14.62	80.87	109.83	16.23	74.29	110.02	7.52	71.24	89.46	18.76
89.91	128.82	14.92	81.26	109.83	16.53	73.79	110.02	7.22	71.44	89.46	19.06
90.30	128.84	15.24	81.56	109.86	16.76	73.60	110.11	7.01	71.63	89.46	19.26
90.60	128.80	15.50	81.75	109.80	17.00	73.01	110.08	6.58	71.93	89.46	19.50
90.70	128.80	15.70	81.95	109.80	17.30	72.62	110.00	6.20	71.93	89.46	19.76
90.89	128.77	15.97	82.05	109.83	17.63	72.71	110.05	5.95	72.12	89.46	20.04
91.19	128.80	16.30	82.34	109.80	17.80	72.32	109.97	5.47	72.42	89.46	20.29
91.48	128.82	16.52	82.54	109.77	18.07	72.32	109.97	5.17	72.71	89.49	20.59
91.88	128.84	16.84	82.84	109.80	18.30	72.12	110.00	4.90	72.71	89.49	20.85
92.17	128.84	17.04	83.13	109.83	18.63	71.73	110.00	4.60	73.01	89.53	21.19
92.37	128.84	17.34	83.33	109.72	18.82	71.83	110.05	4.35	73.40	89.53	21.48
92.66	128.87	17.67	83.52	109.77	19.07	71.44	109.97	3.97	73.60	89.53	21.77
92.86	128.87	17.87	83.72	109.75	19.35	71.24	110.08	3.78	73.79	89.53	22.06
93.15	128.87	18.17	84.11	109.75	19.65	70.85	109.94	3.34	73.99	89.53	22.32

Table A1.9 (cont.) Mass flow rate data for R407C in the 0.049-in. capillary tube.

Mdot	Tsat	Tsub	Mdot	Tsat	Tsub	Mdot	Tsat	Tsub	Mdot	Tsat	Tsub
93.35	128.87	18.37	84.21	109.72	19.92	70.55	109.91	2.91	74.19	89.53	22.60
93.55	128.87	18.67	84.51	109.72	20.22	70.36	110.08	2.78	74.58	89.56	22.88
93.94	128.84	18.84	84.90	109.75	20.55	70.16	110.11	2.51	74.88	89.49	23.05
94.14	128.84	19.14	85.29	109.80	20.90	69.86	110.11	2.21	75.17	89.53	23.35
94.33	128.84	19.34	85.29	109.75	21.05	69.57	110.02	1.82	75.47	89.56	23.60
94.53	128.82	19.62	85.69	109.75	21.35	69.37	110.08	1.58	75.47	89.53	23.80
94.73	128.80	19.80	85.98	109.80	21.70	69.18	110.16	1.36	75.56	89.53	24.02
95.02	128.80	20.10	86.18	109.75	21.95	68.98	110.19	1.19	75.86	89.53	24.25
95.22	128.77	20.27	86.47	109.83	22.33	68.68	110.19	0.89	76.15	89.56	24.54
95.51	128.80	20.60	86.67	109.66	22.36	68.49	110.16	0.56	76.25	89.53	24.78
95.81	128.82	20.92	86.87	109.80	22.80	68.29	110.16	0.26	76.64	89.53	25.03
96.10	128.80	21.10	87.16	109.69	22.99						
96.40	128.80	21.40	87.55	109.80	23.40						
96.59	128.80	21.60	87.55	109.72	23.72						
96.89	128.80	21.90	87.75	109.69	23.99						
97.28	128.80	22.20	88.14	109.75	24.35						
97.48	128.80	22.40	88.44	109.72	24.72						
97.67	128.80	22.70	88.63	109.72	25.02						
97.97	128.80	22.90	88.73	109.69	25.19						

Table A1.10 Mass flow rate data for R410A in the 0.039-in. capillary tube.

Mdot	Tsat	Tsub	Mdot	Tsat	Tsub	Mdot	Tsat	Tsub	Mdot	Tsat	Tsub
54.91	131.79	0.29	44.26	112.40	0.20	57.71	112.06	25.26	36.44	92.46	0.56
51.03	131.62	0.42	44.97	112.40	0.40	57.57	112.06	24.96	37.01	92.43	0.63
53.37	132.09	0.99	45.68	112.38	0.58	57.50	112.08	24.78	36.94	92.29	0.69
51.32	131.85	1.05	46.24	112.36	0.96	57.28	112.06	24.46	38.14	92.34	0.94
50.89	132.00	1.00	47.24	112.26	1.16	57.17	112.04	24.24	37.98	92.29	1.09
50.32	131.95	0.35	47.34	112.20	1.40	57.13	112.06	24.06	38.26	92.21	1.21
50.00	131.80	0.10	46.94	112.30	1.80	56.95	112.04	23.84	38.16	92.21	1.51
50.95	131.69	0.19	46.40	112.40	2.20	56.86	112.04	23.54	38.17	92.24	1.74
51.67	131.60	0.40	46.24	112.46	2.56	56.80	112.03	23.33	38.21	92.34	2.14
52.83	131.50	0.90	46.43	112.50	2.90	56.63	112.03	23.13	38.36	92.34	2.34
53.70	131.40	1.20	46.45	112.54	3.24	56.61	112.03	22.93	38.37	92.31	2.51
53.46	131.42	1.62	46.50	112.56	3.46	56.43	112.04	22.64	38.53	92.36	2.76
53.15	131.87	2.47	46.71	112.54	3.74	56.34	112.01	22.41	38.62	92.41	3.11
53.15	132.12	3.12	46.69	112.52	4.02	56.19	112.01	22.11	38.74	92.41	3.31
53.01	132.17	3.57	47.01	112.50	4.20	56.06	112.01	21.81	38.91	92.38	3.48
53.52	132.19	3.99	47.00	112.46	4.46	55.90	112.04	21.64	39.03	92.34	3.64
53.57	132.17	4.27	47.10	112.48	4.88	55.87	112.06	21.36	39.04	92.41	4.01
52.70	131.87	4.37	47.29	112.46	5.16	55.69	112.06	21.06	39.16	92.34	4.14
53.37	131.82	4.62	47.55	112.46	5.46	55.58	112.08	20.78	39.40	92.36	4.46
53.86	131.82	4.92	47.77	112.44	5.74	55.48	112.14	20.64	39.50	92.36	4.66
53.92	131.82	5.22	47.98	112.44	6.14	55.39	112.18	20.38	39.56	92.31	4.91
54.11	131.82	5.52	48.11	112.42	6.42	55.19	112.14	20.04	39.87	92.34	5.24
54.35	131.82	5.72	48.26	112.40	6.70	55.11	112.16	19.76	39.91	92.29	5.49
54.51	131.84	6.04	48.45	112.38	7.08	55.01	112.16	19.46	40.09	92.31	5.81
54.72	131.80	6.30	48.68	112.38	7.38	54.86	112.20	19.20	40.31	92.34	6.14
54.93	131.82	6.62	48.79	112.38	7.78	54.69	112.20	18.90	40.60	92.34	6.44
55.01	131.79	6.89	49.09	112.42	8.22	54.35	112.18	18.58	40.67	92.36	6.76
55.18	131.77	7.17	49.30	112.38	8.48	54.38	112.22	18.32	40.55	92.26	6.96
55.38	131.74	7.44	49.37	112.40	8.90	54.03	112.20	18.00	40.93	92.29	7.19
55.55	131.72	7.72	49.53	112.38	9.18	54.05	112.22	17.72	41.05	92.26	7.46
55.77	131.72	8.02	49.87	112.38	9.58	53.86	112.22	17.42	41.20	92.26	7.76
55.76	131.72	8.32	49.98	112.36	9.86	53.76	112.24	17.14	41.46	92.29	7.99
56.10	131.70	8.60	50.01	112.38	10.18	53.64	112.24	16.74	41.42	92.26	8.26
56.17	131.69	8.89	50.31	112.36	10.46	53.49	112.24	16.54	41.63	92.26	8.56
56.36	131.67	9.17	50.39	112.34	10.74	53.40	112.24	16.24	41.74	92.24	8.74

Table A1.10 (cont.) Mass flow rate data for R410A in the 0.039-in. capillary tube.

Mdot	Tsat	Tsub	Mdot	Tsat	Tsub	Mdot	Tsat	Tsub	Mdot	Tsat	Tsub
56.49	131.65	9.45	50.50	112.34	11.04	53.29	112.24	15.94	41.85	92.26	8.96
56.63	131.62	9.72	50.75	112.34	11.34	53.06	112.26	15.66	42.02	92.24	9.24
56.84	131.65	10.05	50.86	112.30	11.70	52.75	112.26	15.36	42.18	92.26	9.46
56.94	131.60	10.30	51.07	112.30	12.00	52.62	112.26	15.06	42.36	92.21	9.71
57.11	131.57	10.57	51.23	112.28	12.28	52.48	112.26	14.76	42.48	92.26	10.06
57.36	131.57	10.87	51.37	112.28	12.68	52.42	112.26	14.46	42.51	92.16	10.16
57.46	131.55	11.15	51.63	112.24	12.94	52.30	112.26	14.16	42.60	92.19	10.49
57.63	131.57	11.47	51.72	112.26	13.26	52.06	112.28	13.88	42.97	92.24	10.84
58.30	132.05	12.25	51.96	112.26	13.56	52.07	112.28	13.68	42.97	92.19	11.09
58.45	132.05	12.55	52.08	112.26	13.86	51.90	112.28	13.38	43.25	92.24	11.34
58.61	132.00	12.80	52.19	112.26	14.16	51.81	112.30	13.10	43.27	92.19	11.59
58.68	131.99	13.09	52.34	112.26	14.46	51.53	112.28	12.78	43.65	92.21	11.91
58.51	131.64	13.04	52.55	112.26	14.76	51.28	112.28	12.48	43.73	92.29	12.29
58.63	131.50	13.20	52.82	112.26	15.06	51.04	112.24	12.24	43.77	92.21	12.41
58.87	131.55	13.55	52.86	112.26	15.46	51.01	112.24	11.94	44.00	92.21	12.71
59.03	131.59	13.89	53.11	112.26	15.76	50.98	112.26	11.66	44.23	92.21	13.01
59.25	131.62	14.22	53.26	112.24	16.14	50.84	112.28	11.38	44.25	92.19	13.19
59.47	131.65	14.55	53.44	112.24	16.44	50.72	112.28	11.08	44.51	92.24	13.54
59.65	131.67	14.87	53.62	112.26	16.76	50.60	112.28	10.78	44.60	92.24	13.74
59.87	131.72	15.22	53.83	112.28	17.18	50.43	112.30	10.60	44.74	92.26	14.06
60.10	131.74	15.54	53.96	112.26	17.46	49.99	112.32	10.32	44.85	92.16	14.26
60.30	131.75	15.85	54.09	112.26	17.76	49.70	112.30	10.00	44.86	92.16	14.56
60.45	131.77	16.17	54.24	112.26	18.06	49.66	112.32	9.82	45.16	92.24	14.94
60.60	131.79	16.49	54.46	112.26	18.36	49.60	112.32	9.52	45.28	92.19	15.19
60.79	131.80	16.80	54.55	112.26	18.56	49.49	112.36	9.26	45.48	92.16	15.46
60.99	131.79	17.09	54.73	112.28	18.88	49.31	112.36	8.96	45.68	92.21	15.81
61.21	131.80	17.40	54.86	112.24	19.14	49.14	112.34	8.64	45.76	92.16	16.06
61.32	131.79	17.69	54.99	112.26	19.46	49.02	112.34	8.34	45.91	92.16	16.36
61.51	131.77	17.97	55.15	112.28	19.68	48.85	112.34	8.14	46.07	92.14	16.64
61.71	131.79	18.29	55.20	112.28	19.98	48.72	112.34	7.84	46.28	92.14	16.94
61.81	131.79	18.59	55.34	112.26	20.16	48.50	112.32	7.52	46.48	92.14	17.24
61.86	131.77	18.87	55.45	112.24	20.44	48.45	112.32	7.22	46.53	92.09	17.49
62.22	131.75	19.25	55.59	112.22	20.62	48.28	112.34	6.94	46.66	92.14	17.84
62.32	131.74	19.44	55.66	112.20	20.90	48.19	112.34	6.64	46.74	92.09	18.09
62.46	131.74	19.74	55.85	112.20	21.10	47.89	112.34	6.34	46.90	92.09	18.39

Table A1.10 (cont.) Mass flow rate data for R410A in the 0.039-in. capillary tube.

Mdot	Tsat	Tsub	Mdot	Tsat	Tsub	Mdot	Tsat	Tsub	Mdot	Tsat	Tsub
62.64	131.72	20.02	55.93	112.20	21.30	47.70	112.34	6.04	46.95	92.14	18.64
62.77	131.70	20.30	55.98	112.22	21.52	47.48	112.34	5.74	47.23	92.04	18.84
62.99	131.69	20.59	56.17	112.20	21.80	47.29	112.32	5.42	47.29	92.07	19.17
63.02	131.69	20.89	56.31	112.18	22.08	47.07	112.34	5.14	47.39	92.04	19.44
63.35	131.65	21.15	56.51	112.18	22.38	46.93	112.34	4.84	47.54	92.04	19.64
63.39	131.65	21.45	56.65	112.18	22.78	46.73	112.38	4.58	47.70	92.02	19.92
63.65	131.62	21.82	56.77	112.20	23.10	46.62	112.38	4.28	47.91	92.02	20.24
63.68	131.60	22.10	57.05	112.16	23.36	46.46	112.40	4.00	47.91	91.99	20.46
63.95	131.59	22.39	57.11	112.14	23.64	46.38	112.42	3.72	48.03	91.97	20.71
64.01	131.57	22.67	57.24	112.14	23.94	46.21	112.40	3.50	48.28	91.97	20.96
64.25	131.54	22.94	57.33	112.10	24.20	46.09	112.38	3.18	48.38	91.99	21.23
64.39	131.55	23.35	57.45	112.10	24.50	46.08	112.40	2.90	48.50	91.99	21.50
64.55	131.55	23.65	57.57	112.08	24.68	45.81	112.38	2.58	48.67	91.97	21.76
64.76	131.54	23.94	57.74	112.06	24.96	45.64	112.38	2.28	48.73	91.92	21.99
64.87	131.55	24.35	57.84	112.04	25.24	45.34	112.38	1.98	48.79	91.92	22.29
65.11	131.54	24.64	57.93	112.04	25.44	45.35	112.38	1.68	49.00	91.94	22.63
65.20	131.54	24.94				45.18	112.40	1.50	49.14	91.90	22.94
						45.01	112.40	1.20	49.28	91.92	23.33
						44.81	112.40	0.90	49.58	91.94	23.68
									49.62	91.94	24.04
									49.79	91.87	24.26
									49.95	91.92	24.60
									50.05	91.97	24.92
									50.17	91.99	25.14
									50.31	91.99	25.34

Table A1.11 Mass flow rate data for R410A in the 0.042-in. capillary tube.

Mdot	Tsat	Tsub	Mdot	Tsat	Tsub	Mdot	Tsat	Tsub	Mdot	Tsat	Tsub
62.69	131.88	0.28	53.73	112.05	0.45	70.95	111.98	26.48	43.38	93.13	0.33
63.56	131.68	0.58	53.78	112.13	0.43	70.85	112.00	26.30	42.08	93.13	0.43
65.47	131.46	1.06	54.71	112.15	0.55	70.75	112.02	26.12	43.99	93.15	0.55
65.86	131.41	1.61	55.34	112.17	0.67	70.55	112.00	25.90	47.64	93.10	0.70
64.88	131.68	2.68	56.40	112.13	0.93	70.36	112.02	25.72	47.29	93.05	0.75
64.81	131.83	3.43	57.67	112.05	1.15	70.36	112.02	25.42	49.02	92.98	0.78
65.11	131.88	3.98	57.96	112.03	1.43	70.26	112.02	25.22	45.90	92.88	0.88
65.34	131.85	4.45	57.10	112.17	1.97	70.06	112.03	25.03	47.88	92.86	0.96
65.61	131.85	4.95	56.70	112.31	2.51	69.96	112.03	24.83	47.42	92.81	1.01
65.75	131.81	5.31	56.90	112.37	2.87	69.77	112.03	24.63	48.91	92.74	1.14
65.99	131.76	5.66	56.86	112.43	3.33	69.77	112.05	24.45	49.55	92.71	1.31
66.32	131.76	6.06	57.00	112.43	3.63	69.57	112.03	24.13	49.15	92.74	1.64
66.46	131.75	6.45	57.43	112.45	4.15	69.47	112.05	23.95	48.56	92.81	2.01
66.63	131.71	6.71	57.69	112.41	4.61	69.37	112.07	23.77	48.58	93.03	2.63
66.78	131.66	6.96	57.99	112.41	5.11	69.27	112.09	23.49	48.79	93.03	2.93
66.97	131.66	7.36	58.41	112.41	5.61	69.18	112.09	23.29	49.54	92.98	3.18
67.27	131.61	7.61	58.65	112.37	6.07	69.07	112.09	22.99	49.76	93.03	3.53
67.48	131.63	7.93	58.93	112.37	6.47	69.00	112.11	22.81	49.83	92.98	3.78
67.62	131.63	8.33	59.18	112.37	6.97	68.83	112.11	22.51	49.85	93.03	4.13
67.89	131.66	8.66	59.50	112.33	7.43	68.56	112.11	22.31	50.30	93.03	4.43
68.22	131.68	8.98	59.68	112.33	7.83	68.60	112.13	22.03	50.38	93.03	4.73
68.34	131.71	9.31	60.01	112.33	8.23	68.43	112.11	21.71	50.48	92.98	4.98
68.50	131.71	9.61	60.28	112.27	8.57	68.23	112.11	21.51	49.93	92.86	5.16
68.73	131.71	9.91	60.50	112.25	8.95	68.13	112.09	21.19	50.19	92.93	5.53
68.98	131.73	10.23	60.71	112.23	9.33	68.03	112.11	21.01	50.41	92.96	5.86
69.10	131.73	10.53	60.95	112.23	9.73	67.82	112.11	20.71	50.36	92.86	6.06
69.47	131.75	10.85	61.29	112.21	10.11	67.62	112.11	20.41	50.49	92.81	6.31
69.57	131.73	11.13	61.37	112.19	10.39	67.50	112.13	20.23	50.70	92.74	6.54
69.86	131.73	11.43	61.58	112.19	10.79	67.22	112.11	19.91	50.94	92.71	6.91
69.96	131.71	11.71	61.81	112.19	11.09	67.23	112.11	19.61	51.21	92.76	7.26
70.06	131.70	12.00	62.13	112.19	11.39	66.98	112.13	19.43	51.35	92.71	7.51
70.26	131.71	12.31	62.11	112.19	11.69	66.92	112.13	19.13	51.49	92.71	7.81
70.55	131.70	12.60	62.22	112.17	11.97	66.66	112.11	18.81	51.84	92.71	8.11
70.75	131.70	12.90	62.42	112.17	12.27	66.53	112.11	18.51	51.95	92.76	8.46
70.85	131.68	13.18	62.61	112.17	12.57	66.17	112.09	18.19	52.05	92.79	8.79

Table A1.11 (cont.) Mass flow rate data for R410A in the 0.042-in. capillary tube.

Mdot	Tsat	Tsub	Mdot	Tsat	Tsub	Mdot	Tsat	Tsub	Mdot	Tsat	Tsub
71.04	131.66	13.46	62.84	112.17	12.77	66.13	112.11	18.01	52.31	92.71	9.01
71.34	131.70	13.90	62.91	112.17	13.07	65.98	112.09	17.69	52.59	92.71	9.31
71.63	131.68	14.18	63.07	112.15	13.35	65.82	112.11	17.41	52.67	92.79	9.79
71.63	131.65	14.45	63.36	112.15	13.55	65.57	112.11	17.11	52.82	92.74	10.04
71.83	131.53	14.63	63.53	112.13	13.83	65.44	112.09	16.79	53.13	92.76	10.36
71.93	131.46	14.86	63.65	112.13	14.13	65.29	112.09	16.49	53.17	92.81	10.81
72.32	131.65	15.35	63.86	112.15	14.45	64.99	112.09	16.19	53.36	92.76	11.06
72.71	131.81	15.81	64.04	112.13	14.73	64.96	112.11	15.91	53.49	92.74	11.34
72.81	131.75	16.15	64.19	112.11	15.01	64.71	112.09	15.59	53.92	92.81	11.71
73.01	131.68	16.38	64.30	112.09	15.29	64.60	112.11	15.31	53.93	92.81	12.01
73.11	131.63	16.63	64.58	112.07	15.47	64.50	112.13	15.03	54.25	92.84	12.34
73.50	131.66	16.96	64.71	112.09	15.79	64.34	112.11	14.71	54.52	92.79	12.59
73.60	131.70	17.40	64.90	112.07	16.07	64.13	112.13	14.43	54.68	92.84	12.94
73.99	131.80	17.80	65.02	112.07	16.37	63.95	112.15	14.15	54.90	92.88	13.28
73.99	131.66	17.96	65.19	112.03	16.63	63.78	112.17	13.87	55.18	92.88	13.58
74.19	131.61	18.31	65.44	112.05	16.95	63.63	112.15	13.55	55.37	92.86	13.86
74.38	131.56	18.56	65.51	112.03	17.33	63.33	112.19	13.29	55.60	92.84	14.04
74.68	131.55	18.85	65.81	112.03	17.53	63.31	112.21	13.01	56.16	92.84	14.34
74.88	131.55	19.25	65.98	112.02	17.82	63.03	112.21	12.71	56.33	92.88	14.58
75.27	131.80	19.80	66.34	112.02	18.12	62.92	112.23	12.43	56.59	92.84	14.84
75.37	131.65	20.05	66.31	112.02	18.42	62.90	112.23	12.13	56.56	92.84	15.14
75.47	131.60	20.40	66.63	112.02	18.72	62.66	112.27	11.87	56.83	92.81	15.51
75.66	131.56	20.66	66.62	112.00	19.00	62.58	112.27	11.57	57.08	92.86	15.86
76.06	131.56	21.06	66.82	111.98	19.38	62.36	112.31	11.31	56.89	92.74	16.04
76.15	131.58	21.38	67.13	111.98	19.68	62.03	112.29	10.99	57.17	92.79	16.39
76.35	131.68	21.78	67.18	111.96	19.96	61.98	112.29	10.69	57.45	92.81	16.81
76.64	131.63	22.03	67.42	111.96	20.26	61.76	112.29	10.39	57.58	92.79	17.09
76.94	131.60	22.40	67.74	111.96	20.56	61.67	112.29	10.09	57.63	92.74	17.44
76.94	131.58	22.68	67.72	111.94	20.84	61.44	112.29	9.79	57.80	92.71	17.71
77.14	131.58	22.98	67.95	111.92	21.12	61.24	112.25	9.45	58.03	92.76	18.06
77.33	131.56	23.26	68.07	111.94	21.44	61.15	112.25	9.15	58.17	92.71	18.41
77.63	131.55	23.55	68.22	111.92	21.72	61.11	112.25	8.85	58.35	92.69	18.69
77.73	131.55	23.95	68.49	111.96	22.06	60.86	112.23	8.53	58.53	92.67	18.97
77.92	131.51	24.21	68.63	111.96	22.36	60.78	112.21	8.21	58.76	92.71	19.31
78.22	131.58	24.58	68.73	111.94	22.64	60.59	112.19	7.89	58.89	92.69	19.59

Table A1.11 (cont.) Mass flow rate data for R410A in the 0.042-in. capillary tube.

Mdot	Tsat	Tsub	Mdot	Tsat	Tsub	Mdot	Tsat	Tsub	Mdot	Tsat	Tsub
78.91	132.18	25.48	68.94	111.98	22.98	60.39	112.17	7.57	58.93	92.67	19.87
			69.18	111.98	23.18	60.07	112.17	7.27	59.15	92.69	20.19
			69.37	111.96	23.46	59.98	112.15	6.95	59.34	92.69	20.49
			69.47	111.98	23.78	59.77	112.11	6.61	59.38	92.67	20.71
			69.67	112.00	24.10	59.58	112.09	6.29	59.69	92.69	20.99
			69.86	111.98	24.28	58.69	112.11	6.01	59.71	92.69	21.24
			69.96	111.98	24.58	58.02	112.09	5.69	59.87	92.67	21.45
			70.06	112.00	24.90	57.93	112.09	5.39	60.00	92.67	21.69
			70.26	112.00	25.20	57.75	112.09	5.09	60.27	92.67	21.91
			70.36	111.98	25.38	57.53	112.11	4.81	60.38	92.64	22.09
			70.55	111.98	25.68	57.37	112.13	4.53	60.54	92.64	22.33
			70.75	112.00	26.00	57.14	112.13	4.13	60.71	92.67	22.63
			70.85	112.00	26.30	57.11	112.17	3.87	60.77	92.64	22.88
			70.95	112.00	26.50	56.96	112.15	3.55	60.92	92.59	23.08
						56.78	112.17	3.27	61.03	92.59	23.34
						56.65	112.19	2.99	61.19	92.59	23.66
						56.53	112.21	2.71	61.24	92.62	23.99
						56.48	112.23	2.33	61.37	92.57	24.25
						56.28	112.27	2.07	61.50	92.54	24.51
						56.18	112.27	1.77	61.71	92.57	24.80
						55.95	112.29	1.49	62.01	92.62	25.09
						55.93	112.33	1.23	62.04	92.59	25.32
						55.84	112.37	0.97	62.12	92.67	25.68
						55.60	112.37	0.67	62.35	92.62	25.89

Table A1.12 Mass flow rate data for R410A in the 0.049-in. capillary tube.

Mdot	Tsat	Tsub	Mdot	Tsat	Tsub	Mdot	Tsat	Tsub	Mdot	Tsat	Tsub
			80.28	111.84	0.34	107.11	111.48	24.98	68.76	92.74	0.54
			83.92	111.96	0.46	106.81	111.50	24.80	69.18	92.79	0.69
			83.72	111.88	0.78	106.72	111.60	24.50	69.57	92.65	0.75
			83.23	112.06	1.56	106.42	111.52	24.12	69.57	92.67	1.07
			82.93	112.08	2.18	105.93	111.56	23.76	70.16	92.55	1.25
			83.82	112.08	2.78	105.63	111.52	23.32	70.26	92.52	1.52
			84.51	112.02	3.22	105.14	111.50	22.90	70.75	92.57	1.87
			84.70	111.92	3.62	104.85	111.60	22.70	70.65	92.50	2.10
			85.10	111.94	4.14	104.36	111.52	22.22	71.83	92.48	2.48
			85.59	111.90	4.50	104.06	111.50	21.90	72.32	92.48	2.78
			85.59	111.90	5.00	103.96	111.58	21.58	72.52	92.48	3.18
			86.37	111.94	5.44	103.67	111.56	21.26	72.81	92.50	3.50
			86.86	112.00	5.90	103.18	111.58	20.88	73.11	92.50	3.90
			87.26	112.00	6.20	103.08	111.54	20.54	73.50	92.52	4.22
			87.85	112.00	6.60	102.88	111.56	20.16	73.60	92.48	4.58
			87.85	111.92	6.82	102.49	111.58	19.98	74.09	92.57	4.97
			88.63	111.94	7.14	102.10	111.66	19.66	74.38	92.50	5.20
			88.63	111.92	7.52	102.10	111.64	19.34	74.68	92.52	5.52
			88.73	111.96	7.86	101.70	111.74	19.24	74.97	92.52	5.82
			89.22	111.88	8.18	101.41	111.66	18.86	75.47	92.60	6.20
			90.01	111.98	8.58	101.21	111.60	18.50	75.66	92.50	6.40
			90.11	111.90	8.80	100.62	111.78	18.38	76.06	92.57	6.77
			90.40	111.94	9.14	100.43	111.72	18.02	76.25	92.57	7.07
			90.89	111.96	9.46	100.23	111.70	17.80	76.35	92.52	7.32
			91.09	111.90	9.70	99.74	111.70	17.50	76.94	92.48	7.68
			91.38	111.88	9.98	99.54	111.80	17.30	77.14	92.57	8.07
			91.68	111.88	10.28	99.25	111.74	16.94	77.53	92.55	8.35
			91.97	111.84	10.54	99.25	111.84	16.84	77.92	92.57	8.67
			92.07	111.78	10.78	98.95	111.86	16.56	78.02	92.50	8.90
			92.47	111.86	11.16	98.76	111.92	16.32	78.32	92.50	9.20
			93.06	111.90	11.50	98.56	111.84	16.04	78.61	92.48	9.48
			93.45	111.96	11.86	98.07	111.88	15.78	78.81	92.45	9.75
			93.65	111.96	12.16	98.07	111.92	15.52	79.20	92.50	10.10
			93.84	111.94	12.44	97.87	111.90	15.20	79.30	92.45	10.35
			93.94	111.90	12.70	97.58	111.94	14.94	79.49	92.38	10.58

Table A1.12 (cont.) Mass flow rate data for R410A in the 0.049-in. capillary tube.

Mdot	Tsat	Tsub	Mdot	Tsat	Tsub	Mdot	Tsat	Tsub	Mdot	Tsat	Tsub
			94.33	111.80	12.90	97.38	111.90	14.70	79.79	92.38	10.78
			94.92	111.76	13.16	96.89	111.82	14.32	80.28	92.40	11.10
			94.73	111.62	13.32	96.50	111.82	14.02	80.38	92.33	11.33
			95.22	111.74	13.64	96.50	111.82	13.72	80.48	92.33	11.53
			95.61	111.76	13.96	96.20	111.84	13.44	80.97	92.33	11.83
			95.81	111.74	14.24	95.91	111.84	13.24	80.77	92.28	11.98
			96.30	111.78	14.58	95.51	111.88	12.98	81.36	92.30	12.30
			96.20	111.72	14.82	95.12	111.92	12.72	81.85	92.40	12.60
			96.79	111.74	15.14	94.92	111.92	12.42	81.56	92.16	12.66
			97.18	111.74	15.44	94.33	111.88	12.08	81.95	92.18	12.98
			97.28	111.76	15.76	94.23	111.94	11.84	82.25	92.16	13.36
			97.97	111.86	16.26	94.14	111.92	11.52	82.64	92.18	13.68
			97.97	111.76	16.46	93.74	111.94	11.24	83.33	92.23	14.13
			98.46	111.80	16.80	93.65	111.96	10.96	83.43	92.18	14.38
			98.85	111.86	17.16	93.55	112.00	10.80	83.72	92.18	14.68
			99.25	111.84	17.44	92.76	111.98	10.48	83.92	92.13	14.93
			99.25	111.78	17.68	92.27	111.98	10.18	84.41	92.11	15.31
			99.74	111.82	18.12	91.88	112.02	9.92	84.80	92.16	15.76
			99.84	111.78	18.38	91.48	112.02	9.62	85.39	92.26	16.36
			100.43	111.70	18.60	91.29	112.04	9.34	85.59	92.08	16.58
			100.52	111.76	18.96	91.09	112.08	9.08	85.98	92.13	17.03
			100.72	111.74	19.34	90.50	112.08	8.78	86.57	92.18	17.48
			100.92	111.78	19.68	90.60	112.08	8.48	86.96	92.26	17.86
			101.31	111.70	19.80	90.11	112.10	8.20	87.06	92.21	18.21
			101.70	111.58	19.88	90.11	112.04	7.84	87.55	92.18	18.48
			101.61	111.56	20.16	89.52	112.08	7.58	88.04	92.23	18.93
			101.80	111.52	20.32	89.12	112.04	7.24	87.95	92.16	19.16
			102.00	111.46	20.46	88.93	112.02	6.92	88.54	92.26	19.56
			102.59	111.50	20.70	88.93	112.14	6.74	88.73	92.21	19.91
			102.59	111.42	20.92	88.54	112.04	6.34	89.13	92.23	20.13
			102.78	111.39	21.09	88.24	112.14	6.14	89.32	92.21	20.45
			102.88	111.48	21.38	88.24	112.10	5.80	89.62	92.23	20.76
			103.47	111.44	21.54	87.65	112.10	5.40	90.11	92.28	21.13
			103.77	111.41	21.81	87.45	112.10	5.20	90.21	92.26	21.48
			104.06	111.44	22.04	87.55	112.14	4.94	90.80	92.30	21.92

Table A1.12 (cont.) Mass flow rate data for R410A in the 0.049-in. capillary tube.

Mdot	Tsat	Tsub	Mdot	Tsat	Tsub	Mdot	Tsat	Tsub	Mdot	Tsat	Tsub
			104.65	111.39	22.19	86.96	112.10	4.50	91.09	92.33	22.33
			104.65	111.42	22.52	86.67	112.00	4.10	91.39	92.23	22.60
			105.14	111.50	22.80	86.37	112.10	3.90	91.68	92.26	23.00
			104.95	111.44	22.94	85.49	112.10	3.60	92.07	92.26	23.32
			105.54	111.46	23.26	85.29	112.08	3.28	92.37	92.21	23.60
			105.83	111.44	23.44	84.80	112.08	2.98	92.66	92.28	23.99
			106.03	111.50	23.70	84.51	112.12	2.62	92.86	92.23	24.26
			106.13	111.44	23.94	84.31	112.26	2.46	93.06	92.21	24.53
			106.52	111.52	24.22	83.92	112.12	1.92	93.25	92.26	24.88
			106.42	111.44	24.34	83.23	112.20	1.70	93.65	92.13	25.05
			106.81	111.46	24.66	81.36	112.22	1.42	93.74	92.11	25.32
			107.11	111.54	24.94	80.97	112.31	1.11	94.14	92.16	25.67
						81.16	112.37	0.87			
						80.28	112.30	0.50			